



**HAL**  
open science

# Characterization of Membrane Foulants in Full-scale and Lab-scale Membrane Bioreactors for Wastewater Treatment and Reuse.

Gerald Matar, Gerald Kamil Matar

## ► To cite this version:

Gerald Matar, Gerald Kamil Matar. Characterization of Membrane Foulants in Full-scale and Lab-scale Membrane Bioreactors for Wastewater Treatment and Reuse.. Environmental Sciences. King Abdullah University of Science and Technology, 2015. English. NNT: . tel-02323062

**HAL Id: tel-02323062**

**<https://hal.science/tel-02323062>**

Submitted on 21 Oct 2019

**HAL** is a multi-disciplinary open access archive for the deposit and dissemination of scientific research documents, whether they are published or not. The documents may come from teaching and research institutions in France or abroad, or from public or private research centers.

L'archive ouverte pluridisciplinaire **HAL**, est destinée au dépôt et à la diffusion de documents scientifiques de niveau recherche, publiés ou non, émanant des établissements d'enseignement et de recherche français ou étrangers, des laboratoires publics ou privés.

**Characterization of Membrane Foulants  
in Full-scale and Lab-scale Membrane  
Bioreactors for Wastewater Treatment  
and Reuse**

**Dissertation by  
Gerald Kamil Matar**

**In Partial Fulfillment of the Requirements  
For the Degree of  
Doctor of Philosophy**

**King Abdullah University of Science and Technology, Thuwal,  
Kingdom of Saudi Arabia**

**November, 2015**

## **Examination Committee Approval Form**

The dissertation of Gerald Kamil Matar is approved by the examination committee.

Committee Chairperson: Assoc. Prof. Pascal Saikaly

Committee Member: Prof. Suzana Nunes

Committee Member: Prof. Johannes Vrouwenvelder

Committee Member: Assoc. Prof. Pierre Le-Clech

Committee Member: Asst. Prof. Uli Stingl

© November, 2015

**Gerald Kamil Matar**

All Rights Reserved

## ABSTRACT

### **Characterization of Membrane Foulants in Full-scale and Lab-scale Membrane Bioreactors for Wastewater Treatment and Reuse**

Gerald Kamil Matar

Membrane bioreactors (MBRs) offer promising solution for wastewater treatment and reuse to address the problem of water scarcity. Nevertheless, this technology is still facing challenges associated with membrane biofouling. This phenomenon has been mainly investigated in lab-scale MBRs with little or no insight on biofouling in full-scale MBR plants. Furthermore, the temporal dynamics of biofouling microbial communities and their extracellular polymeric substances (EPS) are less studied. Herein, a multidisciplinary approach was adopted to address the above knowledge gaps in lab- and full-scale MBRs. In the full-scale MBR study, 16S rRNA gene pyrosequencing with multivariate statistical analysis revealed that the early and mature biofilm communities from five full-scale MBRs differed significantly from the source community (i.e. activated sludge), and random immigration of species from the source community was unlikely to shape the community structure of biofilms. Also, a core biofouling community was shared between the five MBR plants sampled despite differences in their operating conditions. In the lab-scale MBR studies, temporal dynamics of microbial communities and their EPS products were monitored on different hydrophobic and hydrophilic membranes during 30 days. At the early stages of filtration (1 d), the same early colonizers belonging to the class *Betaproteobacteria* were identified on all the

membranes. However, their relative abundance decreased on day 20 and 30, and sequence reads belonging to the phylum *Firmicutes* and *Chlorobi* became dominant on all the membranes on day 20 and 30. In addition, the intrinsic membrane characteristic did not select any specific EPS fractions at the initial stages of filtration and the same EPS foulants developed with time on the hydrophobic and hydrophilic membranes. Our results indicated that the membrane surface characteristics did not select for specific biofouling communities or EPS foulants, and the same early colonizers were selected from the source community (i.e. activated sludge), and then went through significant changes to form a mature biofilm. Our findings from these studies could support future research aimed at developing enhanced biological-based strategies to control biofouling in MBRs.

**Keywords:** wastewater treatment; membrane bioreactor; membrane biofouling; microbial communities; hydrophilicity; hydrophobicity.

## ACKNOWLEDGMENTS

First and foremost, I would like to express my appreciation and gratitude to my supervisor Professor Pascal E. Saikaly for providing me with his tremendous support and guidance throughout every stage of my Ph.D.

Very special thanks to Professor Suzana Nunes for offering me the modified hollow-fiber membranes to complete my PhD work, and for providing me with her scientific feedback as part of my PhD committee.

I also thank Prof. Johannes Vrouwenvelder, Prof. Pierre Le-Clech and Prof. Uli Stingl for their scientific feedback and willingness to serve on my PhD committee.

My appreciation also goes to Dr. Samik Bagchi for his tremendous effort and contribution to the analysis of pyrosequencing data. My gratitude also goes to Dr. Graciela Gonzalez-Gil for the methodical and systematical feedback she provided for the extraction protocols of extracellular polymeric substances, and for constructive guidance on different aspect of research and life.

I would like to thank all my colleagues in the Microbial Ecology and Biotechnology group directed by Professor Pascal Saikaly, especially Zhongwei Wang for his assistance in constructing and operating the lab-scale membrane bioreactor. I am also thankful to the entire WDRC family for their support role and attitude.

I thankfully acknowledge financial support from King Abdullah University of Science and Technology.

Last, but not least, I dedicate this thesis to my parents, my brothers and sister, and to Youmna, without their continuous support this dissertation would not have been achievable.

## TABLE OF CONTENTS

<b>Examination Committee Approval Form .....</b>	<b>2</b>
<b>ABSTRACT .....</b>	<b>4</b>
<b>LIST OF ABBREVIATIONS.....</b>	<b>10</b>
<b>LIST OF FIGURES .....</b>	<b>13</b>
<b>LIST OF TABLES .....</b>	<b>18</b>
<b>CHAPTER 1 INTRODUCTION .....</b>	<b>19</b>
<b>1.1. Fresh water demand.....</b>	<b>19</b>
<b>1.2. Membrane Bioreactors (MBRs).....</b>	<b>21</b>
<b>1.3. Fouling in MBRs.....</b>	<b>23</b>
<b>1.4. Biofouling in MBRs.....</b>	<b>27</b>
1.4.1. Factors that affect biofouling in MBRs.....	28
1.4.2. Sequential steps that develop membrane biofouling.....	30
<b>1.5. Biofouling control strategies.....</b>	<b>32</b>
1.5.1. Membrane surface modification.....	32
1.5.2. Critical flux concept.....	32
1.5.3. Chemical dosage to increase flocs size .....	33
<b>1.6. Knowledge Gaps.....</b>	<b>35</b>
<b>1.7. Objectives.....</b>	<b>37</b>
<b>1.8. Thesis roadmap .....</b>	<b>38</b>
<b>References .....</b>	<b>41</b>
<b>CHAPTER 2 454-Pyrosequencing Reveals Biodiversity of Sessile and Planktonic Bacterial Community in Five Full-scale Membrane Bioreactors .....</b>	<b>46</b>
<b>ABSTRACT .....</b>	<b>48</b>
<b>2.1. Introduction .....</b>	<b>49</b>
<b>2.2. Materials and methods.....</b>	<b>51</b>
2.2.1. Full-scale MBRs and sample collection.....	51
2.2.2. DNA extraction, PCR amplification and 16S rRNA gene pyrosequencing....	53
2.2.3. Processing of pyrosequencing data .....	54
2.2.4. Alpha and beta diversity estimates.....	55
2.2.5. Statistical analysis .....	56
<b>2.3. Results .....</b>	<b>57</b>
2.3.1. Alpha diversity measures .....	57
2.3.2. Bacterial community composition and taxonomy.....	59
2.3.3. Beta diversity measures.....	62
2.3.4. Core genera and OTUs.....	67

2.3.5. Effect of source community .....	72
<b>2.4. Discussion .....</b>	<b>73</b>
<b>References .....</b>	<b>80</b>
<b>CHAPTER 3 Microbial Succession and Mature Biofilm Formation on Different Membrane Surfaces Operated Under Low Flux Conditions in a Lab-scale Membrane Bioreactor .....</b>	<b>83</b>
<b>ABSTRACT .....</b>	<b>85</b>
<b>3.1. Introduction .....</b>	<b>86</b>
<b>3.2. Materials and Methods .....</b>	<b>89</b>
3.2.1. Description of the lab-scale MBR .....	89
3.2.2. Membranes characteristics and sampling frequency .....	91
3.2.3. DNA extraction, PCR amplification and 16S rRNA gene pyrosequencing .....	93
3.2.4. Processing of pyrosequencing data .....	95
3.2.5. Diversity estimates .....	96
<b>3.3. Results .....</b>	<b>96</b>
3.3.1. Reactor performance and transmembrane pressure measurements .....	96
3.3.2. Bacterial alpha diversity measures .....	98
3.3.3. Effect of membrane surface chemistry on the microbial community structure of early colonizers .....	100
3.3.4. Microbial community succession .....	103
3.3.5. Shared OTUs .....	108
<b>3.4. Discussion .....</b>	<b>109</b>
3.4.1. Composition of the early colonizers .....	109
3.4.2. Successional steps towards a mature biofilm .....	114
<b>3.5. Conclusion .....</b>	<b>118</b>
<b>References .....</b>	<b>119</b>
<b>CHAPTER 4 Temporal Changes in Extracellular Polymeric Substances on Hydrophobic and Hydrophilic Membrane Surfaces in a Submerged Membrane Bioreactor .....</b>	<b>124</b>
<b>ABSTRACT .....</b>	<b>125</b>
<b>4.1. Introduction .....</b>	<b>126</b>
<b>4.2. Materials and Methods .....</b>	<b>128</b>
4.2.1. Membranes manufacture and characteristics .....	128
4.2.2. Lab-scale MBR construction and operation .....	129
4.2.3. EPS extraction .....	132
4.2.4. Analysis of the EPS solution .....	133
4.2.4.1. Liquid chromatography with organic carbon detection .....	133
4.2.4.2. Fluorescence excitation – emission matrices .....	133
4.2.4.3. Fourier transform infrared spectroscopy .....	133

4.2.4.4. Proteins and polysaccharides quantification .....	134
4.2.5. Confocal laser scanning microscopy.....	134
4.2.6. Statistical analysis .....	135
<b>4.3. Results .....</b>	<b>136</b>
4.3.1. TMP measurements.....	136
4.3.2. Characterisation of the initial fouling layer.....	137
4.3.3 Temporal changes in fouling characteristics.....	140
4.3.3.1. LC-OCD .....	140
4.3.3.2. FEEM .....	144
4.3.4. Visualization of the biofilm architecture.....	145
<b>4.4 Discussion .....</b>	<b>147</b>
4.4.1. Effect of surface hydrophilicity and charge on biofouling .....	147
4.4.2. Dynamics of the EPS deposition on different membrane surfaces .....	148
4.4.3. Effect of permeate production on membrane biofouling .....	151
<b>4.5. Conclusion.....</b>	<b>153</b>
<b>References .....</b>	<b>155</b>
<b>CHAPTER 5 CONCLUSION .....</b>	<b>160</b>
<b>5.1. General conclusions.....</b>	<b>160</b>
<b>5.2. Proposed approaches for future studies on MBR biofouling.....</b>	<b>164</b>
<b>Appendix A - Effect of rinsing on the structure and composition of biofouling communities in MBRs.....</b>	<b>167</b>
<b>Appendix B - Lab-scale MBR routine measurements, COD and Nutrients removal.....</b>	<b>170</b>
<b>Appendix C - Characterization of the hollow-fiber membranes. ....</b>	<b>172</b>
<b>Appendix D - Pyrosequencing results of RNA samples.....</b>	<b>174</b>
<b>Appendix E - Optimization of different approaches for EPS extraction from hollow fiber membranes. ....</b>	<b>176</b>
<b>Appendix F - Scanning electron micrographs and confocal laser scanning microscopy of biofilm samples on membrane surfaces.....</b>	<b>178</b>
<b>Appendix G - Different lab-scale reactors designs and construction. ....</b>	<b>181</b>

## LIST OF ABBREVIATIONS

ARDRA:	Amplified Ribosomal Dexoyribonucleic Acid Restriction Analysis
CAS:	Conventional Activated Sludge
CLSM:	Confocal Laser Scanning Microscopy
COD:	Chemical Oxygen Demand
COM:	Commercial Membrane
DGGE:	Denaturing Gradient Gel Electrophoresis
DNA:	Deoxyribonucleic Acid
DO:	Dissolved Oxygen
DOM:	Dissolved Organic Matter
EPS:	Extracellular Polymeric Substances
EOM:	Effluent Organic Matter
FEEM:	Fluorescence Excitation-Emission Matrix
FISH:	Fluorescent in situ Hybridization
FTIR:	Fourier Transform Infrared
HF:	Hollow Fiber
HRT:	Hydraulic Retention Time
LC-OCD:	Liquid Chromatography Organic Carbon Detection
MBR:	Membrane Bioreactor
MF:	Microfiltration
MLSS:	Mixed Liquor Suspended Solids
MLVSS:	Mixed Liquor Volatiles Suspended Solids
nAg:	Silver Nano Particles

NCBI:	National Center for Biotechnology Information
NF:	Nanofiltration
NMDS:	Nonmetric Multidimensional Scaling
NMR:	Nuclear Magnetic Resonance Spectroscopy
OCT:	Optical Coherence Tomography
OTU:	Operational Taxonomic Unit
PAC:	Powdered Activated Carbon
PBS:	Phosphate Buffer Saline
PCoA:	Principal Coordinate Analysis
PCR:	Polymerase Chain Reaction
PDA:	Polydopamine
PE:	Polyethylene
PES:	Polyethersulfone
PP:	Polypropylene
POX:	Polyoxadiazole
PS:	Polysulfone
PTA:	Fluorinated Polytriazole
PTFE:	Polytetrafluorethylene
PVDF:	Polyvinylidene Fluoride
QIIME:	Quantitative Insights Into Microbial Ecology
RNA:	Ribonucleic Acid
rRNA:	Ribosomal RNA

RO:	Reverse Osmosis
SEM:	Scanning Electron Microscopy
SMP:	Soluble Microbial Products
SPSU:	Sulfonated Polysulfone
SPTA:	Sulfonated Polytriazole
SRA:	Sequence Read Archive
SRT:	Sludge Retention Time
T-RFLP:	Terminal Restriction Fragment Length Polymorphism
TMP:	Transmembrane Pressure
UF:	Ultrafiltration
UPGMA:	Unweighted Pair Group Method with Arithmetic Mean
WW:	Wastewater

## LIST OF FIGURES

### Chapter 1 Introduction

<b>Figure 1.1.</b> Projected global water scarcity in 2025 (adapted from International Water Management Institute).....	19
<b>Figure 1.2.</b> Membrane separation processes, pore size, molecular weight cut-off (MWCO) and examples of sizes of solutes and particles [5].....	20
<b>Figure 1.3.</b> Universal MBR system configuration [2].....	22
<b>Figure 1.4.</b> Research trends in MBRs - number of publications in key subject areas (Scopus 2010) [2].....	23
<b>Figure 1.5.</b> Progressive pore blockage leading to rapid TMP increase (adapted from Le-Clech et al. 2006) [11].....	24
<b>Figure 1.6.</b> Fouling mechanisms for MBR operated with a constant flux (adapted from Zhang et al. 2006) [17].....	26
<b>Figure 1.7.</b> Research studies conducted on "MBR biofouling" between 1998-2014 (Scopus database on: September 2015).....	28
<b>Figure 1.8.</b> Biofouling in submerged MBRs: 1) Development of conditioning film; 2) Attachment of Pioneer microorganisms; 3) EPS production; 4) Development of microcolonies; 5) Detachment. (Adapted from Vanysacker et al. 2014) [42].	31

### Chapter 2 454-Pyrosequencing Reveals Biodiversity of Sessile and Planktonic Bacterial Community in Five Full-scale Membrane Bioreactors

<b>Figure 2.1.</b> Heatmap distribution of bacterial phyla and proteobacterial classes derived from the 15 pooled samples. The color intensity in each cell shows the percentage of class/phylum in the corresponding sample. The hierarchical clustering on the left was created by unweighted-pair group method using arithmetic means (UPGMA). The numbers from 1 to 5 correspond to the 5 full-scale MBRs.....	59
<b>Figure 2.2.</b> Relative abundance of bacteria retrieved from the five MBR plants classified at the class level. Bacterial classes that represent < 0.1% of the total bacterial community composition were classified as "others". The numbers 1 to 5 correspond to the five different MBR plants. ....	61
<b>Figure 2.3.</b> Relative abundance of the 79 annotated bacterial genera retrieved from the five MBRs. The numbers 1 to 5 correspond to the five different MBR plants. Only bacterial genera with relative abundance > 0.1% are presented in this figure. ....	62
<b>Figure 2.4.</b> Principal coordinate analysis (PCoA) of the 15 pooled samples based on unweighted UniFrac distance showing the relatedness of the bacterial community structure of samples collected from AS and biofilms (Early and Mature). The numbers from 1 to 5 refer to the five different MBRs. ....	63

- Figure 2.5.** Principal coordinate analysis (PCoA) of the 15 pooled samples based on Bray-Curtis distance showing the relatedness of the bacterial community structure of samples collected from AS and biofilms (Early and Mature). ..... 64
- Figure 2.6.** Boxplot showing unweighted UniFrac distance within and between Early, Mature and AS communities in all five full-scale MBRs. The red lines within the box represent the median while the plus signs are for outliers. .... 65
- Figure 2.7.** Nonmetric multidimensional scaling (NMDS) plot of the 15 pooled samples based on unweighted UniFrac distance showing the total (green triangles), dominant (red squares) and rare taxa (blue triangles). The numbers from 1 to 5 correspond to the five different MBRs..... 66
- Figure 2.8.** Relative abundance of the top 20 core genera among AS, early or mature samples from the five different MBRs. Core genera indicates genera shared across all samples in the same category (i.e. AS, Early or Mature). ..... 68
- Figure 2.9.** Venn diagram showing shared and unique OTUs within each biomass category, A: Early, B: Mature, C: AS. .... 70
- Figure 2.10.** Venn diagram showing the shared and unique OTUs in each MBR plant. A: MBR 1, B: MBR 2, C: MBR 3, D: MBR 4, E: MBR 5. .... 71
- Figure 2.11.** NMDS analysis, visualizing the results of a random sampling procedure, to estimate the probability that the biofilm communities (Early and Mature) represented random samples of their respective AS communities. A total of 1000 random subsamples of the AS communities were assembled for each MBR. Five examples; A: MBR 1, B: MBR 2, C: MBR 3, D: MBR 4, and E: MBR 5 are shown, to illustrate the distribution of the randomly produced AS communities in relation to the biofilm community. White, red, blue, and green circles represent the random subsamples of the AS community, the AS community, the early biofilm community, and the mature biofilm community. NMDS was calculated based on the Horn Index. Plotted NMDS values were selected from ten independent random starting positions. The minimum stress values for each MBR ranged from 0.44 to 0.46. .... 72

### **Chapter 3** Microbial Succession and Mature Biofilm Formation on Different Membrane Surfaces Operated Under Low Flux Conditions in a Lab-scale Membrane Bioreactor

- Figure 3.1.** Membrane cassette designed to hold simultaneously five different hollow-fiber membrane modules. .... 93
- Figure 3.2.** COD and ammonium concentrations in the synthetic wastewater influent and effluent, and nitrate (NO<sub>3</sub>) and nitrite (NO<sub>2</sub>) concentrations in the wastewater effluent. .... 97
- Figure 3.3.** Transmembrane pressure (TMP) profiles for the five membranes during filtration. .... 98
- Figure 3.4.** Classification at the family level of the early colonizers that attached to the hydrophobic and hydrophilic membranes after 1 day of operation, under 10 L/m<sup>2</sup>.h

flux and without permeate flux. The POX (Polyoxadiazole), PTA (Polytriazole), SPTA (Sulfonated polytriazole), SPSU (Sulfonated polysulfone) and COM (commercial membrane) membranes were operated under 10 L/m<sup>2</sup>.h flux (F) and without permeate flux (noF). MLSS correspond to the mixed liquor suspended solids sample, and D1 corresponds to the samples collected at the day 1. Others refer to bacterial family with relative abundance < 1%...... 101

**Figure 3.5.** Venn diagram representing the core shared OTUs between all biofilm samples extracted from the five different membranes operated with 10 L/m<sup>2</sup>.h at day 1 (left) and day 30 (right), respectively. The horizontal axis represents the OTUs number corresponding to each membrane type..... 102

**Figure 3.6.** Non-metric Multi-Dimensional Scaling (NMDS) based on unweighted Unifrac distance for the genomic DNA extracted from the five different membranes operated with a permeate flux of 10 L/m<sup>2</sup>.h and without permeate production (0 L/m<sup>2</sup>.h). The numbers from 1 to 30 correspond to the date of sample collection. Red circles correspond to hydrophobic membranes, blue triangles correspond to hydrophilic membranes, and green squares correspond to MLSS samples. The MLSS sample from day 10 was excluded from the data set because it did not amplify properly..... 103

**Figure 3.7.** Heat map distribution of bacterial phyla and proteobacterial classes derived from 40 biofilm and three mixed liquor samples. The color intensity in each cell reflects the abundance of class/phylum in the corresponding sample, light gray corresponds to low abundance and dark blue and black corresponds to higher abundance, respectively. Hierarchical clustering on the top was created using unweighted-pair group method using arithmetic means (UPGMA). POX (Polyoxadiazole), PTA (Polytriazole), SPTA (Sulfonated polytriazole), SPSU (Sulfonated polysulfone) and COM (commercial membrane) membranes were operated under 10 L/m<sup>2</sup>.h flux (F) and without permeate flux (noF). MLSS correspond to the mixed liquor suspended solids sample. Other bacteria refer to phyla with relative abundance < 1%. D1, D10, D20 and D30 refer to sampling days 1, 10, 20 and 30, respectively..... 105

**Figure 3.8.** The relative abundance and phylogenetic classification of the different genera and family detected in the MLSS. The letters F, G and C correspond to family, genus and class, respectively. The corresponding phyla and proteobacterial class is presented in bracket..... 106

**Figure 3.9.** The relative abundance and phylogenetic classification of the top 10 dominant shared OTUs between the five different membranes operated with 10 L/m<sup>2</sup>.h flux. The letters F, G and C correspond to family, genus and class, respectively. The corresponding phyla and proteobacterial class is presented in bracket..... 108

## Chapter 4 Temporal Changes in Extracellular Polymeric Substances on Hydrophobic and Hydrophilic Membrane Surfaces in a Submerged Membrane Bioreactor

- Figure 4.1.** Schematic of the lab-scale membrane bioreactor (MBR). ..... 130
- Figure 4.2.** Transmembrane pressure (TMP) profiles for the four membranes during filtration (with permeate production). ..... 136
- Figure 4.3.** Fourier transform infrared (FTIR) spectroscopic analysis of the foulant material extracted from the four different membrane surfaces during early stages of filtration, operated with 10 L/m<sup>2</sup>.h permeate production (1 day). ..... 138
- Figure 4.4.** FTIR spectroscopic analysis of the foulant material extracted from the four different membrane surfaces inserted in the membrane tank, without permeate flux after 1 day of MBR operation. .... 138
- Figure 4.5.** Concentrations of proteins and polysaccharides in the extracellular polymeric substances (EPS) samples extracted from the four membrane surfaces on day 1 and 30, and quantified using colorimetric methods (Lowry et al., 1951; Dubois et al., 1956) (A); and TOC concentrations (mg/cm<sup>2</sup>) accumulated on the four different membranes operated in continuous mode for 1 and 30 days (B). ..... 139
- Figure 4.6.** Evolution of the relative abundance of different organic fractions extracted from the surfaces of four different membranes operated with 10 L/m<sup>2</sup>.h permeate flux, and analyzed using LC-OCD over a 30 d MBR operation. The black arrows correspond to the chronological order of the membrane sample collection. .... 140
- Figure 4.7.** Temporal dynamics of organic foulants extracted from the surfaces of four different membranes operated with 10 L/m<sup>2</sup>.h permeate flux, and analyzed using liquid chromatography with organic carbon detection (LC-OCD). The black arrows correspond to the chronological order of the membrane sample collection. .... 141
- Figure 4.8.** Non-metric multidimensional scaling (NMDS) results of the EPS solutions extracted from four different membranes with (10 L/m<sup>2</sup>.h) and without permeate production (0 L/m<sup>2</sup>.h). The red circles correspond to the EPS samples that clustered together based on their percent similarity. .... 142
- Figure 4.9.** Biplot of the EPS solution, extracted from the different membrane surfaces. Blue circles and red circles correspond to samples from day 1 and day 30, respectively. The gray arrows point towards different EPS fractions, and PC1 (component 1) and PC2 (component 2) explain 77.4% and 19.5% of the variance between samples, respectively. .... 143
- Figure 4.10.** Evolution of 3D Fluorescence Excitation Emission (FEEM) diagrams for four different membranes operated with permeate production for 1, 10, 20 and 30 days. .... 144
- Figure 4.11.** Confocal laser scanning microscopy (CLSM) images showing the evolution of different EPS fractions accumulated on the four membrane surfaces. Total cells, proteins and  $\alpha$ - and  $\beta$ -Polysaccharides were stained with their corresponding dyes (Table 4.3). The scale bar length corresponds to 50  $\mu$ m. .... 146

**Chapter 5 Conclusion**

**Figure 5.1.** Inter-relation between membrane biofouling in MBRs and the studied parameters that could affect the rate of this phenomenon..... 164

## LIST OF TABLES

### Chapter 1 Introduction

<b>Table 1.1.</b> Summary of common biofouling control strategies in MBRs.....	34
--	----

### Chapter 2 454-Pyrosequencing Reveals Biodiversity of Sessile and Planktonic Bacterial Community in Five Full-scale Membrane Bioreactors

<b>Table 2.1.</b> Characteristics of the 5 full-scale MBR plants.....	52
---	----

<b>Table 2.2.</b> Number of observed OTUs and alpha diversity measures for the pooled samples.....	58
--	----

<b>Table 2.3.</b> Number and percentages of shared genera between samples belonging to the same category (i.e. AS, Early or Mature).....	67
--	----

<b>Table 2.4.</b> Percentages of core OTUs and their corresponding sequences between different samples. For each MBR, AS: Early, AS: Mature and Early: Mature correspond to the shared OTUs and sequences within two types of samples. ....	69
---	----

<b>Table 2.5.</b> Dominant microbial communities identified on biofouled membranes. ....	74
--	----

### Chapter 3 Microbial Succession and Mature Biofilm Formation on Different Membrane Surfaces Operated Under Low Flux Conditions in a Lab-scale Membrane Bioreactor

<b>Table 3.1.</b> Operating conditions of the lab-scale MBR. ....	89
---	----

<b>Table 3.2.</b> Synthetic wastewater influent characteristics (in g/L). ....	90
--	----

<b>Table 3.3.</b> Membrane properties and surface characteristics.....	91
--	----

<b>Table 3.4.</b> Sequence counts, observed OTUs per sample and alpha diversity measures .	99
--	----

<b>Table 3.5.</b> Shared OTUs and sequences between membranes operated under flux (10 L/m <sup>2</sup> .h) and no flux (0 L/m <sup>2</sup> .h).....	104
---	-----

### Chapter 4 Temporal Changes in Extracellular Polymeric Substances on Hydrophobic and Hydrophilic Membrane Surfaces in a Submerged Membrane Bioreactor

<b>Table 4.1.</b> Membrane properties and polymer composition.....	129
--	-----

<b>Table 4.2.</b> Synthetic wastewater influent characteristics (in g/L). ....	131
--	-----

<b>Table 4.3.</b> Characteristics of the dyes used to label different EPS components for the CLSM study. ....	134
---	-----

## CHAPTER 1 INTRODUCTION

### 1.1. Fresh water demand

The worldwide demand for freshwater is continuously increasing due to the steady growth of world's population. Currently, millions of people still lack access to improved water quality. In 2050, it is expected that 40% of the global population will be living in severely water stressed areas [1]. To mitigate the effects of direct exploitation of freshwater resources, membrane filtration systems offer promising solutions to deliver clean water in regions that suffer from severe water scarcity (Figure 1.1).

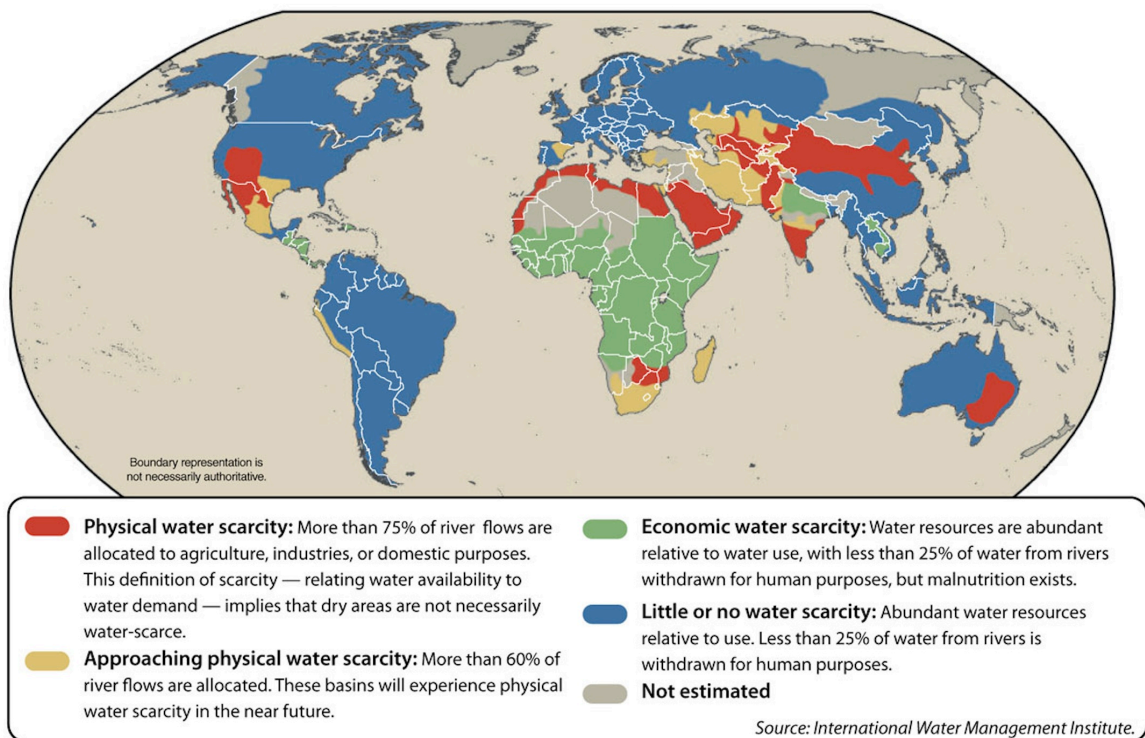


**Figure 1.1.** Projected global water scarcity in 2025 (adapted from International Water Management Institute).

Membrane separation processes have acquired worldwide recognition for drinking water production, wastewater treatment and water reuse. Pressure is applied upstream to push water through a porous membrane surface selective rejection capacity to specifically prevent physical or chemical constituents from passing through the membrane. Membrane based processes can produce high quality water from contaminated water resources, the purified water product as permeate and the concentrated waste being the retentate. According to their pore size and rejection capacity, membranes are classified into reverse osmosis (RO), nanofiltration (NF), ultrafiltration (UF) and microfiltration (MF) membranes [2] (Figure 1.2).

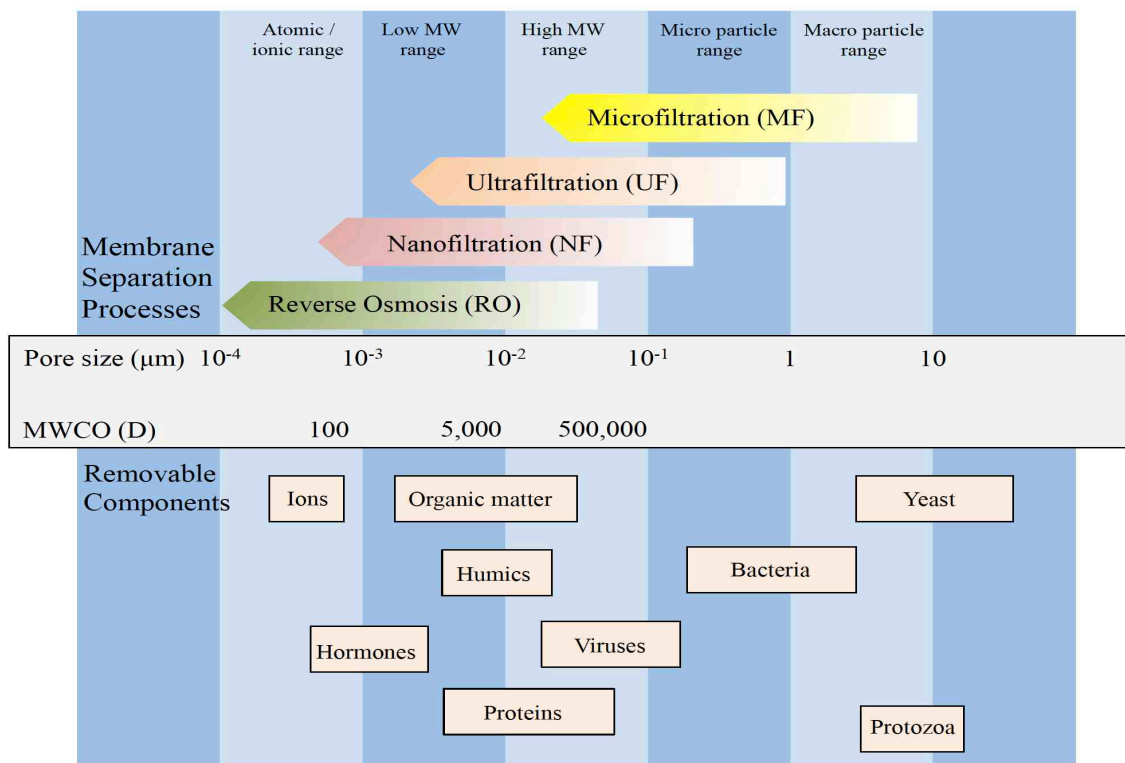


**Figure 1.2.** Membrane separation processes, pore size, molecular weight cut-off (MWCO) and examples of sizes of solutes and particles [5].

Megacities located near the coast produce clean water through seawater desalination to meet daily water demand. The application of desalination technologies becomes more difficult in remote areas, increasing the importance of wastewater reuse as a mean for freshwater preservation. Membrane bioreactors (MBRs) offer reasonable solutions for wastewater treatment and water reuse, fulfilling the increasing demand for daily clean water in these types of areas [3].

In addition, the wide range of fresh water utilization for domestic applications, chemical industries, and food production create deteriorated water quality, resulting in the production of various types of wastewater. According to the United Nations Educational, Scientific and Cultural Organization (UNESCO), appropriate treatment processes should be considered to improve the wastewater quality and to match international regulations before its final discharge in river systems [4]. These regulations are achievable with the MBR technology.

## **1.2. Membrane Bioreactors (MBRs)**

Membrane bioreactors (MBRs) combine suspended growth bioreactors with a membrane filtration process to retain the biomass, in order to replace the sedimentation tank in conventional activated sludge systems (CAS) [2]. MBRs are based on the conventional wastewater treatment model founded on the aeration process of the wastewater to provide oxygen that can remove carbon and nitrogen through oxidation processes (Figure 1.3). While aeration in MBRs accounts for the largest fraction of the overall energy demand ( $0.8 - 2 \text{ kWh/m}^3$ ) [6], it remains essential to provide oxygen for bacterial metabolisms and to reduce membrane fouling.

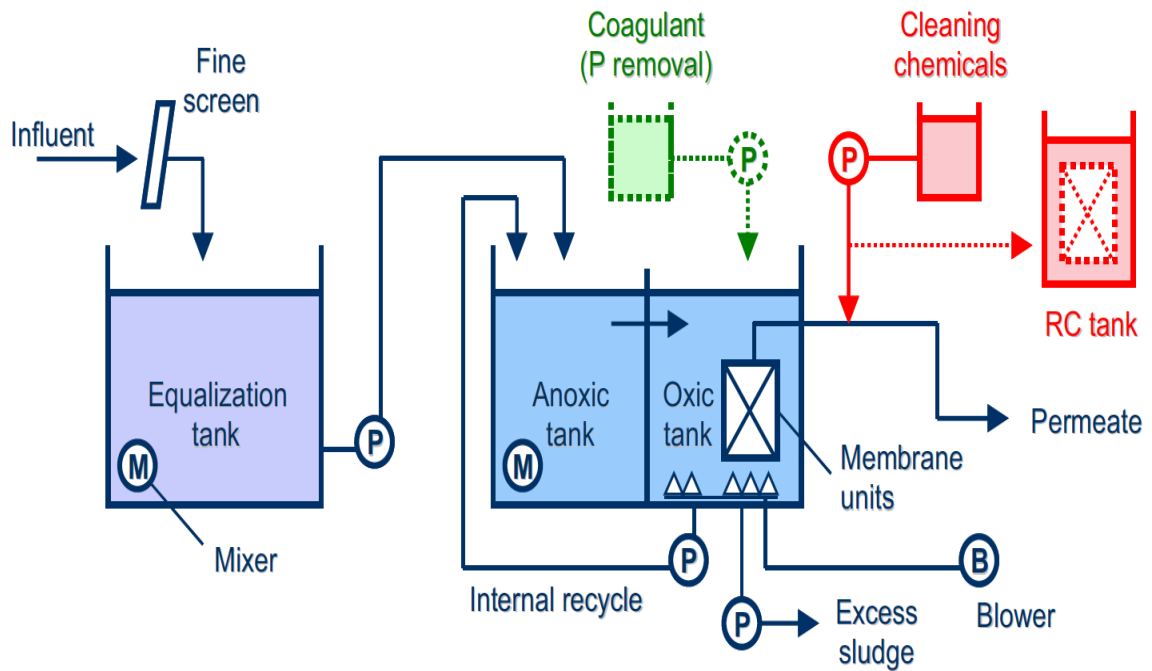


**Figure 1.3.** Universal MBR system configuration [2].

Membrane bioreactors offer several advantages over the conventional activated sludge processes, including: a) relatively smaller footprints by removing the sedimentation tank [7], b) improved and consistent quality of the treated water through the use of membrane modules [8], c) reduced sludge production only when operating the MBRs at very long sludge retention times (SRTs) [8], and e) operating the system at high mixed liquor suspended solids (MLSS) concentrations, which enhances the growth of specific nitrifying bacteria responsible for ammonia removal [9].

Since its creation, the MBR technology has proved increasing merit, confirmed through: i) continuous increases in MBR installations around the world, ii) enlargement in the treatment plant size and capacity, and iii) continuous rise in research studies conducted on different aspects of MBR technology [2] (Figure 1.4).

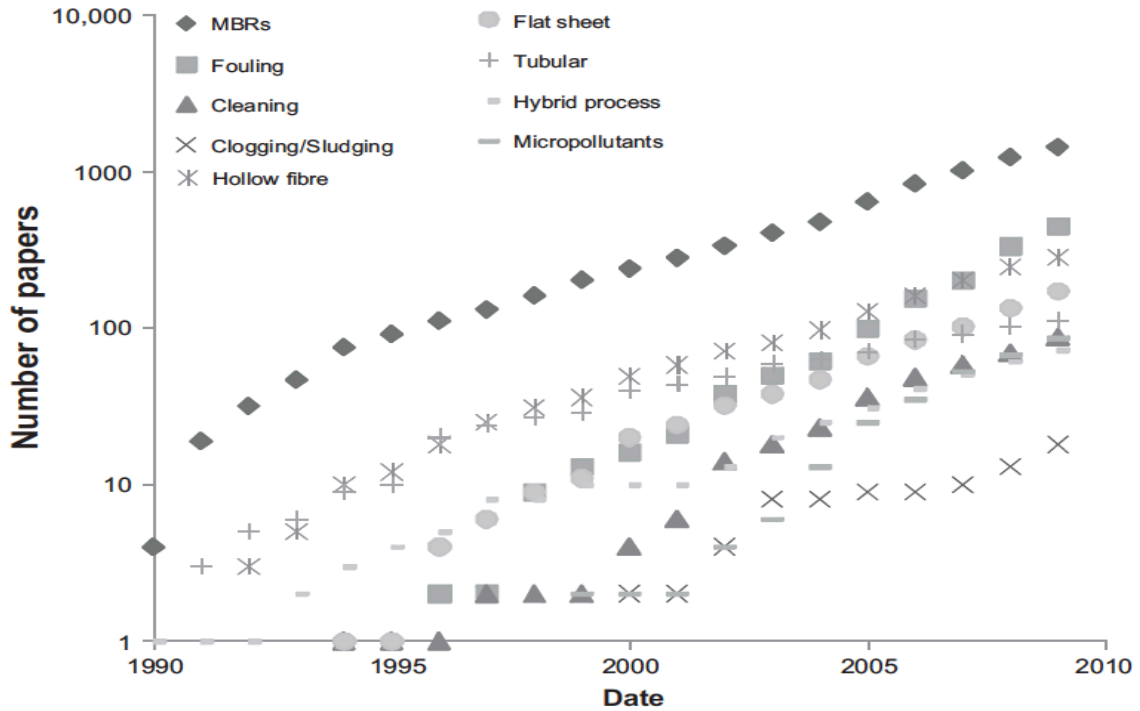


**Figure 1.4.** Research trends in MBRs - number of publications in key subject areas (Scopus 2010) [2].

MBRs gained confidence following new technological aspects that emerged, such as i) shaping the membrane tanks into biotreatment processes that can increase the plant's capacity and improve the product water quality, and ii) better understanding of the main factors that drive the MBR market, such as their competence to provide better governmental requirements for water quality and a relative decrease in membranes operation costs [2].

### 1.3. Fouling in MBRs

Despite the numerous advantages of MBRs, membrane fouling remains one of the major drawbacks of this technology and continues to be the most challenging problem. Membrane fouling in MBRs is a direct result of physical, chemical and biological

interactions between membrane surfaces and microbial communities along with their metabolic products found in the mixed liquor suspended solids (MLSS). While small foulants (macromolecules and colloids) can adsorb into membrane pore walls and lead to membrane pore blocking, large foulants (sludge flocs and particles) can build up directly onto membrane surfaces and establish a thick cake layer [10] (Figure 1.5).

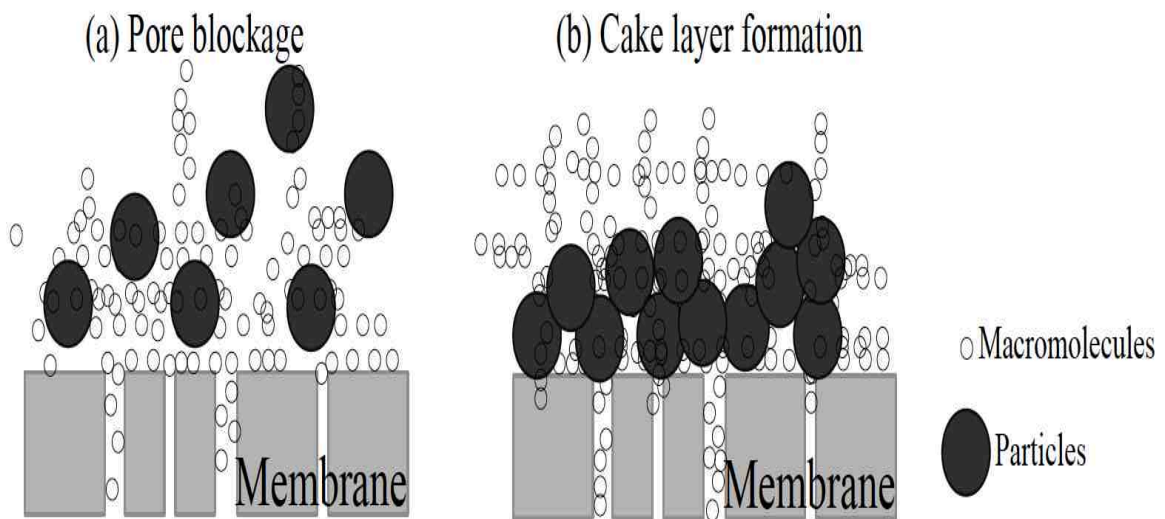


**Figure 1.5.** Progressive pore blockage leading to rapid TMP increase (adapted from Le-Clech et al. 2006) [11].

Conventionally, MBRs are operated either at constant transmembrane pressure (TMP) mode, or at constant flux mode. When constant TMP mode is applied [11], a rapid flux decline occurs at the initial stages of filtration, followed by a decrease in the volume of the produced permeate [12]. A hypothetical three-phase-process-mechanism was suggested to describe the formation of a cake layer on membrane surfaces in MBRs during constant TMP mode operation [13]. Firstly, an initial phase comprised of irreversible deposition of soluble microbial products (SMP) onto membrane surfaces, followed by a second phase during which sludge particles accumulate on top of the initial

SMP layer. The final phase occurs when the flux reaches steady state and stabilizes, which increases the filtration resistance [13].

Typically, MBRs are operated using constant flux mode, where the convection of foulant towards the membrane surface is maintained at a constant rate [2]. Consequently, a sharp increase in TMP is observed [14], leading to higher energy consumption [15], and an increase in the frequency of physical and chemical cleaning in the long term [11]. The fouling mechanism of MBRs operated at constant flux is also characterized by three major stages. During stage one, an initial conditioning-fouling layer composed mainly of extracellular polymeric substances (EPS) covers the membrane surface, following physical and chemical interactions between the membrane surface and the mixed liquor components. The initial fouling layer contributes to an increase in the membrane's irreversible resistance [16] and facilitates the attachment of biomass on the membrane. The second stage is typically characterized by a slow and steady fouling behavior [11], during which biomass particles and colloids attach more easily on the pre-established fouling layer that leads to a progressive TMP increase [11]. The final stage is typically characterized with a sudden TMP jump. Part of the membrane pores foul more than others leading to a significant decrease in permeate flux within the clogged pores [11]. Detailed analysis of three stages fouling mechanism is presented in Figure 1.6.

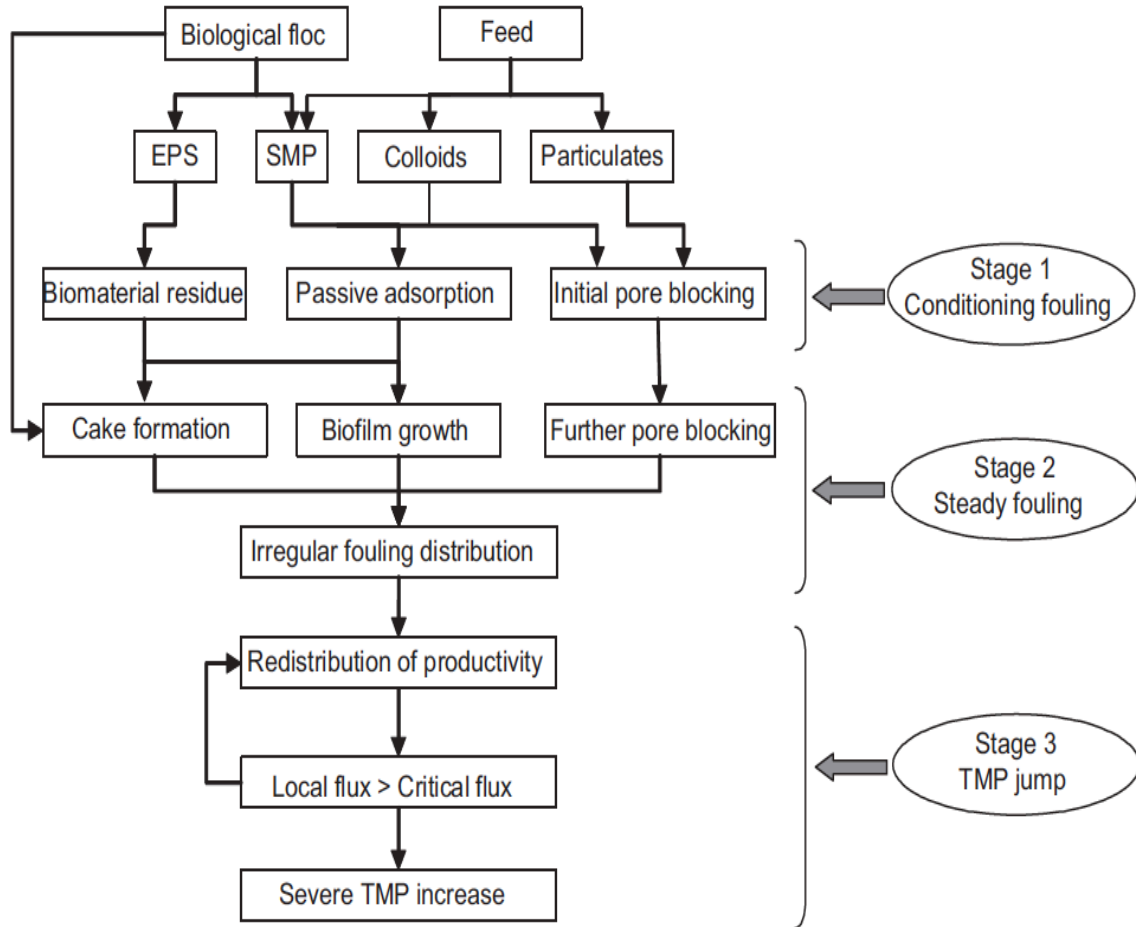


**Figure 1.6.** Fouling mechanisms for MBR operated with a constant flux (adapted from Zhang et al. 2006) [17].

There are two different fouling mechanisms in MBRs; reversible fouling that is removable using chemical or physical cleaning approaches, and irreversible fouling that cannot be removed at all [10] and leads to an unavoidable replacement of the membrane modules [18]. In addition, fouling components in MBRs can result into three different types of fouling; a) organic, b) inorganic, and c) biological fouling. Organic fouling leads to the adsorption and accumulation of dissolved organic substances, especially polysaccharides, proteins, and humics on membrane surfaces [19]. Inorganic fouling causes the deposition and buildup of inorganic salts, especially  $\text{CaSO}_4$ ,  $\text{CaCO}_3$ ,  $\text{SiO}_2$  and

BaSO<sub>4</sub> [20]. Either organic or inorganic fouling can occur on the membrane surface or inside the membrane pores. The accumulation of dissolved organic and inorganic matter inside the membrane pores leads to internal pore blocking [21].

#### **1.4. Biofouling in MBRs**

Membrane biofouling, described previously as the “Achilles’ heel of membrane processes” [22], is a direct result of bacterial attachment on membrane surfaces, along with their rapid growth and fast metabolism that lead to biofilm formation [22]. Beside the dramatic increase in TMP combined with the severe decrease in permeate flux, biofouling might trigger enzymatic biodegradation of membrane surfaces, or even membrane polymer hydrolysis through the production of high localized pH values [23]. In addition, among all three types of fouling in MBRs, biofouling remains the most complicated to understand and very difficult to address. Microbial communities can attach on membrane surfaces, and consequently grow and multiply exponentially, before detaching to colonize new surfaces. Despite the relatively high number of research studies conducted on biofouling in MBRs during the past decade (Figure 1.7), this phenomenon remains very challenging. Due to the complexity of microbial communities and their extracellular polymeric substances (EPS) in the mixed liquor, researchers and engineers continue to deal with membrane biofouling as a “Black Box” [24].

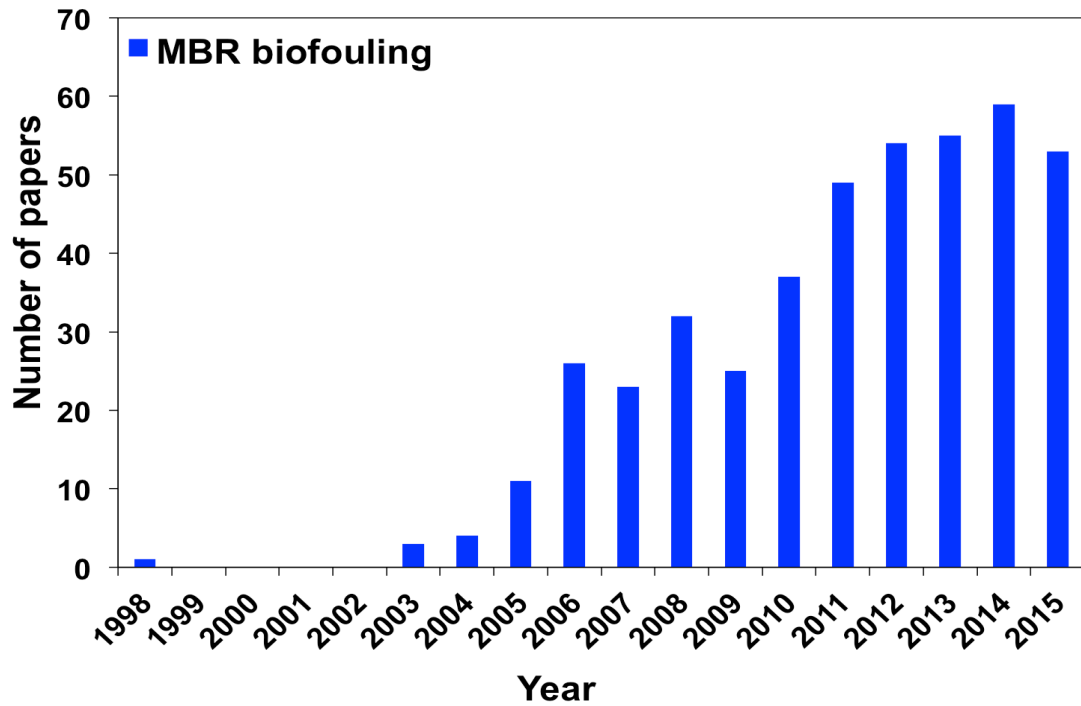


**Figure 1.7.** Research studies conducted on "MBR biofouling" between 1998-2014 (Scopus database on: September 2015).

#### 1.4.1. Factors that affect biofouling in MBRs

Several operating parameters affect directly the rate of biofouling in MBRs, especially i) the type of treated wastewater (i.e. domestic or industrial), ii) the imposed MBR operating conditions (i.e. sludge retention time (SRT), hydraulic retention time (HRT)), iii) the composition and structure of the microbial communities in the mixed liquor, and iv) the membrane module design and specifications (i.e. configuration, pore size, surface hydrophobicity or hydrophilicity) [11, 25, 26].

Considering the effect of SRT on biofouling rate in MBRs, several researchers have reported contradictory results. While Ahmed et al. reported a decrease in the fouling rate when the SRT increased [27], Han et al. indicated that the fouling rate increased with

longer SRT [28]. In addition, Sweity et al. confirmed the positive influence of SRT on the ratio of proteins to polysaccharides in the EPS matrix [29], but Rosenberger and Kraume reported a decrease in the SMP concentrations with sludge age [30].

The type of treated wastewater and the composition of the microbial communities affect directly the fouling rate in MBRs. For instance, feeding the biomass with real or synthetic wastewater could affect significantly the protein fractions in the EPS, and consequently increase the MBR fouling rate [31, 32]. On the other hand, SMP and colloidal materials contribute to membrane pore blockage, and suspended solids increase the cake layer resistance [33]. The concentration of the MLSS affects the biofouling rate in MBRs, however inconsistent conclusions can be highlighted among different research studies. While Chang et al. reported an increase in TMP along with a decrease in the permeate flux when the MLSS concentration increased [34], Brookes et al. reported a TMP decrease when the MLSS concentration decreased [35].

Membrane surface characteristics (i.e. pore size and density, surface roughness, surface hydrophobicity or hydrophilicity), and the membrane module configuration (i.e. hollow-fiber, flat-sheet, tubular) affect the biofouling tendencies in MBRs [2]. Membranes with narrow pores ( $10^{-3}$   $\mu\text{m}$ ) reject a broad variety of materials and produce a cake layer that has higher resistance than membranes with larger pores ( $10^{-1}$   $\mu\text{m}$ ) [11], and membrane surface roughness can cause different biofouling behavior. Considering the membranes' configuration, the most widely applied is the submerged model, while sidestream configurations are installed for specific applications [2]. The packing density of hollow fiber (HF) modules could increase the biofouling rate if the number of hollow-fibers does not allow air bubbles to reach the middle fibers [36]. Finally, biofouling rate

is expected to be more severe for hydrophobic membranes compared to hydrophilic ones, due to the nature of interactions that occur between membrane surfaces and MLSS components (i.e. solutes, microbial communities, EPS and SMP products). Recently, hydrophobic membranes were demonstrated to have stronger interactions with the foulants due to enhanced hydrophobic adhesion, which retained more effluent organic matter (EOM) [37].

#### **1.4.2. Sequential steps that develop membrane biofouling**

Biofouling in MBRs is a mechanism that involves several sequential steps. Initially, series of physical and chemical interactions between MLSS components and membrane surfaces initiate this process. A conditioning layer that covers the membrane surface allows the adsorption of organic and inorganic molecules. The conditioning layer can form within only few minutes, and it is composed mainly of proteins [38], polysaccharides [39], and humic substances [40]. Once developed, the conditioned membrane renders bacterial attachment on membrane surfaces more favorable [41], and the membrane surface characteristics become secondary [11]. In other words, the membrane surface does not select anymore for specific fouling components. Then, bacterial cells initiate hydrophilic, hydrophobic, electrostatic, and lectin-carbohydrate interactions with the conditioning layer. This allows the recruitment and attachment of early microorganisms [42, 43, 44]. Consequently, microbial metabolism and cells proliferation begins. Microbial communities start producing their own EPS matrix, and develop into micro-colonies to resist external threatening environmental factors [45, 46]. Finally, biofilms could detach from membrane surfaces and colonize different spots,

possibly due to air scouring rate and shear stress. The four steps are summarized in Figure 1.8.

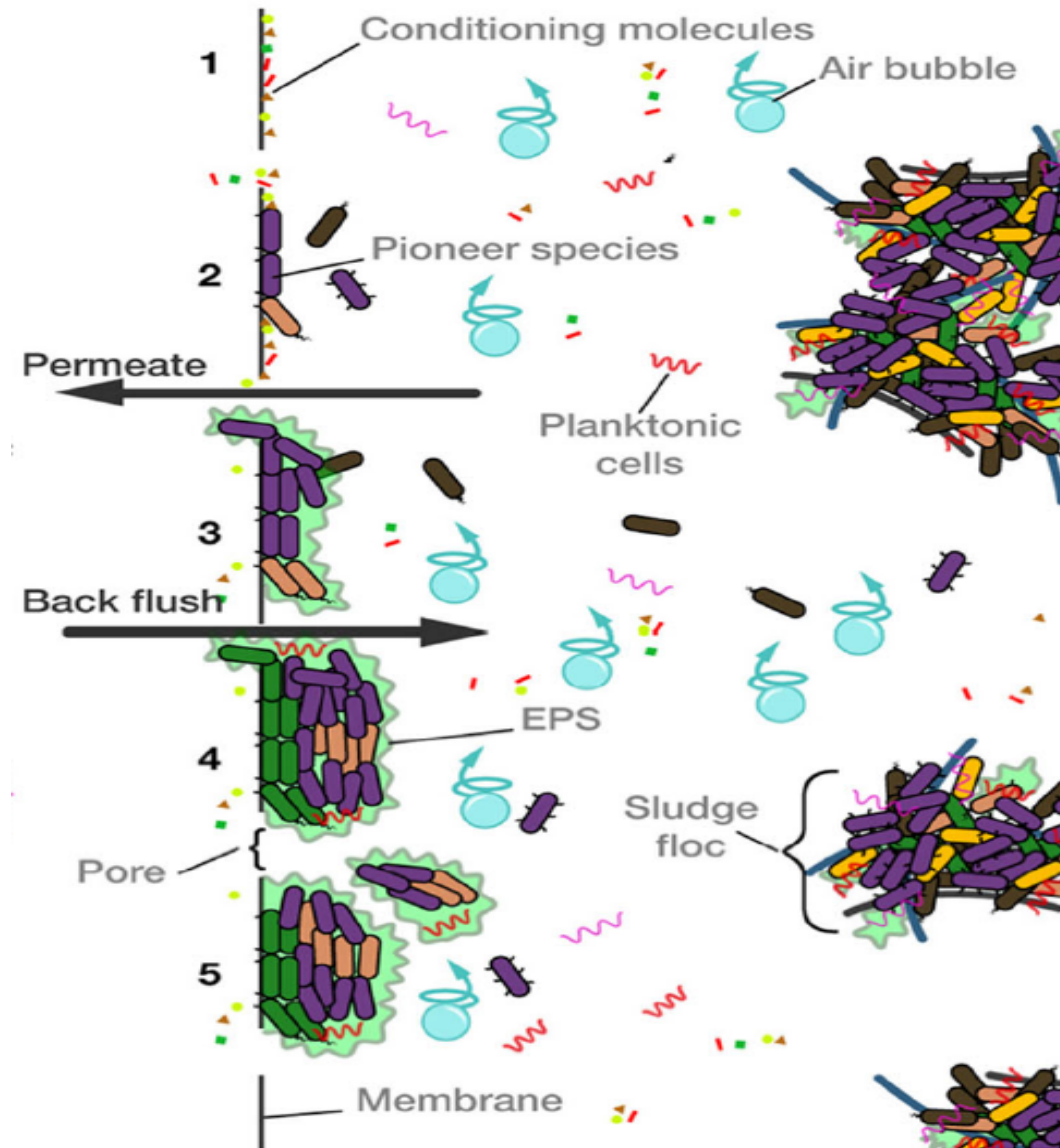


**Figure 1.8.** Biofouling in submerged MBRs: 1) Development of conditioning film; 2) Attachment of Pioneer microorganisms; 3) EPS production; 4) Development of microcolonies; 5) Detachment. (Adapted from Vanysacker et al. 2014) [42].

## **1.5. Biofouling control strategies**

Several biofouling control strategies have been proposed in the literature besides physical and chemical cleaning, including but not limited to i) membrane surface modification to enhance its antifouling potential propensity, ii) operating the MBR system sub-critical flux values and iii) chemical dosages in the mixed liquor to increase the flocs sizes.

### **1.5.1. Membrane surface modification**

Membrane surface modification as an enhanced biofouling control strategy has gained merit during the past decades in membrane filtration systems. For instance, polypropylene (PP) membranes embedded within acrylic acid groups demonstrated enhanced filtration behavior when tested in MBRs [47], and membranes coated with fullerenes C<sub>60</sub> diminished bacterial attachment and reduced membrane biofouling [48]. Likewise, silver nanoparticles (nAg) grafter on membrane surfaces exhibited reduced bacterial attachment on membrane surfaces [49, 50]. Increasing the surface hydrophilicity can potentially reduce the attachment of foulants through strong adsorption of a water layer on the membrane surface and creates a buffer zone. This could reduce the adhesion of microorganisms and fouling components [51]. The significance of membrane surface modification to reduce fouling might be decisive during early stages of filtration, however it is expected to lose its effectiveness following extended filtration periods.

### **1.5.2. Critical flux concept**

Operating the MBR below critical flux (sub-critical flux) values can reduce or delay membrane fouling. The sub-critical flux is the value below which the convection and diffusion of foulants towards the membrane surface are minor, and thus contribute to a

reduced fouling rate of an acceptable level [28]. While this concept remains theoretically possible, several researchers have tested various membrane filtration systems at the sub-critical flux values, and reported that membrane fouling occurred even at low flux conditions [31,52]. When operation the system at sub-critical conditions, macromolecules adsorb slowly on the membrane surface followed by a faster fouling step, which contributes to pore clogging due to accumulation of macromolecules on the membrane surface [11].

### **1.5.3. Chemical dosage to increase flocs size**

The addition of coagulants and powdered activated carbon (PAC) to wastewater has been suggested to reduce membrane fouling in MBRs. Coagulants such as ferric chloride ( $\text{FeCl}_3$ ) and aluminum sulfate ( $\text{Al}_2(\text{SO}_4)_3$ ) can adsorb dissolved organic matter (DOM) and SMPs from the mixed liquor. This can reduce their availability in the mixed liquor and prevent their accumulation on membrane surfaces [53]. Ferric chloride can help with generating large flocs in the MLSS and reduce their impact on MBR biofouling [11]. Aluminum sulfate can aggregate small particles and SMPs to form larger flocs and to reduce membrane biofouling [53]. Similarly, several researchers reported that powdered activated carbon (PAC) enhances the development of robust sludge flocs when PAC is dosed directly to the MLSS tank. This could reduce the release of foulants and decrease the membrane biofouling in MBR [54, 55]. In a different study, sludge enriched with PAC resisted high salinity and prohibited the release of foulants from the sludge flocs and exhibited lower fouling tendency [56]. The common biofouling control strategies in MBRs are summarized in Table 1.1.

**Table 1.1.** Summary of common biofouling control strategies in MBRs

Control strategy	Key Findings	References
<b>Membrane surface modification</b>	Membranes with higher hydrophilic surface properties reduced partial membrane biofouling	[47]
	Ceramic membranes coated with fullerene C <sub>60</sub> prevented bacterial adhesion	[48]
	nAg embedded on the membrane reduced bacterial attachment	[49, 50]
<b>Physical control</b>	High aeration ratio in the membrane tank increased membrane flux	[57]
	Periodical backwashing doubled the membrane flux	[58]
<b>Chemical dosage to increase flocs size</b>	PAC added to the MLSS tank reduced soluble EPS concentration and decrease membrane fouling rate	[55, 54]
	Coagulation/flocculation increased flocs size and reduced MBR fouling rate	[53, 59]
<b>Biological control</b>	Quorum Quenching bacteria encapsulated vessels delayed reaching a high TMP	[60]
	Enzymatic disruption allowed 45 hours of operation at 15 L/m <sup>2</sup> .h before reaching maximum TMP	[61]

Despite intensive effort focused on determining sustainable approaches to prevent and control biofouling in MBRs, a comprehensive and effective control strategy is still yet to be discovered [11].

## 1.6. Knowledge Gaps

Despite continuous expansion in research studies that focus on biofouling in MBRs (Figure 1.7), essential information is still missing that could help building a complete picture to better understand the biofouling phenomenon.

- The majority of the studies that characterized the biofouling microbial communities were conducted in lab-scale MBR systems, with few studies that focused on pilot-scale MBRs [21, 62], and none on real-scale MBRs. In addition, the microbial ecology of microorganisms responsible for biofouling has not been thoroughly tackled. While few studies characterized the community structure of early colonizers [63, 43], the majority of microbial studies focused on mature biofilms in MBRs [21, 12, 64].
- Several researchers have modified membrane surfaces by adding silver nanoparticles [50] or increasing the membrane's hydrophilicity [47] to mitigate biofouling. However, the fouling propensities of these membranes were evaluated with model microorganisms or commercial foulants using flow-cell systems, which does not reflect the real biofouling mechanism in MBRs.
- Few studies have compared the biofouling behavior of different polymeric membranes. Recently, one study looked at species diversity of biofouling communities on three different membranes during 24 h of filtration [42], and another study compared the passive bacterial adsorption (without filtration) on three different polymeric membranes during a 15 d test [65]. However, a clear conclusion on the capability of membrane surfaces to select specific biofouling communities according to the membrane polymeric material could not be identified.

- Studies that monitor the temporal dynamics of biofouling microbial communities and their corresponding EPS products in MBRs using different polymeric membranes are still lacking. To the best of our knowledge, only one study monitored during 15 d the changes in biofouling communities and their EPS products using only one membrane type [64].
- Recently, numerous studies correlated the structure and composition of membrane biofouling communities with different MBR operating conditions. For instance, lab-scale MBRs operated under three different SRTs of 3, 5 and 10 d revealed an increase in microbial diversity when the SRT increased [66]. Also, the imposed permeate flux affected the composition of microbial communities. Different biofouling microbial communities developed on membrane surfaces at high flux of 30 L/m<sup>2</sup>.h compared with flux of 15 L/m<sup>2</sup>.h [67]. Furthermore, variations in the aeration intensities resulted in differences in the relative abundances of microbial communities in two lab-scale MBRs [71]. Nevertheless, the effect of different membrane surface chemistry on the community structure of membrane biofouling has not been addressed.
- Several researchers have used conventional molecular techniques to characterize the structure and composition of microbial communities responsible for membrane biofouling; including terminal length fragment length polymorphism (T-RFLP) [63], denaturing gradient gel electrophoresis (DGGE) [66], 16S rRNA clone libraries, and fluorescence in situ hybridization (FISH) [21]. However, these conventional molecular techniques target only the dominant species and fail to characterize the rare species that might contribute greatly to MBR biofouling. Next-generation high-

throughput sequencing allows deep characterization of the rare and the dominant microbial communities by generating hundreds of thousands of short sequencing reads. Pyrosequencing has been intensively applied to characterize the community structure of the mixed liquor from different full-scale wastewater treatment plants [68, 69, 70] and lab-scale MBRs operated under different conditions [14, 65, 71].

### **1.7. Objectives**

In order to better understand the membrane biofouling phenomenon in MBRs, it is important to deeply investigate the microbial ecology of bacterial communities responsible for membrane biofouling and to intensively characterize their corresponding EPS products. Therefore, the application of state-of-the-art 454-pyrosequencing, different chemical analytical tools and microscopic techniques, could help achieving a much-improved picture of membrane biofouling in MBRs [72].

Therefore, the objectives of this PhD dissertation can be summarized in the following key points:

1. Characterizing the community structure of early colonizers (5 hr) and mature biofilms that developed on membrane surfaces in several full-scale MBR plants equipped with the same membrane type while treating different domestic wastewaters.
2. Investigating the effect of different hydrophobic and hydrophilic hollow-fiber membranes in selecting specific biofouling microbial communities during early stages of membrane filtration (1d) and how these communities evolve to develop a mature biofilms (30 d) in a lab-scale MBR fed with the same synthetic wastewater.

3. Studying the microbial community structure and composition that attached to different membrane surfaces under passive adsorption (without flux) and active filtration modes (10 L/m<sup>2</sup>.h flux).
4. Assessing the impact of membrane surface chemistry (hydrophilicity or hydrophobicity) on initial membrane biofouling and EPS composition, and consequently examining their temporal dynamics in long-term experiments under low flux (10 L/m<sup>2</sup>.h flux) and passive adsorption modes (without flux) in a lab-scale MBR.

### **1.8. Thesis roadmap**

This thesis contains 5 chapters, some of which are submitted as scientific research articles to peer reviewed journals and published as conference proceedings in international conferences.

Chapter 2 presents the outcome of collaborative work between King Abdullah University of Science and Technology and Missouri University of Science and Technology. High-throughput 16S rRNA gene pyrosequencing combined with multivariate statistical analysis was applied to characterize the biofilm (early and mature) and activated sludge bacterial communities in five full-scale MBRs treatment plants. These plants were located in the region of Seattle (Washington, USA) and equipped with the same type of membrane while treating domestic wastewater. This work is submitted to Applied Microbiology and Biotechnology, authored by Gerald K. Matar, Samik Bagchi, Kai Zhang, Daniel B. Oerther and Pascal E. Saikaly and entitled “454-Pyrosequencing Reveals Biodiversity of Sessile and Planktonic Bacterial Community in Five Full-scale Membrane Bioreactors”. I performed the DNA extraction and optimized

the PCR protocols. I contributed to the discussion of the results during the statistical analysis, I wrote the first draft and P. E. Saikaly corrected the manuscript.

Chapter 3 is the result of collaboration between Professor Pascal Saikaly and Professor Suzana Nunes and focuses on characterizing the structure and composition of early colonizers that attach on different membrane surfaces and to assess the temporal changes in the biofouling microbial communities on the different membranes. 16S rRNA gene pyrosequencing and multivariate statistical analysis were applied to characterize the succession of biofouling microbial communities following 1, 10, 20 and 30 d of filtration in a lab-scale MBR operated with five different hollow-fiber membranes. This work is authored by Gerald Matar, Samik Bagchi, Husnul Maab, Wen-Tso Liu, Suzana Nunes, Johannes Vrouwenvelder, Pascal Saikaly and it is entitled “Microbial Succession and Mature Biofilm Formation on Different Membrane Surfaces Operated Under Low Flux Conditions in a Lab-scale Membrane Bioreactor” and it is currently under preparation for submission to a peer-reviewed journal. Prof. Suzana Nunes provided the membranes, which I tested during 30 days. I designed and constructed the lab-scale MBR and the membrane cassette. I designed the experiment and conducted all experimental work, including sample collection and DNA extraction, and I contributed to the statistical analysis. I prepared the first draft and P. E. Saikaly corrected it.

Chapter 4 focuses on studying the temporal changes in EPS products that accumulate on four hydrophobic and hydrophilic membranes in a lab-scale MBR during 30 d of filtration to assess their impact on MBR fouling at the early (1 d) and longer (30 d) stages of filtration. Several analytical tools, including conventional colorimetric tests, LC-OCD, FEEM, FTIR and CLSM were used to intensively characterize the EPS products that

develop on membrane surfaces. This work is submitted to Water Research, authored by Gerald Matar, Graciela Gonzalez-Gil, Husnul Maab, Suzana Nunes, Pierre Le-Clech, Johannes Vrouwenvelder, Pascal Saikaly and it is entitled “Temporal Changes in Extracellular Polymeric Substances on Hydrophobic and Hydrophilic Membrane Surfaces in a Submerged Membrane Bioreactor”. Prof. Suzana provided the hollow-fiber membranes. I designed the experiment and conducted all the experimental work using the same lab-scale MBR from chapter 3, and I performed all the chemical analysis and microscopic imaging to deeply characterize the EPS products. I prepared the manuscript and all co-authors corrected and provided strong comments.

Chapter 5 summarizes the conclusions of the three studies, and provides potential implications and key aspects to consider in future studies that focus on MBR biofouling, to reduce its occurrence in full-scale MBRs and to minimize its drawbacks on the overall systems’ performance.

The thesis is structured as a paper dissertation, and it consists of a number of scientific articles, except for the introduction chapter. Therefore, some repetitions in individual chapters were necessary, and small adaptations were made to improve the content of the chapters.

## References

1. WHO/UNICEF. Joint monitoring programme for water supply and sanitation progress on sanitation and drinking-water: 20130, Update; New York, 2013.
2. Judd, S. J. **The MBR book: principles and applications of membrane bioreactors for water and wastewater treatment.** Elsevier, 2010.
3. Henze, M. E. **Biological wastewater treatment: principles, modelling and design:** IWA Publishing, 2008.
4. Ringeisen, B. R. et al. **WWAP The United Nations World Water Development Report 2014: Water and Energy; Paris UNESCO.** 2014.
5. Peter-Varbanets, M., Zurbrugg, C., Swartz, C., Pronk, W. Decentralized systems for potable water and the potential of membrane technology. **Water Res.**, v. 43, n. 2, p. 245-265, 2009.
6. Martin, I., Pidou, M., Soares, A., Judd, S.J., Jefferson, B.. Modelling the energy demands of aerobic and anaerobic membrane bioreactors for wastewater treatment. **Environment. Technol.**, v. 32, n. 9, p. 921-932, 2011.
7. Santos, A., Ma, W., Judd, S.J. Membrane bioreactors: two decades of research and implementation. **Desalination**, v. 273, n. 1, p. 148-154, 2011.
8. Lesjean, B., Tazi-Pain, A., Thauere, D., Moeslang, H., Buisson, H. Ten persistent myths and the realities of membrane bioreactor technology for municipal applications. **Water Sci. Technol.**, v. 63, n. 1, p. 32-39, 2011.
9. Judd, S. J. The status of membrane bioreactor technology. **Trends in Biotechnology**, v. 26, n. 2, p. 109-116, 2008.
10. Meng, F., Chae, S.R, Drews, A., Kraume, M., Shin, H.S., Yang, F. Recent advances in membrane bioreactors (MBRs): membrane fouling and membrane material. **Water Res.**, v. 43, n. 6, p. 1489-1512, 2009.
11. Le-Clech, P., Chen, V., Fane, T.A.G. Fouling in membrane bioreactors used in wastewater treatment. **J. Membr. Sci.**, v. 284, n. 1, p. 17-53, 2006.
12. Gao, D.W., Wen, Z.D., Li, B., Liang, H. Microbial community structure characteristics associated membrane fouling in A/O-MBR system. **Biores. Technol.**, v. 154, p. 87-93, 2014.
13. Bae, T. H and . Tak. T. M. Interpretation of fouling characteristics of ultrafiltration membranes during the filtration of membrane bioreactor mixed liquor. **J. Membr. Sci.**, v. 264, p. 151-160, 2005.
14. Lim, S.Y., Kim, S., Yeon, K.M., Sang, B.I., Chun, J., Lee. C.H. Correlation between microbial community structure and biofouling in a laboratory scale membrane bioreactor with synthetic wastewater. **Desalination**, v. 287, n. 209-215, 2012.
15. Liao, B.Q., Bagley, D.M., Kraemer, H.E., Leppard, G.G., Liss, S.N. A review of biofouling and its control in membrane separation bioreactors. **Water Environment Res.**, p. 425-436, 2004.
16. Ognier, S., Wisniewski, C., Grasmick, A. Influence of macromolecules adsorption

- during filtration of a membrane bioreactor mixed liquor suspension. **J. Membr. Sci.**, v. 209, p. 27-37, 2002.
17. Zhang, J., Chua, H.C., Zhou, J., Fane, A.G. Factors affecting the membrane performance in submerged MBR. **J. Membr. Sci.**, v. 284, p. 54-66, 2006.
  18. Mahendran, B., Lin, H., Liao, B., Liss, S.N. Surface properties of biofouled membranes from a submerged anaerobic membrane bioreactor after cleaning. **J. Environment. Eng.**, v. 137, n. 6, p. 504-513, 2010.
  19. Subhi, N., Leslie, G., Chen, V., Le-Clech, P. Organic fouling of ultrafiltration membrane: detailed characterization by liquid chromatography with organic carbon detector (LC--OCD). **Sep. Sci. Technol.**, v. 48, n. 2, p. 199-207, 2012.
  20. Shirazi, S., Lin, C.J., Chen, D. Inorganic fouling of pressure-driven membrane processes-a critical review. **Desalination**, v. 250, n. 1, p. 236-248, 2010.
  21. Miura, Y., Watanabe, Y., Okabe, S. Membrane biofouling in pilot-scale membrane bioreactors (MBRs) treating municipal wastewater: impact of biofilm formation. **Environ. Sci. Technol.**, v. 41, n. 2, p. 632-638, 2007.
  22. Flemming, H.C., Schaule, G., Griebe, T., Schmitt, J., Tamachkiarowa, A. Biofouling—the Achilles heel of membrane processes. **Desalination**, v. 113, n. 2, p. 215-225, 1997.
  23. Ghayeni, S.B.S., Beatson, P.J, Schneider, R.P, Fane, A.G. Water reclamation from municipal wastewater using combined microfiltration-reverse osmosis (ME-RO): Preliminary performance data and microbiological aspects of system operation. **Desalination**, v. 116, p. 65-80, 1998.
  24. Malaeb, L., Le-Clech, P., Vrouwenvelder, J.S., Ayoub, G.M., Saikaly, P.E. Do biological-based strategies hold promise to biofouling control in MBRs? **Water Res.**, v. 47, n. 15, p. 5447-5463, 2013.
  25. Meng, F., Shi, B., Yang, F., Zhang, H. Effect of hydraulic retention time on membrane fouling and biomass characteristics in submerged membrane bioreactors. **Bioprocess. Biosys. Eng.**, v. 30, n. 5, p. 359-367, 2007.
  26. Yamato, N., Kimura, K., Miyoshi, T., Watanabe, Y. Difference in membrane fouling in membrane bioreactors (MBRs) caused by membrane polymer materials. **J. Membr. Sci.**, v. 280, n. 1, p. 911-919, 2006.
  27. Ahmed, Z., Cho, J., Lim, B.R., Song, K.G., Ahn, K.H. Effects of sludge retention time on membrane fouling and microbial community structure in a membrane bioreactor. **J. Membr. Sci.**, v. 287, n. 2, p. 211-218, 2007.
  28. Han, S.S., Bae, T.H., Jang, G.G., Tak, T.M. Influence of sludge retention time on membrane fouling and bioactivities in membrane bioreactor system. **Process Biochem.**, v. 40, n. 7, p. 2393-2400, 2005.
  29. Sweity, A., Ying, W., Ali-Shtayeh, M.S., Yang, F., Bick, A., Oron, G., Herzberg, M. Relation between EPS adherence, viscoelastic properties, and MBR operation: Biofouling study with QCM-D. **Water Res.**, v. 45, p. 6430-6440, 2011.
  30. Rosenberger, S. and Kraume, M. Filterability of activated sludge in membrane bioreactors. **Desalination**, v. 146, p. 373-379, 2002.
  31. Le-Clech, P., Jefferson, B., Chang, I.S., Judd, S.J. Critical flux determination by the

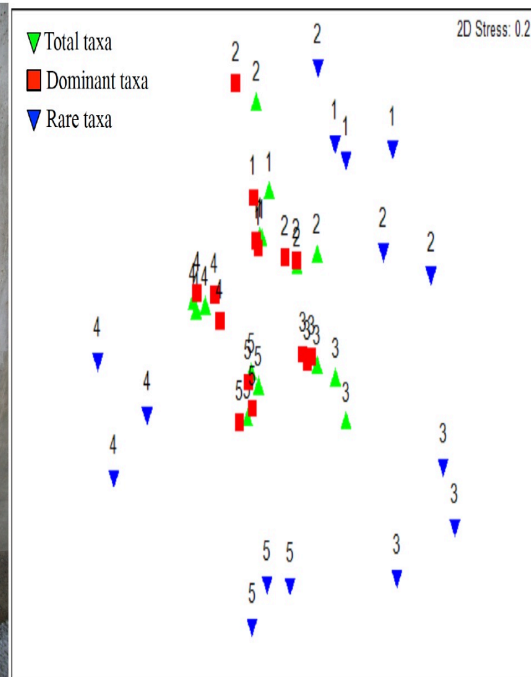
- flux-step method in a submerged membrane bioreactor. **J. Membr. Sci.**, v. 227, p. 81-93, 2003.
32. Jefferson, B., Brookes, A., Le-Clech, P., Judd, S.J. Methods for understanding organic fouling in MBRs. **Water Sci. Technol.**, v. 49, p. 237-244, 2004.
  33. Itonaga, T., Kimura, K., Watanabe, Y. Influence of suspension viscosity and colloidal particles on permeability of membrane used in membrane bioreactor (MBR). **Water Sci. Technol.**, v. 50, p. 301-309, 2004.
  34. Chang, I. S., Kim, S. N. Wastewater treatment using membrane filtration-effect of biosolids concentration on cake resistance. **Process Biochem.**, v. 40, p. 1307-1314, 2005.
  35. Brookes, A., Jefferson, B., Guglielmi, G., Judd, S.J. Sustainable flux fouling in a membrane bioreactor: impact of flux and MLSS. **Sep. Sci. Tech.**, v. 41, p. 1279-1291, 2006.
  36. Yeo, A.P.S., Law, A.W.K., Fane, A.G. Factors affecting the performance of a submerged hollow fiber bundle. **J. Membr. Sci.**, v. 280, p. 969-982, 2006.
  37. Qu, F., Liang, H., Zhou, J., Nan, J., Shao, S., Zhang, J., Li, G. Ultrafiltration membrane fouling caused by extracellular organic matter (EOM) from *Microcystis aeruginosa*: Effects of membrane pore size and surface hydrophobicity. **J. Membr. Sci.**, v. 449, p. 58-66, 2014.
  38. Ng, T.C.A., Ng, H.Y. Characterisation of initial fouling in aerobic submerged membrane bioreactors in relation to physico-chemical characteristics under different flux conditions. **Water Res.**, v. 44, p. 2336-2348, 2010.
  39. Garg, A., Jain, A., Bhosle, N.B. Chemical characterization of a marine conditioning film. **Inter. Biodet. Biodeg.**, v. 63, p. 7-11, 2009.
  40. Khan, M.T., O.Manes, C.L., Aubry, C., Gutierrez, L., Croue, J.P. Kinetic study of seawater reverse osmosis membrane fouling. **Environ. Sci. Technol.**, v. 47, n. 19, p. 10884-10894, 2013.
  41. Tansel, B., Sager, J., Garland, J., Xu, S., Levine, L., Bisbee, P. Deposition of extracellular polymeric substances (EPS) and microtopographical changes on membrane surfaces during intermittent filtration conditions. **J. Membr. Sci.**, v. 285, n. 1, p. 225-231, 2006.
  42. Vanyacker, L., Boerjan, B., Declerck, P., Vankkelecom, I.F.J. Biofouling ecology as a means to better understand membrane biofouling. **Appl. Microbiol. Biotechnol.**, v. 98, n. 19, p. 8047-8072, 2014.
  43. Zhang, K., Choi, H., Dionysiou, D.D., Sorial, G.A., Oerther, D.B. Identifying pioneer bacterial species responsible for biofouling membrane bioreactors. **Environ. Microbiol.**, v. 8, n. 3, p. 433-440, 2006.
  44. Park, N., Kwon, B., Kim, I.S., Cho, J. Biofouling potential of various NF membranes with respect to bacteria and their soluble microbial products (SMP): Characterizations, flux decline, and transport parameters. **J. Membr. Sci.**, v. 258, p. 43-54, 2005.
  45. Flemming, H.C., Neu, T.R., Wozniak, D.J. The EPS matrix: the "house of biofilm cells". **J. Bacteriol.**, v. 189, n. 22, p. 7945-7947, 2007.

46. Flemming, H.C., Wingender, J. The biofilm matrix. **Nature Rev. Microbiol.**, v. 8, n. 9, p. 623-633, 2010.
47. Li, W., Zhou, J., Gu, J.S., Yu, H.Y. Fouling control in a submerged membrane-bioreactor by the membrane surface modification. **J. Appl. Polymer Sci.**, v. 115, n. 4, p. 2302-2309, 2010.
48. Chae, S.R., Wang, S., Hendren, Z.D., Wiesner, M.R., Watanabe, Y., Gunsch, C.K. Effects of fullerene nanoparticles on *Escherichia coli* K12 respiratory activity in aqueous suspension and potential use for membrane biofouling control. **J. Membr. Sci.**, v. 329, n. 1, p. 68-74, 2009.
49. Sheng, Z., Liu, Y. Effects of silver nanoparticles on wastewater biofilms. **Water Res.**, v. 45, n. 18, p. 6039-6050, 2011.
50. Zodrow, K., Brunet, L., Mahendra, S., Li, D., Zhang, A, Li, Q., Alvarez, P.J.J. Polysulfone ultrafiltration membranes impregnated with silver nanoparticles show improved biofouling resistance and virus removal. **Water Res.**, v. 43, n. 3, p. 715-723, 2009.
51. Elimelech, M., Phillip, W. A. The future of seawater desalination: energy, technology, and the environment. **Science**, v. 333, n. 6043, p. 712-717, 2011.
52. Vrouwenvelder, J., Paassen, J.A.M., Van Agtmaal, J.M.C., Van Loosdrecht, M.C.M., Kruithof, J.C. A critical flux to avoid biofouling of spiral wound nanofiltration and reverse osmosis membranes: fact or fiction? **J. Membr. Sci.**, v. 326, n. 1, p. 36-44, 2009.
53. Song, K.G., Kim, Y., Ahn, K.H. Effect of coagulant addition on membrane fouling and nutrient removal in a submerged membrane bioreactor. **Desalination**, v. 221, p. 467-474, 2008.
54. Remy, M., Potier, V., Temmink, H., Rulkens, W. Why low powdered activated carbon addition reduces membrane fouling in MBRs. **Water Res.**, v. 44, p. 861-867, 2010.
55. Ying, Z., Ping, G. Effect of powdered activated carbon dosage on retarding membrane fouling in MBR. **Sep. Purif. Technol.**, v. 52, n. 1, p. 154-160, 2006.
56. Remy, M., Temmink, H., Van den Brink, P., Rulkens, W. Low powdered activated carbon concentrations to improve MBR sludge filterability at high salinity and low temperature. **Desalination**, v. 276, p. 403-407, 2011.
57. Psoch, C., Schiewer, S. Anti-fouling application of air sparging and backflushing for MBR. **J. Membr. Sci.**, v. 283, n. 1, p. 273-280, 2006.
58. Vera, L., Gonzales, E., Diaz, O., Delgado, S. Application of a backwashing strategy based on transmembrane pressure set-point in a tertiary submerged membrane bioreactor. **J. Membr. Sci.**, v. 470, p. 504-512, 2014.
59. Zhang, H., Sun, B., Zhao, X., Gao, Z. Effect of ferric chloride on fouling in membrane bioreactor. **Sep. Purif. Technol.**, v. 63, n. 2, p. 341-347, 2008.
60. Jahangir, D., Oh, H.S., Kim, S.R., Park, P.K., Lee, C.H, Lee, J.K. Specific location of encapsulated quorum quenching bacteria for biofouling control in an external submerged membrane bioreactor. **J. Membr. Sci.**, v. 411, n. 130, p. 136, 2012.
61. Jiang, W., Xia, S., Liang, J., Zhang, Z., Hermanowics, S.W. Effect of quorum

- quenching on the reactor performance, biofouling and biomass characteristics in membrane bioreactors. **Water Res.**, v. 47, n. 1, p. 187-196, 2013.
62. Calderon, K., Rodelas, B., Cabirol, N., Gonzalez-Lopez, J., Noyola, A. Analysis of microbial communities developed on the fouling layers of a membrane-coupled anaerobic bioreactor applied to wastewater treatment. **Biores. Technol.**, v. 102, n. 7, p. 4618-4627, 2011.
  63. Piasecka, A., Souffrea, C., Vandepitte, K., Vanysacker, L., Bilad, R.M., De Bie, T., Hellemans, B., De Meester, L., Yan, X., Declerck, P., Vankelcom, I.F.J. Analysis of the microbial community structure in a membrane bioreactor during initial stages of filtration. **Biofouling**, v. 28, n. 2, p. 225-238, 2012.
  64. Gao, D., Fu, Y., Ren, N. Tracing biofouling to the structure of the microbial community and its metabolic products: A study of the three-stage MBR process. **Water Res.**, v. 47, p. 6680-6690, 2013.
  65. Lee, S.H., Hong, T.I., Kim, B., Hong, S., Park, H.D. Comparison of bacterial communities of biofilms formed on different membrane surfaces. **World J. Microbiol. Biotechnol.**, v. 30, n. 2, p. 777-782, 2014.
  66. Duan, L., Moreno-Andrade, I., Huang, C-L., Xia, S., Hermanowics, S.W. Effects of short solids retention time on microbial community in a membrane bioreactor. **Biores. Technol.**, v. 100, n. 1, p. 3489-3496, 2009.
  67. Huang, L.N., De Wever, H., Diels, L. Diverse and distinct communities induced biofilm fouling in membrane bioreactors operated under different conditions. **Environ. Sci. Technol.**, v. 42, p. 8360-8366, 2008.
  68. Wang, X., Hu, M., Xia, Y.; Wen, X., Ding, K. Pyrosequencing analysis of bacterial diversity in 14 wastewater treatment systems in China. **Appl. Environ. Microbiol.**, v. 78, n. 19, p. 7042-7047, 2012.
  69. Shanks, O.C., Newton, R.J., Kelty, C.A., Huse, S.M., Sogin, M.L., McLellan, S.L. Comparison of the microbial community structures of untreated wastewaters from different geographic locales. **Appl. Environ. Microbiol.**, v. 79, n. 9, p. 2906-2913, 2013.
  70. Ye, L., Zhang, T. Bacterial communities in different sections of a municipal wastewater treatment plant revealed by 16S rDNA 454 pyrosequencing. **Appl. Environ. Microbiol.**, v. 97, n. 6, p. 2681-2690, 2013.
  71. Ma, J., Wang, Z., Yang, Y., Mei, X., Wu, Z. Correlating microbial community structure and composition with aeration intensity in submerged membrane bioreactors by 454 high-throughput pyrosequencing. **Water Res.**, v. 47, n. 2, p. 859-869, 2013.
  72. Rittmann, B.E. Microbial ecology to manage processes in environmental biotechnology. **Trends Biotechnol.**, v. 24, n. 6, p. 261-266, 2006.

## CHAPTER 2 454-Pyrosequencing Reveals Biodiversity of Sessile and Planktonic Bacterial Community in Five Full-scale Membrane Bioreactors

### Early Colonizers



### Mature Biofilm



Peer reviewed journal article

**Gerald K. Matar**, Samik Bagchi, Kai Zhang, Daniel B. Oerther and Pascal E. Saikaly (2015) “454-Pyrosequencing Reveals Biodiversity of Sessile and Planktonic Bacterial Community in Five Full-scale Membrane Bioreactors”. *Submitted to Applied Microbiology and Biotechnology*

Abstract, Oral presentation

**G. Matar**, Samik Bagchi, Kai Zhang, Daniel B. Oerther and Pascal E. Saikaly (2015). “Pyrosequencing of 16S rRNA gene reveals large differences in the sessile bacterial community in five full-scale membrane bioreactors.” **250<sup>th</sup> American Chemical Society National Meeting & Exposition**, Boston, MA – USA, August 16-20, 2015

Conference proceedings, oral presentation

**G. Matar**, S. Bagchi, K. Zhang, D. B. Oerther and P. E. Saikaly (2013). “Analysis of bacterial community structure and composition of early and mature biofilms from five full-scale MBR plants using 454 pyrosequencing.” **International Water Association: Proceedings of the International Conference: 10th IWA Leading Edge Conference on Water and Wastewater Technologies**, Bordeaux, France, June 2-6, 2013

Conference proceedings, oral presentation

**G. Matar**, S. Bagchi, K. Zhang, D. B. Oerther and P. E. Saikaly (2013). “Microbial characterization of early and mature biofilms on the membrane surfaces of full-scale MBR plants in Seattle, Washington, USA.” **International Water Association: 9th International Conference on Biofilm Reactors**, Paris, France, May 28-31, 2013

**ABSTRACT**

Membrane biofouling remains poorly understood in full-scale membrane bioreactor (MBR). Studies that characterized the microbial communities responsible for membrane biofouling in lab-scale MBRs are numerous, yet similar studies on full-scale MBRs are still lacking. Five full-scale MBR plants were selected from the same geographic location and treated predominately municipal wastewater. The five MR plants were equipped with the same type of membrane (KUBOTA flat-sheet microfiltration membranes) that were operated under the same flux and air-scouring rate. Membrane biofilm (early and mature) and activated sludge samples were collected during December, and high-throughput 16S rRNA gene pyrosequencing combined with multivariate statistical analysis was applied to thoroughly characterize the community structure and composition of membrane biofilms (early and mature) and activated sludge. Our results revealed that community structures of early and mature membrane biofilms were distinct from the communities in the activated sludge. High number of unique OTUs that corresponded to the rare resulted into differences in the microbial communities between the five MBR plants. Consequently, microbial communities from the activated sludge, early and mature biofilms clustered together according to the MBR treatment plant. Furthermore, the structure of the activated sludge and biofilm communities differed among the five MBRs suggesting that the source communities (i.e. AS) and local environmental and operational conditions on the membrane surface selected specifically microorganisms from AS to form membrane biofilms.

**Keywords** Biofouling. Membrane bioreactor. Early colonizers. Mature biofilm. 16S rRNA gene pyrosequencing

## 2.1. Introduction

Membrane bioreactors (MBRs) offer several advantages over conventional wastewater treatment technologies (e.g. conventional activated sludge process), such as producing less sludge and providing high quality permeate without encountering a large footprint [1, 2]. Despite these advantages, membrane fouling, particularly biofouling (i.e. biofilm formation), remains a major hindrance to the wide spread of MBRs. Membrane biofouling causes a drop in the performance of the system, including flux decline or increase in trans-membrane pressure (TMP) depending on the mode of operation, thus resulting in higher energy consumption [1, 3, 4]. As a result, frequent membrane cleaning is required, and in the case of irreversible fouling, membrane replacement is required.

Several control strategies have been suggested to mitigate biofouling in MBRs including physical cleaning (e.g. back-washing, back-pulsing, air sparging), chemical cleaning (e.g. acids, bases, oxidants, chelating agents, polymeric coagulants, surfactants), membrane modification (e.g. charge, hydrophobicity, roughness), and biological-based antifouling strategies (e.g. quorum quenching, enzymatic disruption, energy uncoupling) [5]. However, these strategies often fail to adequately control biofouling. Finding more efficient strategies to control biofouling in MBRs requires a more fundamental understanding of biofilm formation.

Several sequential steps are generally considered to be involved in the progression of biofilm formation on surfaces, including: i) formation of a conditioning film followed by a series of recruitment processes, ii) attachment of pioneer colonizers, iii) growth of pioneer colonizers, which change the surface characteristics enabling the recruitment of new organisms resulting in early biofilm formation, and iv) subsequent development of

mature biofilms [6, 7, 8]. This sequence of events in the colonization of surfaces is well understood for human dental plaque and other solid surfaces [6, 9, 10, 11], and it has been observed in the colonization of reverse osmosis (RO) membrane and spacer surfaces [8]. However, this detailed level of understanding on biofilm formation on membrane surfaces in MBRs is less studied. In addition, only few microbiological studies have been conducted on MBRs to better understand and characterize the microbial community underlying the biofouling process. While most studies have characterized the microbial communities in mature biofilms [1, 4, 12, 13, 14], some researchers claim that characterizing the early colonizers on membrane surfaces might help develop better control strategies; yet, few studies have addressed these early colonizers [7, 15, 16, 17]. However, studies characterizing the microbial community of both early colonizers and mature biofilm in MBRs are lacking. Moreover, the majority of existing microbiological studies have focused on lab-scale MBRs [4, 7, 13, 14, 15, 16, 17, 18] with very few on pilot-scale MBRs [1, 12]. A common outcome of the aforementioned MBR studies was that the biofilm microbial community was distinct from the suspended community. However, we still have no clear understanding of what shapes the biofilm community in MBRs.

The biofouling community composition in MBRs has been mainly investigated using conventional molecular biology techniques such as terminal restriction fragment length polymorphism (T-RFLP) of PCR-amplified 16S rRNA genes [17], denaturing gradient gel electrophoresis (DGGE) of 16S rRNA gene fragments [4, 12], clone library analysis of 16S rRNA genes [1, 4, 7, 12, 15, 17], and fluorescence *in situ* hybridization (FISH) [1, 13]. These conventional molecular biology tools can only capture a mere snapshot of

dominant members, with little information on rare taxa [19]. On the other hand, high-throughput sequencing technologies provide enough sequencing depth to cover the complexity of bacterial community comprising both dominant and rare taxa [20, 21]. Only very few studies [14, 16] applied high-throughput sequencing to characterize the biofouling communities in MBRs.

In this study we applied high-throughput 16S rRNA gene pyrosequencing combined with multivariate statistical analysis to characterize the biofilm (early and mature) and activated sludge bacterial communities in five full-scale MBRs equipped with the same type of membrane and treating domestic wastewater. This study is motivated by several questions: i) Is there a core microbial community responsible for membrane biofouling in the different full-scale MBRs? ii) Does the activated sludge community vary with location and how does this variation affect the biofouling community (early and mature)? iii) Is the assembly of biofilm community (early and mature) in MBRs the result of random immigration of species from the suspended community or the result of specific selection of certain species due to the local environmental conditions? To the best of the author's knowledge this is the first study characterizing the early and mature biofouling communities in full-scale MBRs from different locations and operated under different conditions.

## **2.2. Materials and methods**

### **2.2.1. Full-scale MBRs and sample collection**

Fifteen full-scale MBR treatment plants were identified in the region of Seattle (Washington, U.S.A.) and due to technical reasons only five MBR plants were selected to

conduct this study. The five MBR plants (referred to herein as MBR 1, 2, 3, 4 and 5) were equipped with KUBOTA flat-sheet microfiltration (MF) membranes (KUBOTA Membranes, USA) and treated predominantly municipal wastewater. Details of influent wastewater characteristics and operational parameters of the five MBR plants are listed in Table 2.1.

**Table 2.1.** Characteristics of the 5 full-scale MBR plants.

Environmental and operational variables <sup>a</sup>						
MBR plant	Influent BOD (mg/L)	Influent NH <sub>3</sub> (mg/L)	Influent TKN (mg/L)	Influent TP (mg/L)	SRT (days)	HRT (hours)
MBR 1	250	36	50	0	22	8.6
MBR 2	200	28	35.5	8	31	8.4
MBR 3	400	86	120	15	49	27.9
MBR 4	700	57	80	8	15	16.7
MBR 5	300	22	31	8	29	16.9

<sup>a</sup>BOD: biochemical oxygen demand; TKN: total kjeldahl nitrogen; TP: total phosphorous; SRT: solids retention time; HRT: hydraulic retention time.

Old membrane modules that have been in operation for at least six months were removed from the membrane basin and duplicate membrane samples (5 cm<sup>2</sup> each) were sectioned from different locations on the membrane surfaces, on which mature biofilms have already developed. Immediately afterwards, new membrane modules were deployed in the membrane basin to replace the old membrane modules and after 5 hours of filtration, the new membrane modules were removed and duplicate membrane samples (5 cm<sup>2</sup> each) were sectioned from different locations on the membrane surfaces, on which early biofilms or colonizers have already developed. Activated sludge (AS) samples (20 mL each) were collected from the membrane basin of each MBR treatment plant at the same time when the early and biofilm samples were collected. All membrane and

activated sludge samples from the five MBR treatment plants were collected over a period of two weeks. In total, 30 samples were collected including duplicate samples of early and mature biofilms and activated sludge from five full-scale MBR plants. All samples were immediately stored on ice and transported to the laboratory, where they were stored at  $-80^{\circ}\text{C}$  until further analysis.

### **2.2.2. DNA extraction, PCR amplification and 16S rRNA gene pyrosequencing**

Before DNA extraction the membrane samples were rinsed with 1 X PBS (phosphate-buffered saline: 8 g NaCl, 0.2 g KCl, 1.44 g  $\text{Na}_2\text{HPO}_4$ , and 0.24 g  $\text{KH}_2\text{PO}_4$  per liter distilled water, pH 7.4) to remove loosely deposited sludge [4]. Genomic DNA was extracted from the mature biofilms, early biofilms and AS samples using the PowerSoil DNA extraction kit (MO BIO Laboratories, inc., Carlsbad, CA) according to the manufacturer's protocol. The quality (A260/A280) and quantity (A260) of the extracted genomic DNA was determined with a Nanodrop® 1000 spectrophotometer (Thermo Fisher Scientific, Waltham, MA).

Genomic DNA was extracted from the mature biofilms, early biofilms and AS samples using the PowerSoil DNA extraction kit (MO BIO Laboratories, inc., Carlsbad, CA) according to the manufacturer's protocol. The quality (A260/A280) and quantity (A260) of the extracted genomic DNA was determined with a Nanodrop® 1000 spectrophotometer (Thermo Fisher Scientific, Waltham, MA) [22]. These primers targeted the V1–V3 region of the bacterial 16S rRNA gene. Barcodes that allow sample multiplexing during pyrosequencing were incorporated between the 454 adapter and the forward primer. PCR was performed using a C1000 Thermal Cycler (BIO-RAD, Hercules, CA) with the following PCR conditions: initial denaturation at  $95^{\circ}\text{C}$  for 5

minutes, followed by 25 cycles of denaturation at 95°C for 30 seconds, annealing at 55°C for 30 seconds, and extension at 72°C for 30 seconds. The PCR was completed with a final extension at 72°C for 5 minutes [22].

Triplicate PCR products from each sample were pooled and confirmed by gel electrophoresis. Then, gel bands were excised and purified using the Qiaquick gel extraction kit (QIAGEN, Valencia, CA) according to the manufacturer's protocol. The concentration of the PCR products was measured on Qubit® 2.0 Fluorometer using the PicoGreen® dsDNA quantitation assay (Invitrogen, Carlsbad, CA). The purified barcoded amplicons were pooled in equimolar concentrations and pyrosequenced on the Roche 454 FLX Titanium genome sequencer (Roche, Indianapolis, IN) at the Bioscience Core Laboratory at King Abdullah University of Science and Technology, according to the manufacturer's instructions.

### **2.2.3. Processing of pyrosequencing data**

The 16S rRNA gene amplicons were processed using the Quantitative Insights Into Microbial Ecology (QIIME v1.7.0) pipeline [23]. All raw reads were first denoised, filtered for quality check and demultiplexed to trim the barcoded primers and to remove all the low quality sequence reads, such as sequences below 200 base pairs (bp) and above 1000 bp, sequences containing more than 6 ambiguous base pairs and sequences with quality score below 25. Chimeric sequences were identified and removed from the sequences using Chimera Slayer as implemented in QIIME. A total of 743,970 reads from the 30 samples passed through this QA/QC step. The sequences were clustered into operational taxonomic units (OTUs) using UCLUST [24], with 97% sequence identity threshold. Representative sequence from each OTU was phylogenetically aligned using

PyNAST [25] and assigned to a taxonomic identity using the Greengenes 13\_5 database [26].

To compensate for stochastic sampling efforts and reduce effects of variation among replicates [27], duplicate samples were pooled together to create combined OTU files. This resulted into 15 pooled samples encompassing a total of 22,877 OTUs. The OTU table was further clustered based on biomass category into three subsets i.e. Early, Mature and AS or by MBRs into five subsets. Shared OTUs within each of the three subsets (i.e. AS, Early or Mature) or MBR was visualized by Venn diagram in R ‘vegan scalpel’ program. The distribution of the different bacterial phyla and proteobacterial classes was visualized in a heatmap using R ‘vegan scalpel’ program.

The 454 pyrosequencing reads have been deposited into the Sequence Read Archive (SRA) of the National Center for Biotechnology Information (NCBI) under study accession number SRP064009.

#### **2.2.4. Alpha and beta diversity estimates**

For alpha diversity measurements, both non-phylogeny based metrics (observed OTUs, Shannon diversity index (H) and Chao 1 richness estimator) and phylogeny based metric (phylogenetic diversity (PD<sub>whole</sub>)) were calculated with QIIME at the 3% distance level for each pooled sample using rarefied OTU dataset. Community comparisons between samples was performed with unweighted UniFrac and Bray-Curtis distance (beta diversity) and visualized by principal coordinate analysis (PCoA) in QIIME. To remove inherent heterogeneity of sampling depth, we subsampled the dataset (normalized abundance values) to an even depth of 4,000 sequences across the pooled samples. This number was chosen, as it was slightly less than the pooled sample with the lowest reads

(i.e. Early biofilm from MBR 2, which had 4,007 reads). We also assessed the beta diversity of total, dominant and rare taxa for the pooled samples. Rare taxa were arbitrarily defined as OTUs that encompass < 12 sequences [28]. Unweighted UniFrac distance was calculated for total, general and rare OTUs and visualized by nonmetric multidimensional scaling (NMDS) using the software PRIMER 6 (version 6.1.13) and PERMANOVA+ add on (version 1.0.3) (PRIMER-E LTD, United Kingdom). Jackknife beta diversity and clustering analysis was performed to determine robustness of clustering of samples by the Unweighted Pair Group Method with Arithmetic means (UPGMA).

The OTU table was separated based on biomass category into three subsets i.e. Early, Mature and AS. Average unweighted UniFrac distance within and between Early, Mature and AS communities was calculated for each category by distance comparison command in QIIME.

### **2.2.5. Statistical analysis**

Reproducibility between duplicate samples was evaluated by one way pairwise analysis of similarity (ANOSIM) based on Spearman's rank correlation at a 999 permutation using the statistical software PRIMER 6 (version 6.1.13) and PERMANOVA+ add on (version 1.0.3) (PRIMER-E LTD, United Kingdom). ANOSIM produces a test statistic (R) which can range from -1 to 1 [29]. An R value of 0 indicates no separation in community structure and a value of 1 indicates separation [30].

To estimate the probability that a biofilm community (early or mature) represents a random sample of the respective suspended community (i.e. activated sludge), a random subsampling of the activated sludge community from each MBR was done as described

in Besemer et al (2012) [19]. In brief, OTUs from each activated sludge community were sampled with replacement until the number of OTUs in this randomly assembled community equaled the richness of the respective biofilm community. This procedure was repeated to yield 1000 random subsamples of each activated sludge community. The probability of the biofilm community to fall within the distribution of these random subsamples was calculated as the percentage of the distances of the random subsamples to their centroid [19]. The results of the random sampling procedure were visualized in NMDS.

## **2.3. Results**

### **2.3.1. Alpha diversity measures**

16S rRNA gene pyrosequencing was conducted on replicates from each type of sample (i.e., AS, early and mature biofilms). One-way pairwise analysis of similarity (ANOSIM) showed high similarity (98.4%; R: -0.25) between replicate samples. Spearman correlation coefficient was 92% ( $p < 0.001$ ). To limit the phenomenon of stochastic sampling, the obtained sequence reads from each replicate sample were pooled together [27] resulting in a total of 15 samples. A total of 743,970 high-quality reads were generated for the pooled samples after denoising, quality filtering and removal of chimeric sequences. The sequences were clustered into 22,877 OTUs at a 97% sequence identity threshold.

The alpha diversity measurements of the pooled samples using rarefied OTUs are summarized in Table 2.2. The diversity values across the fifteen samples ranged as follows: observed OTUs (939-6,943), Chao 1 (1,765-8,113), H (6.41-8.22) and PD

(74.59-226.01). All four indices, that is, observed OTU, Chao 1, H and PD, demonstrated that the early biofilm samples have higher diversity than the mature samples among the five MBR plants. On the basis of observed OTUs, the AS sample from MBR 4 had the highest diversity followed by MBR 3, MBR 2, MBR 1 and MBR 5. Almost a similar pattern was observed for AS samples using Chao 1 and PD. Good's coverage (84.20-97.91%, averaging 95%) revealed that the 16S rRNA gene sequences identified in these samples represent the majority of bacterial diversity present in each sample.

**Table 2.2.** Number of observed OTUs and alpha diversity measures for the pooled samples.

MBR plant	Sample description	Alpha diversity measures				Good's coverage (%)
		Number of observed OTUs	Richness estimate (Chao 1)	Shannon diversity index (H)	Phylogenetic diversity (PD)	
MBR 1	Early	2,531	4,377±101	8.20±0.01	138.04±0.58	95.77
	Mature	2,104	3,615±86	7.86±0.01	124.07±0.6	93.80
	AS	2,836	4,705±58	8.22±0.01	147.85±0.53	96.35
MBR 2	Early	1,002	2,231±95	7.88±0.01	80.50±0.57	84.20
	Mature	939	1,765±39	6.61±0.01	74.59±0.32	93.24
	AS	3,158	5,573±95	7.65±0.01	174.55±0.55	96.12
MBR 3	Early	3,852	8,113±3	7.65±0.01	226.01±0.036	93.92
	Mature	3,847	6,957±87	7.91±0.01	209.94±0.85	94.95
	AS	4,927	6,024±187	6.41±0.01	173.65±1.88	97.29
MBR 4	Early	6,943	7,216±312	8.03±0.01	204.87±2.64	97.48
	Mature	3,477	5,702±265	7.83±0.01	171.70±1.37	96.65
	AS	5,820	7,814±142	7.99±0.01	212.08±2.43	96.51
MBR 5	Early	4,650	5,212±148	7.99±0.01	170.28±1.69	97.91
	Mature	2,497	4,414±60	7.77±0.01	146.81±0.62	95.61
	AS	2,563	4,874±124	7.71±0.01	156.78±0.64	94.33

### 2.3.2. Bacterial community composition and taxonomy

Using PyNAST with the Greengenes database as a reference, 100%, 87%, 68%, 52% and 32% of the V1-V3 16S rRNA gene pyrotags could be assigned to the phylum, class, order, family and genus level, respectively.

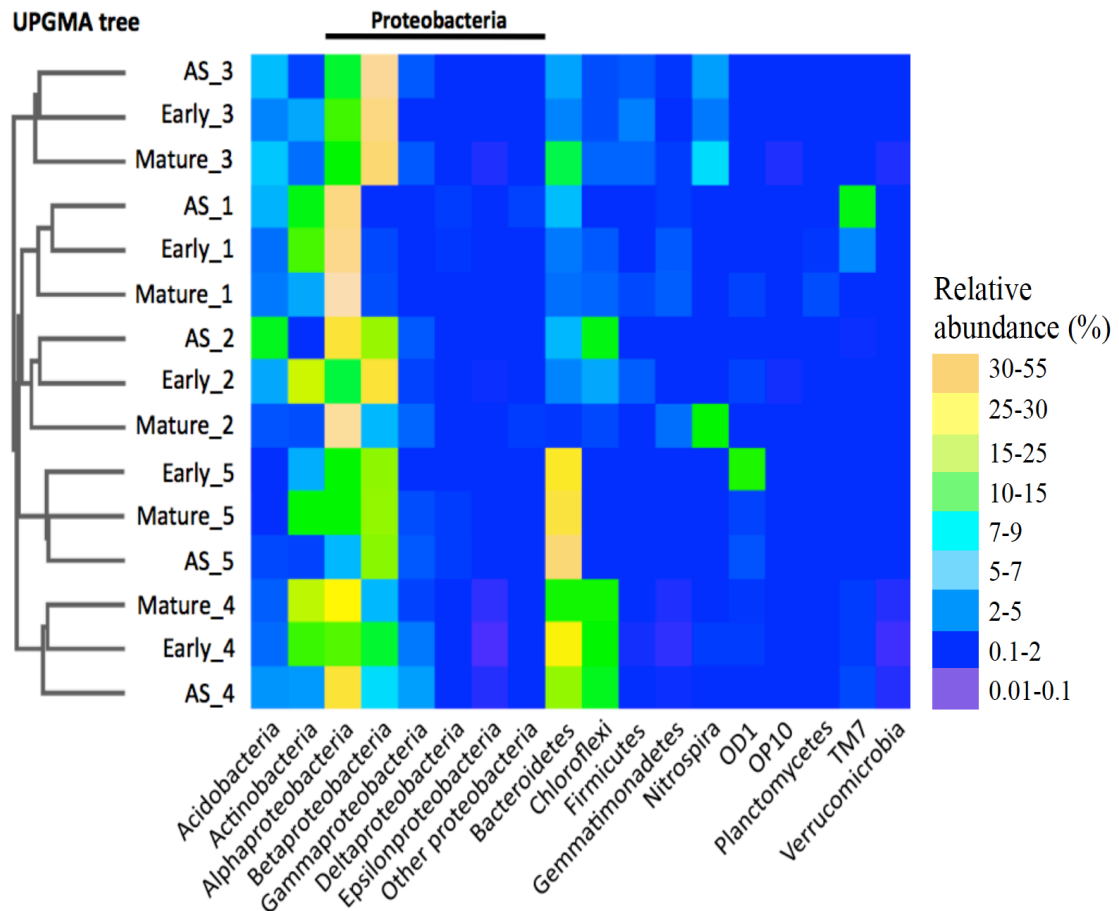


**Figure 2.1.** Heatmap distribution of bacterial phyla and proteobacterial classes derived from the 15 pooled samples. The color intensity in each cell shows the percentage of class/phylum in the corresponding sample. The hierarchical clustering on the left was created by unweighted-pair group method using arithmetic means (UPGMA). The numbers from 1 to 5 correspond to the 5 full-scale MBRs.

The AS and biofilm samples (early and mature) were allocated to 13 phyla, 21 classes and 382 genera. The dominant phylum across the 15 samples was *Proteobacteria* (Figure 2.1), constituting between 35 and 62% of all sequence reads. Other highly represented phyla included *Bacteroidetes* (13.9%), *Actinobacteria* (9.7%), *Acidobacteria* (6.0%), *Chloroflexi* (5.7%), *Nitrospira* (3.8%), *ODI* (3.3%), *Fermicutes* (2.4%), *Gemmatimonadetes* (2.0%) and *Planctomycetes* (2.0%). The numbers in parentheses represent the averages of all the samples (i.e. AS, early and mature) collected from the five MBR plants. The phylum *Bacteroidetes* was relatively more dominant in MBR 4 and 5, while the phylum *Chloroflexi* was more abundant in MBR 4 (Figure 2.1).

The phylum *Actinobacteria* was relatively more dominant in early (13.6%) and mature (9.9%) biofilms than AS (5.5%) samples. Within *Proteobacteria*, *Alphaproteobacteria* (20.9%; 18.7%; 28.8%) was the dominant class, followed by *Betaproteobacteria* (18.4%; 18.1%; 13.7%), *Gammaproteobacteria* (4.3%; 3.1%; 3.6%) and *Deltaproteobacteria* (1.9%; 1.9%; 1.5%) (Figure 2.2). The numbers in parentheses represent the averages of AS, early and mature samples collected from the five MBR plants, respectively.

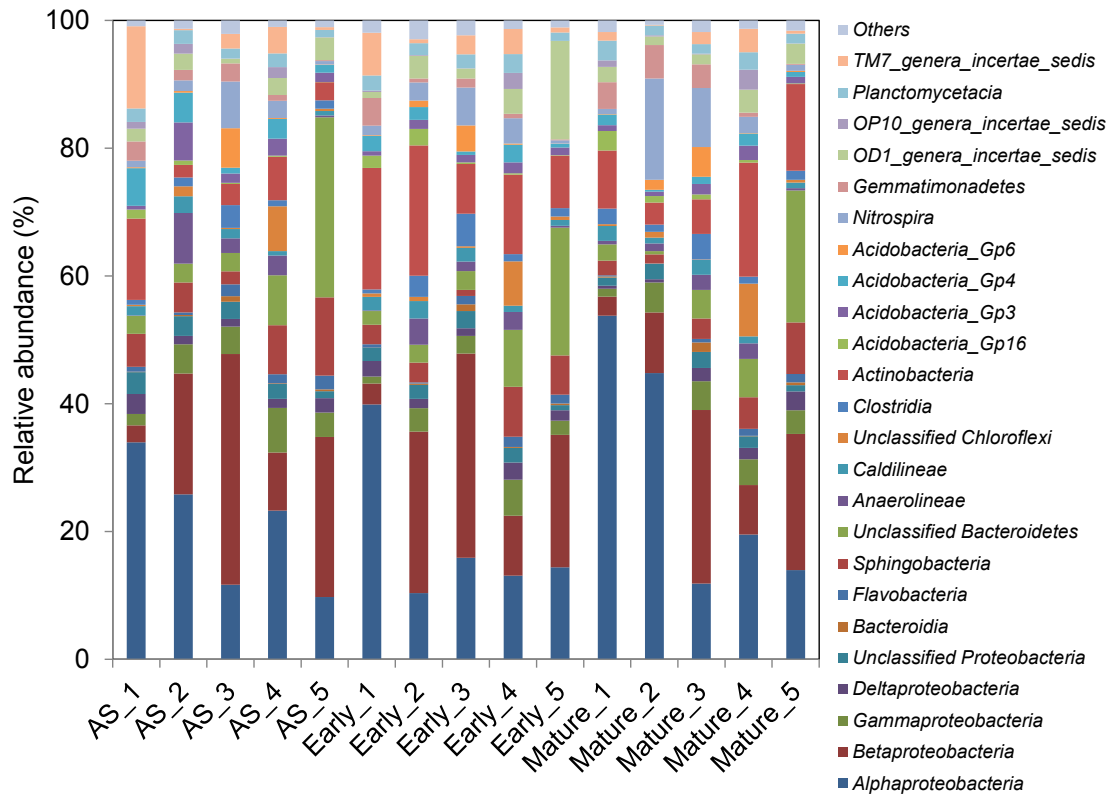


**Figure 2.2.** Relative abundance of bacteria retrieved from the five MBR plants classified at the class level. Bacterial classes that represent  $< 0.1\%$  of the total bacterial community composition were classified as “others”. The numbers 1 to 5 correspond to the five different MBR plants.

The difference in the bacterial community composition between the 5 MBR plants for each sample category (i.e. AS, early or mature) was more pronounced at the genus level (Figure 2.3) than phyla (Figure 2.1) and class level (Figure 2.2).

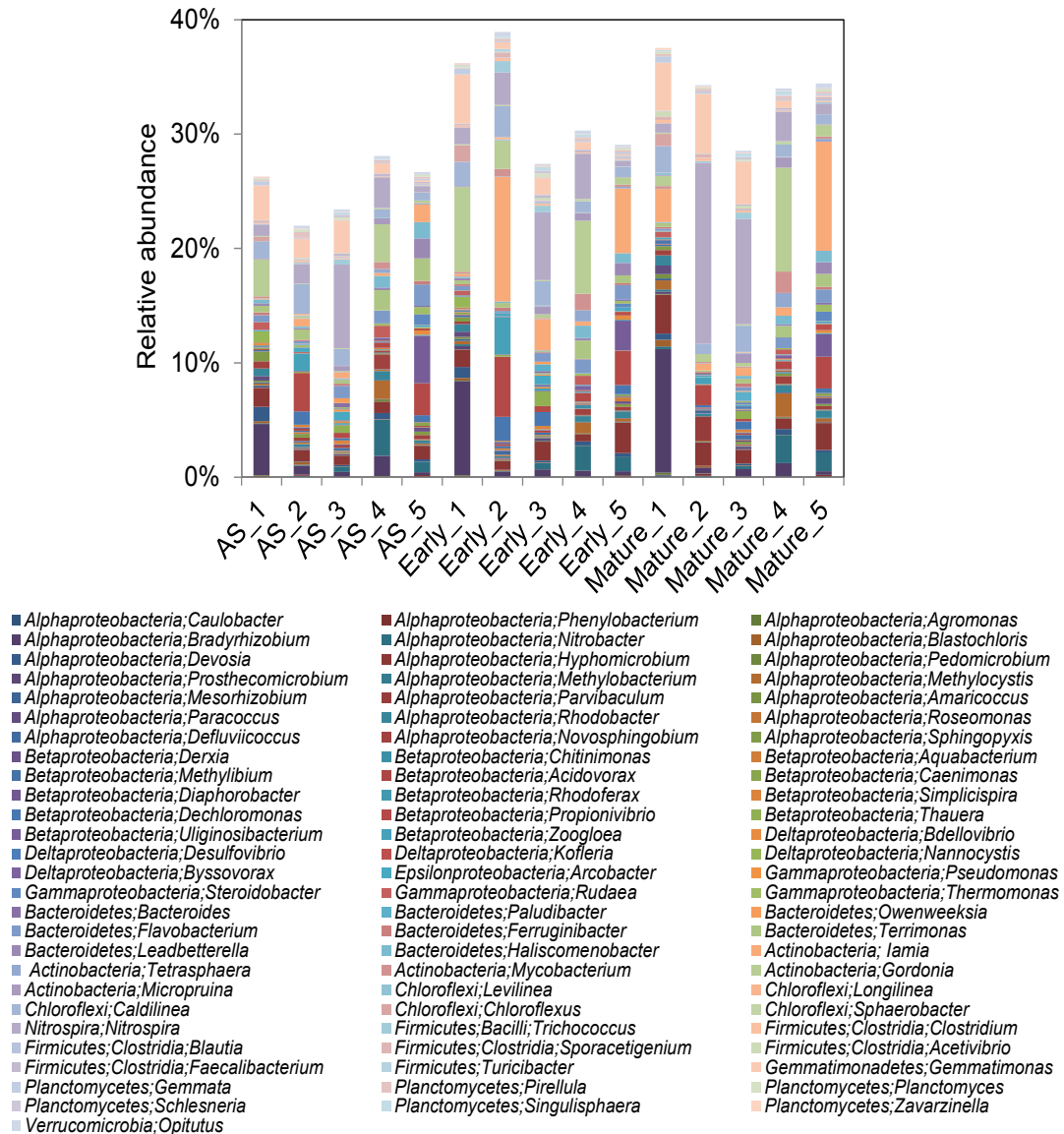


**Figure 2.3.** Relative abundance of the 79 annotated bacterial genera retrieved from the five MBRs. The numbers 1 to 5 correspond to the five different MBR plants. Only bacterial genera with relative abundance > 0.1% are presented in this figure.

### 2.3.3. Beta diversity measures

The bacterial communities in the five MBR plants were compared using both phylogenetic (unweighted UniFrac) and non-phylogenetic (Bray-Curtis distance)

measures. The PCoA results based on unweighted UniFrac distance revealed that the bacterial communities in the 15 samples were clustered into five groups with samples from the same MBR plant grouped together (Figure 2.4).

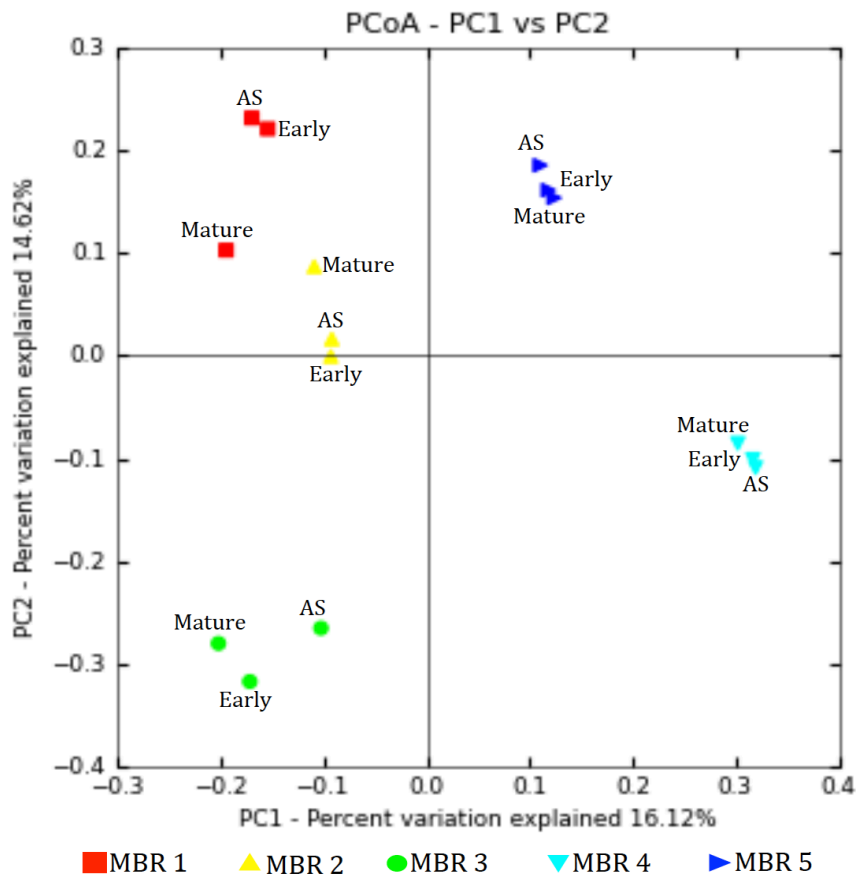


**Figure 2.4.** Principal coordinate analysis (PCoA) of the 15 pooled samples based on unweighted UniFrac distance showing the relatedness of the bacterial community structure of samples collected from AS and biofilms (Early and Mature). The numbers from 1 to 5 refer to the five different MBRs.

Similar results were obtained with Bray-Curtis distance at 3% cutoff-OTU level (Figure 2.5).

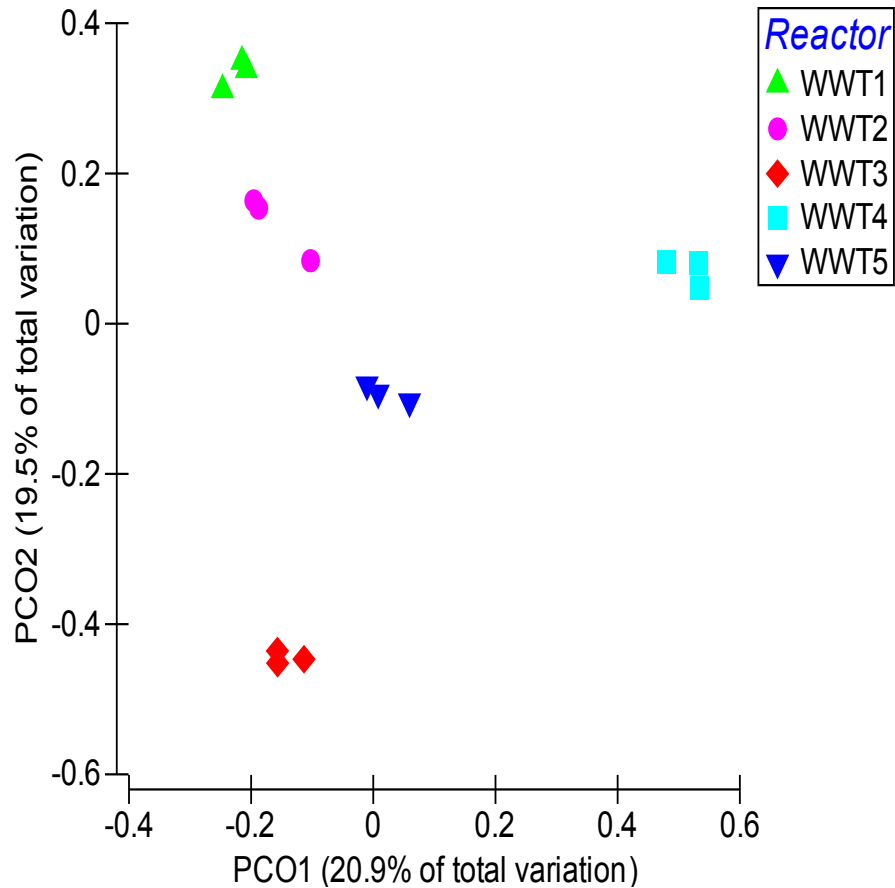


**Figure 2.5.** Principal coordinate analysis (PCoA) of the 15 pooled samples based on Bray-Curtis distance showing the relatedness of the bacterial community structure of samples collected from AS and biofilms (Early and Mature).

Also, hierarchical clustering (Figure 2.1) by UPGMA showed five clear clusters where each cluster corresponds to the AS and biofilm (early and mature) samples collected from the same MBR plant. High dissimilarity was observed between samples

within each category (i.e. AS, Early or Mature) based on unweighted UniFrac distance (Figure 2.6).

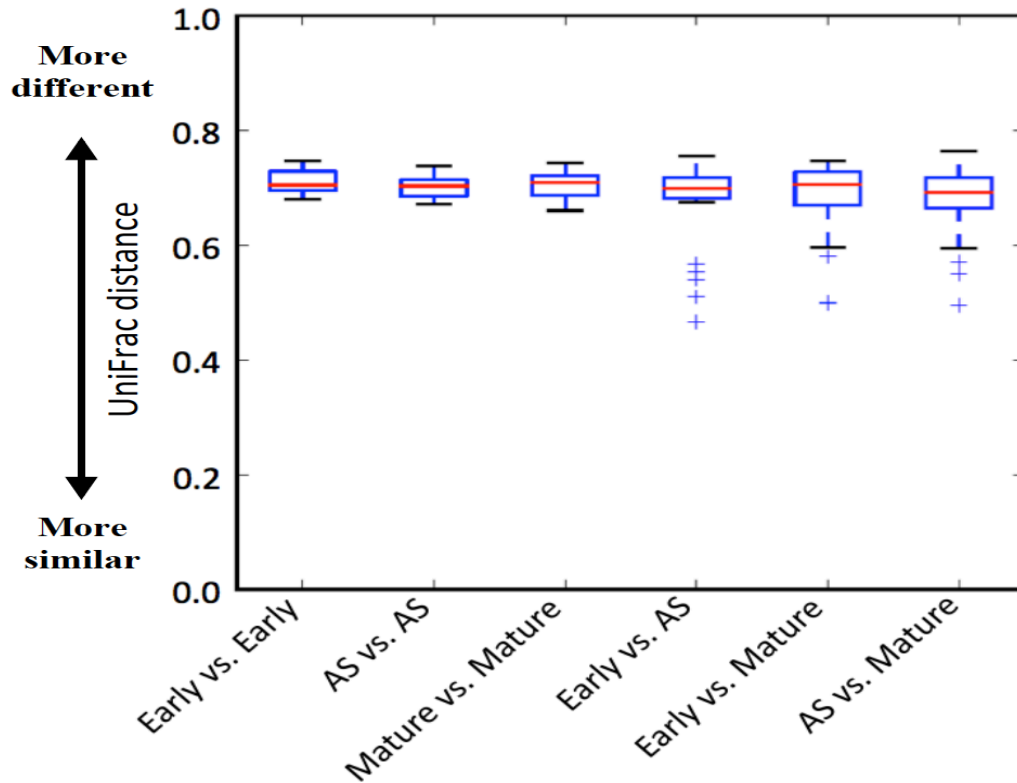


**Figure 2.6.** Boxplot showing unweighted UniFrac distance within and between Early, Mature and AS communities in all five full-scale MBRs. The red lines within the box represent the median while the plus signs are for outliers.

To compare the bacterial communities in the five MBR plants based on total, dominant and rare OTUs, the bacterial community in each sample was separated into rare (blue triangles), dominant (red squares) and total taxa (green triangles) and visualized in NMDS plot generated based on unweighted UniFrac distance (Figure 2.7). The NMDS results showed that the bacterial communities in the five MBR plants were more

dispersed based on rare OTUs than the total and dominant OTUs as can be seen by their wide distribution in the NMDS plot (Figure 2.7). Also, the total and dominant bacterial taxa were clustered together. These results suggest that the difference in the bacterial communities in the five MBR plants was mainly due to differences in the composition of the rare OTUs.

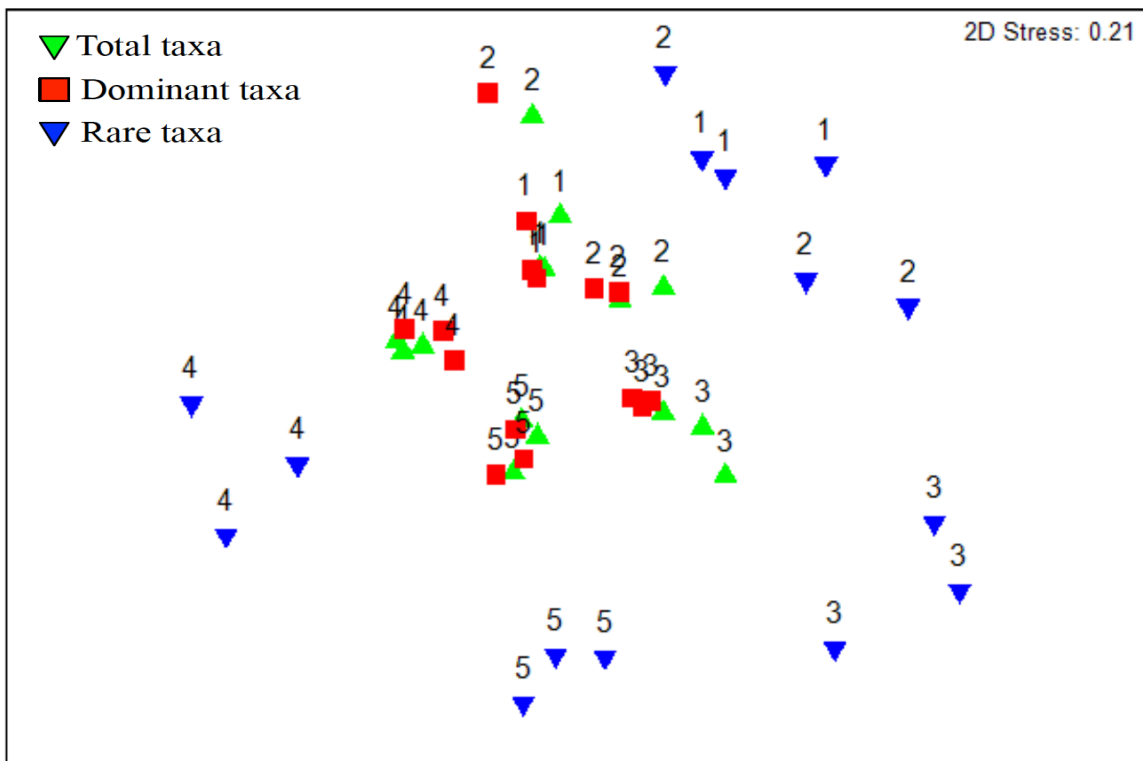


**Figure 2.7.** Nonmetric multidimensional scaling (NMDS) plot of the 15 pooled samples based on unweighted UniFrac distance showing the total (green triangles), dominant (red squares) and rare taxa (blue triangles). The numbers from 1 to 5 correspond to the five different MBRs.

Although hierarchical clustering (Figure 2.1), PCoA (Figure 2.4 and Figure 2.5) and NMDS analysis (Figure 2.7) showed that the AS and biofilm samples from each MBR plant were clustered together, comparison of unweighted UniFrac distance between

samples revealed that the AS samples from the five MBR plants were highly dissimilar from the biofilm samples (early and mature) (Figure 2.6). Also, the early biofilms were dissimilar from the mature biofilms.

#### 2.3.4. Core genera and OTUs

Core genera or OTUs indicate genera or OTUs shared across all samples in the same category (i.e. AS, early or mature) or across all 15 samples. Of the 382 classified genera (32% of sequence reads), 79 genera (30.5% of sequence reads) (Figure 2.3) were present at a relative abundance  $\geq 0.1\%$  in at least one of the 15 samples. Of these 79 genera, 48, 58 and 52 were shared between all AS, early biofilm and mature biofilm samples, respectively (Table 2.3).

**Table 2.3.** Number and percentages of shared genera between samples belonging to the same category (i.e. AS, Early or Mature).

Sample (Combined) <sup>a</sup>	Total number of classified genera <sup>b</sup>	Number of shared genera	Percentage of shared genera	Percentage in classified sequences <sup>c</sup>
AS	222	48	21.62	72.07-89.95
Early	214	58	27.10	64.47-83.87
Mature	208	52	25.00	74.79-91.87

<sup>a</sup>Combined samples correspond to the five AS samples, five early biofilms or five mature biofilms collected from the five MBRs.

<sup>b</sup>Total number of classified genera in each category (i.e. AS, Early or Mature).

<sup>c</sup>Range of percentage of sequences of the shared genera in the total classified sequences in each sample.

The relative abundance and phylogenetic classification of the 20 most abundant core genera across all 15 samples are presented in Figure 2.8. These core genera mainly belong to the *Proteobacteria* (*Alphaproteobacteria* and *Betaproteobacteria*), *Actinobacteria*, *Bacteroidetes*, *Chloroflexi*, *Gemmatimonadetes* and *Nitrospira* phyla.

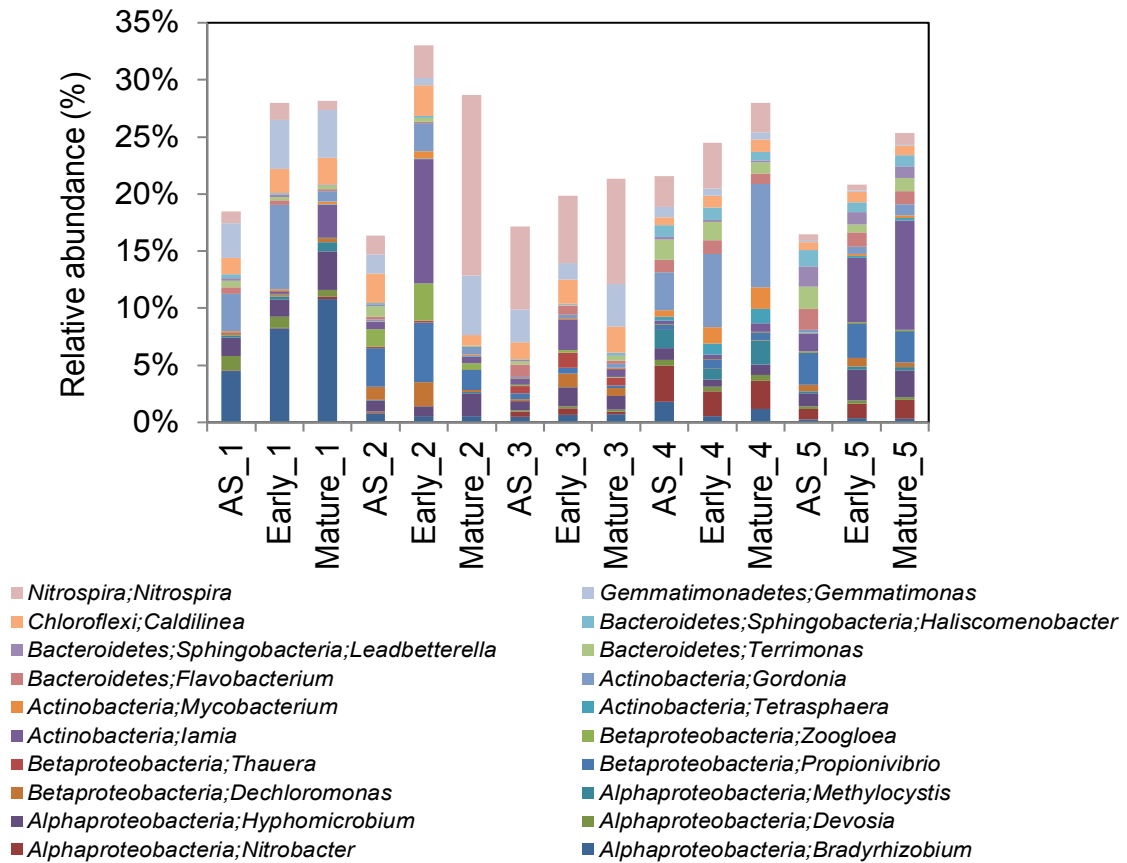


**Figure 2.8.** Relative abundance of the top 20 core genera among AS, early or mature samples from the five different MBRs. Core genera indicates genera shared across all samples in the same category (i.e. AS, Early or Mature).

To assess the number of core OTUs within the same category (i.e. AS, early or mature), the five AS, five early and five mature biofilm samples, from the five different MBR plants were combined together. Of the 14,323, 9,518 and 14,090 total observed OTUs, only 138 OTUs (0.96%), 114 OTUs (1.19%) and 228 OTUs (1.62%) were shared respectively by the five combined early biofilms, mature biofilms and AS samples (Table 2.4 and Figure 2.9). However, these core OTUs comprise a high fraction of the total

number of reads in the early biofilm (27.94%), mature biofilm (25.80%) and AS (35.17%) samples, respectively (Table 2.4).

**Table 2.4.** Percentages of core OTUs and their corresponding sequences between different samples. For each MBR, AS: Early, AS: Mature and Early: Mature correspond to the shared OTUs and sequences within two types of samples.

Sample	OTUs			Sequences		
	Total	Shared	Shared (%)	Total	Shared	Shared (%)
Early (Combined) <sup>a</sup>	14,323	138	0.96	310,757	86,829	27.94
Mature (Combined) <sup>a</sup>	9,518	114	1.20	146,745	37,864	25.80
AS (Combined) <sup>a</sup>	14,090	228	1.62	286,468	100,744	35.17
<b>MBR 1</b>						
AS: Early	3,794	1,573	41.46	65,143	56,326	86.47
AS: Mature	4,016	1,121	27.91	53,442	45,826	85.75
Early: Mature	3,536	1,099	31.08	45,677	39,572	86.63
<b>MBR 2</b>						
AS: Early	3,443	717	20.82	43,523	3,1672	72.77
AS: Mature	3,497	600	17.15	47,243	3,1875	67.47
Early: Mature	1,577	364	23.08	11,734	6,103	52.01
<b>MBR 3</b>						
AS: Early	6,615	2,164	32.71	131,490	121,604	92.48
AS: Mature	6,726	2,048	30.44	134,487	123,135	91.56
Early: Mature	5,902	1,797	30.44	76,373	67,775	88.74
<b>MBR 4</b>						
AS: Early	9,338	3,425	36.67	231,592	217,864	94.07
AS: Mature	7,008	2,289	32.66	145,697	138,392	94.99
Early: Mature	7,841	2,579	32.89	194,763	184,864	94.92
<b>MBR 5</b>						
AS: Early	5,418	1,795	33.13	125,477	115,733	92.23
AS: Mature	3,684	1,376	37.35	52,344	49,042	93.69
Early: Mature	5,273	1,874	35.54	128,955	119,139	92.39

<sup>a</sup>Combined samples correspond to the five early biofilms, five mature biofilms or five AS samples collected from the five MBRs.

Based on the Venn diagram (Figure 2.9), the unique OTUs for the five combined early biofilms, mature biofilms and AS samples correspond to 79.50% (11,387 OTUs), 78.20% (7,443 OTUs) and 77.70% (10,948 OTUs) of the total observed OTUs in each

category, respectively. By comparing the ratio of the number of reads to the number of core or unique OTUs within the same category (i.e. AS, early or mature), the core OTUs correspond to the dominant OTUs (332 to 929 reads per OTU; averaging 468 reads per OTU), whereas the unique OTUs correspond to the rare OTUs (15 to 20 reads per OTU; averaging 18 reads per OTU) [27].

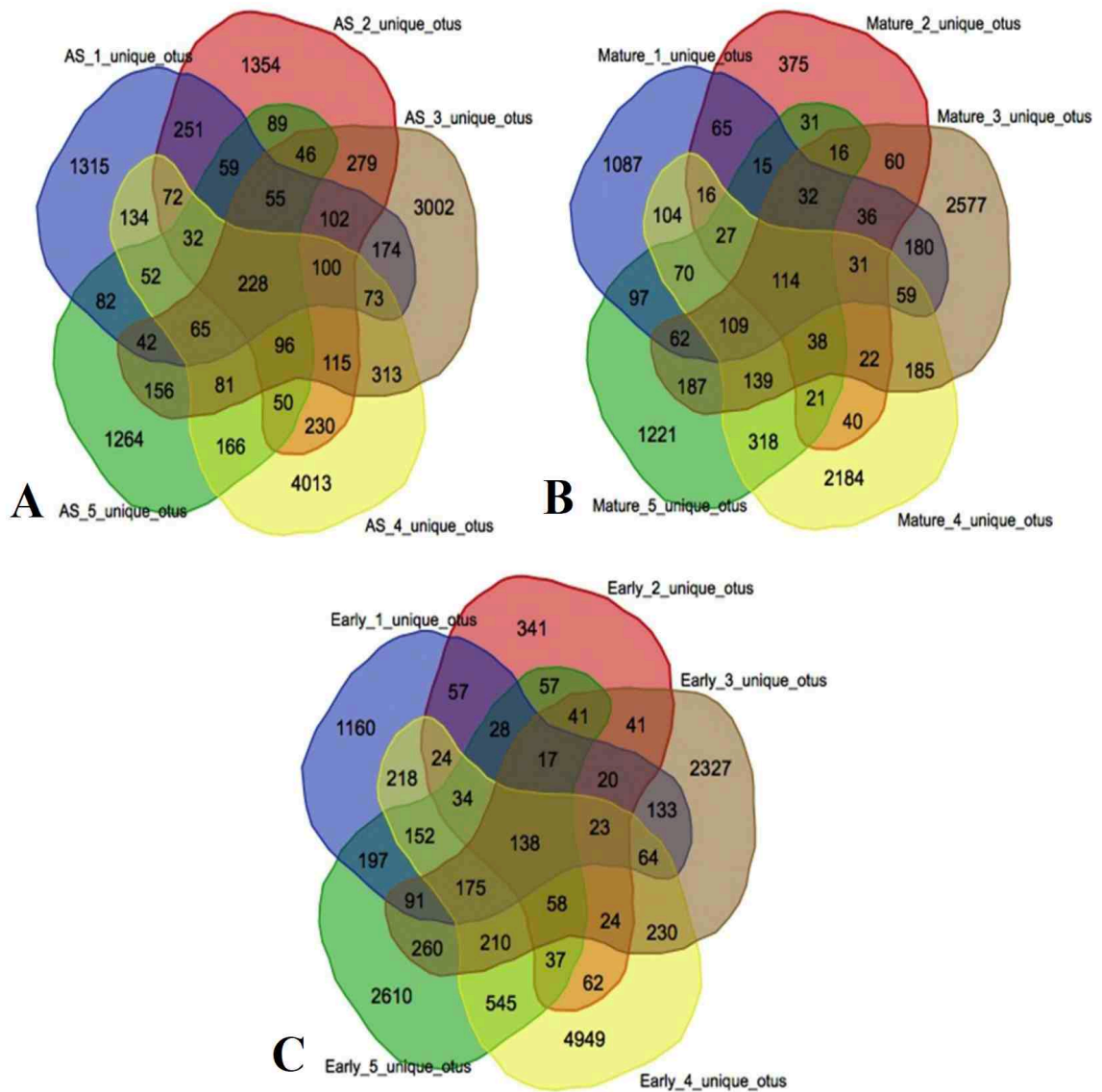


**Figure 2.9.** Venn diagram showing shared and unique OTUs within each biomass category, A: AS, B: Mature, C: Early.

Despite the fact that the AS, early and mature biofilm in each MBR harbored a large number of unique OTUs (Figure 2.10), those found in only one of the three samples, the percentage of shared OTUs between the different samples (i.e. AS, Early and Mature) within each MBR plant was high ranging from 17.15%-41.46%. These shared OTUs comprise a high fraction (52.01%-94.99%, averaging 85.74%) of the total number of reads (Table 2.4). Also, the shared OTUs correspond to the dominant OTUs (32 to 79 reads per OTU; averaging 57 reads per OTU) in each MBR plant, whereas the unique OTUs correspond to the rare OTUs (2 to 4 reads per OTU; averaging 3 reads per OTU).

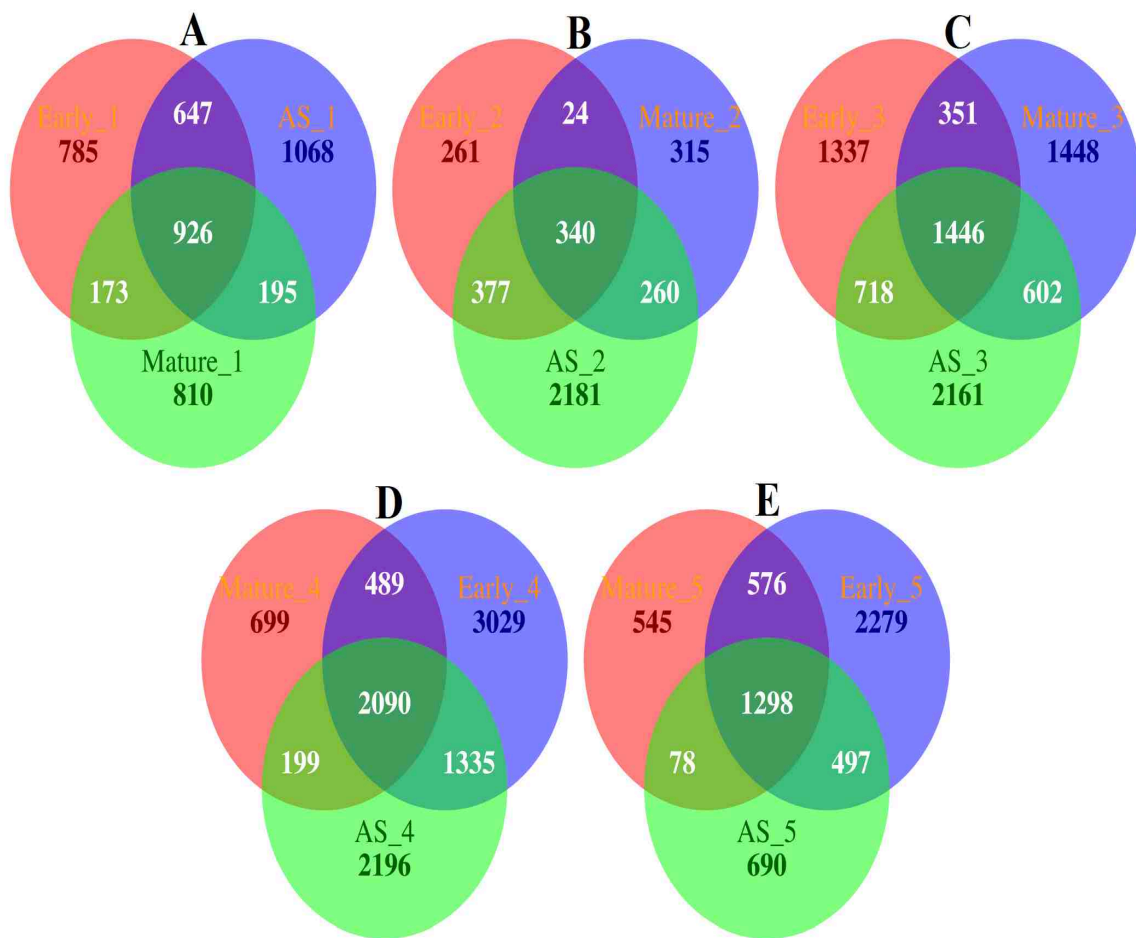


**Figure 2.10.** Venn diagram showing the shared and unique OTUs in each MBR plant. A: MBR 1, B: MBR 2, C: MBR 3, D: MBR 4, E: MBR 5.

### 2.3.5. Effect of source community

To estimate the probability that the biofilm communities (early and mature) represent random samples of their respective AS communities, the biofilm communities were compared to 1000 random subsamples of the AS communities.

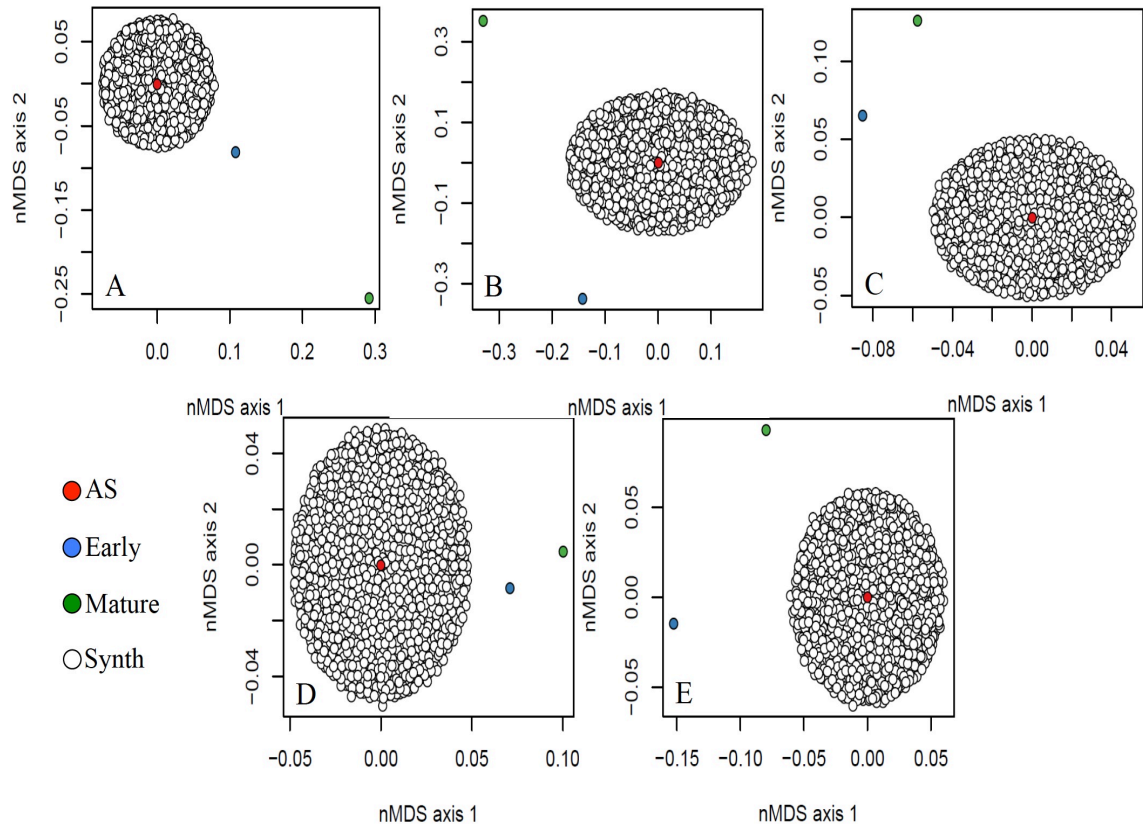


**Figure 2.11.** NMDS analysis, visualizing the results of a random sampling procedure, to estimate the probability that the biofilm communities (Early and Mature) represented random samples of their respective AS communities. A total of 1000 random subsamples of the AS communities were assembled for each MBR. Five examples; A: MBR 1, B: MBR 2, C: MBR 3, D: MBR 4, and E: MBR 5 are shown, to illustrate the distribution of the randomly produced AS communities in relation to the biofilm community. White, red, blue, and green circles represent the random subsamples of the AS community, the AS community, the early biofilm community, and the mature biofilm community. NMDS was calculated based on the Horn Index. Plotted NMDS values were selected from ten independent random starting positions. The minimum stress values for each MBR ranged from 0.44 to 0.46.

The results were visualized on NMDS plot based on the Horn Index (Figure 2.11). In all five MBRs, the biofilm differed significantly from the random assemblages ( $P < 0.001$  for each MBR), indicating that the biofilm communities are unlikely to represent a random sample of the suspended community.

#### **2.4. Discussion**

Despite the numerous studies on characterizing the biofilm microbial community in MBRs [1, 4, 7, 12, 13, 14, 15, 16, 17, 18], we still know little of the bacteria in wastewater treatment plants that cause biofouling. This is mainly due to the fact that the majority of these studies were conducted in lab-scale MBRs where conditions are not as complex as in full-scale systems, and most importantly the dominant biofouling communities detected in these studies (Table 2.5) were different, which raises the question of whether a core or common biofouling community exists in MBR treatment plants. Nevertheless, all these studies concluded that the biofouling community (early and mature) was significantly different from the AS community, which indicate the existence of a specific biofouling community, and biofouling control strategies should mainly focus on these biofouling communities [1, 16]. Also, some researchers suggested that targeting the early colonizers could help in preventing biofouling [7, 15, 17].

Our results are in agreement with previous studies, where *Proteobacteria* was the dominant phylum detected on the biofouled MBR membranes [1, 4, 7, 12, 13, 15, 18]. Other phyla including *Bacteroidetes* [4, 13] and *Actinobacteria* [15, 18] have also been reported to be among the dominant biofouling communities.

**Table 2.5.** Dominant microbial communities identified on biofouled membranes.

System Type and Molecular biology techniques used in the study	Dominant microbial communities on biofouled membranes	Ref
Three polymeric MF flat-sheet membranes: PES, PTFE and PVDF inserted in a lab-scale reactor containing AS and operated in batch mode without feed [454 pyrosequencing]	<i>Gamma-</i> and <i>Betaproteobacteria</i> dominant on all three membranes	[14]
Lab-scale MBR with hydrophilic PVDF hollow-fiber fed synthetic WW [454 pyrosequencing]	Genera <i>Enterobacter</i> and <i>Dyella</i> were closely associated with initial and late biofouling	[16]
Lab-scale MBR with double-flat sheet membranes fed with synthetic WW containing molasses [T-RFLP and clone library analysis of 16S rRNA gene]	25 pioneer operational taxonomic units (OTUs) belonged to the phyla <i>Firmicutes</i> , <i>Proteobacteria</i> , <i>Bacteroidetes</i> and <i>Planctomycetes</i>	[17]
2 hollow-fiber MF membrane types: PE and PVDF in inclined plate MBR fed with real wastewater [FISH]	PE: TMP increased; <i>Betaproteobacteria</i> increased, <i>Bacteroidetes</i> decreased, <i>Gammaproteobacteria</i> remained stable PVDF: TMP increased; <i>Betaproteobacteria</i> remained stable; <i>Bacteroidetes</i> and <i>Gammaproteobacteria</i> increased when	[13]
MF membrane in lab-scale MBRs treating real WW [DGGE and clone library analysis of 16S rRNA gene]	Phylotypes from the phylum <i>Proteobacteria</i> and <i>Bacteroidetes</i> were dominant at low and high flux	[4]
PE hollow-fiber MF in pilot-scale MBR treating real WW [FISH & 16S rRNA gene clone library analysis]	Aeration rate = 3500 L/h: initial biofilm was composed of <i>Alpha-</i> , <i>Beta-</i> , <i>Gamma-</i> , and <i>Deltaproteobacteria</i> ; Aeration rate = 5000 L/h; <i>Betaproteobacteria</i> significantly increased and became dominant	[1]
Flat-sheet MF membrane in pseudo-continuous stirred-tank and pseudo-plug flow lab-scale reactors treating synthetic paper mill WW [clone library analysis of 16S rRNA gene]	Membrane biofilm: <i>Brevundimonas</i> , <i>Acinetobacter</i> , <i>Sphingomonas</i> , and <i>Aquaspirillum</i> were dominant. <i>Acinetobacter</i> is important in early colonization	[15]
Pilot-scale submerged MBR with hollow-fiber MF membrane for treating real WW [DGGE and clone library analysis of 16S rRNA gene]	<i>Gammaproteobacteria</i> selectively adhered and grow on membrane surface. Low-volumetric organic loads: organisms associated with family <i>Xantho-monadacea</i> of <i>Gammaproteobacteria</i> were predominant	[12]
Lab-scale MBR with flat sheet MF membrane treating synthetic paper mill WW [ARDRA & clone library analysis of 16S rRNA gene]	<i>Alphaproteobacteria</i> ( <i>Brevundimonas</i> and <i>Asticcacaulis</i> ) and <i>Acinetobacter</i> were dominant after 4h of filtration	[7]
Intermittently aerated MBR with hollow-fiber MF membrane treating real WW [Quinone profile analysis]	<i>Pseudomonas</i> , <i>Moraxella</i> , <i>Vibrio</i> , <i>Staphylococcus warneri</i> . <i>Micrococcus</i> sp. and <i>Nocardia</i> sp.	[18]
Continuously aerated submerged MBR treating real WW [Quinone profile analysis]	<i>Paracoccus</i> sp. and <i>Flavobacterium</i> sp.	[18]

rRNA: ribosomal RNA; T-RFLP: terminal restriction length polymorphism; FISH: fluorescent in situ hybridization; DGGE: denaturing gradient gel electrophoresis; ARDRA: Amplified Ribosomal Dextroynucleic acid Restriction Analysis; WW: Wastewater.

Similar to the aforementioned studies we observed significant differences in the community structure between the AS and early (after only 5 h of filtration) and mature biofilm samples from the 5 full-scale MBR plants (Figure 2.6). This difference was mainly attributed to the presence of a large number of unique OTUs in each sample (Figure 2.10). These unique OTUs represent the rare OTUs in the community as they correspond to a small fraction of the total sequence reads in each MBR plant. However, this does not suggest that these rare OTUs are of little importance to the community as a whole. Musat et al. (2008) showed that the least abundant species (~0.3% of the total cell number) contributed to more than 40% and 70% of the total uptake of ammonium and carbon, respectively in the oligotrophic, meromictic Lake Cadagno [31]. In contrast, a high percentage of sequence reads was shared between the AS and biofilm samples (early or mature) in each MBR plant (Table 2.4) and these shared sequence reads mainly belong to the dominant OTUs and genera in these samples. For example, the 20 most abundant genera detected in AS samples (Figure 2.8) were also found in the early and mature biofilms, but their relative abundance varied between the samples (i.e. AS, early and mature). The fact that a large fraction of sequence reads was shared between the source community (i.e. AS) and biofilm communities suggests that the AS community contributed to the assembly of biofilms on the membrane surfaces of full-scale MBRs. These results are in agreement with a previous study on seawater reverse osmosis (SWRO) desalination plants from different geographical locations, where the biofouling communities on the SWRO membranes best resembled the source seawater microbes [32]. Furthermore, we found that random immigration of OTUs from the source

community was unlikely to shape the community structure of biofilms (Figure 2.11). This suggests that the local environmental, operational and biotic conditions on the membrane likely selected microorganisms from AS for biofilm formation. This species sorting by local conditions resulted in the presence of unique OTUs (rare taxa) on the early and mature biofilms and in different relative abundances of shared OTUs (dominant taxa) between the source community and biofilms. Previous studies showed that species sorting by local environmental conditions was the major mechanism for shaping biofilm community structure in natural environments such as streams [19, 32]. Also, Besemer et al. (2007, 2009) reported that flow velocity is an important parameter that shapes community assembly of biofilms in streams [33, 34].

In MBRs, several operating parameters have been shown to influence the microbial community structure on membrane surfaces. For example, Huang et al. (2008) compared the biofouling communities of identical membranes operated under different fluxes (15 and 30 L/m<sup>2</sup>.h) and solid retention times (SRTs, 8 and 30 d), and they concluded that the imposed membrane flux affected the community structure and composition of biofouling microorganisms [4]. The low-flux (i.e. 15 L/m<sup>2</sup>.h) biofilm communities from the two MBRs operated at different SRTs were related. In contrast, distinct biofilm communities developed on the high-flux MBRs operated at different SRTs. Also, the microbial communities were significantly different between MBRs operated at different fluxes but same SRT [4]. The authors explained this difference in the results between the low and high-flux to the strong convective force that transports bacterial cells towards the membrane surface at higher permeate flux [4]. Miura et al (2007) reported that the shear force induced by aeration over the membrane surface directly influenced the biofouling

community composition where high shear forces selected for *Betaproteobacteria* [1]. Also, studies have shown that membrane surface characteristics (e.g. physico-chemical property, roughness) influenced bacterial biofilm community structure. Also, studies have shown that the biofilm community structure may be affected by the physicochemical properties of polymeric membranes such as hydrophobicity, roughness and surface charge [13, 14]. Collectively, our findings and the results of the aforementioned studies indicate that the local environmental and operational conditions (i.e. deterministic factors) select microorganisms from AS for biofilm formation on membranes in MBRs.

Our results showed that the difference in the community structure between the 5 MBRs (Figure 2.1 and Figure 2.4) was mainly due to the presence of high number of unique OTUs in each sample (Figure 2.9) and these unique OTUs corresponded to the rare taxa in the community. This was also evidenced in the NMDS analysis, which showed that the bacterial communities in the five MBR plants were more dispersed, based on rare OTUs than the total and dominant OTUs (Figure 2.7). Although the shared OTUs between the biofilm samples in the 5 MBRs were less than 2%, these shared OTUs represented the dominant taxa and corresponded to a high fraction of shared sequence reads between the biofilm communities (Table 2.4). Furthermore, our finding showed that 48, 58 and 52 of the classified genera with relative abundance  $\geq 0.1\%$  were shared between AS, early biofilm and mature biofilm samples, respectively. Classification of the 20 most abundant core genera across the 5 MBR plants revealed the presence of genera that are extensively reported in AS, including *Nitrospira*, *Mycobacterium*, *Thauera*, *Dechloromonas*, *Gemmatimonas*, *Gordonia*, *Tetrasphaera*, and *Zooglea* [36, 37, 38, 39] (Figure 2.8). These results suggest that these shared OTUs and genera between the early

or mature biofilms comprise very common biofouling communities in the full-scale MBRs. Zhang et al. (2011) reported that although the SWRO membrane bacterial communities from five desalination plants located in different parts of the world and operated under different conditions were not identical to each other [32], some common dominant biofouling bacteria (*Leucothrix mucor*, and *Ruegeria* species) were observed [32]. Bereschenko et al. (2010) identified *Sphingomonas* spp. as key biofouling organisms that initiated and dominated biofouling in full-scale freshwater reverse osmosis (RO) treatment facility [8]. The larger number of common biofouling communities detected on the membranes of full-scale MBRs compared to freshwater and seawater RO plants is mainly related to differences in the bacterial community diversity and physiology between wastewater and freshwater and seawater, which renders the control of biofouling in MBRs more challenging than RO plants.

Zhang et al. (2012) identified a set of core genera shared by 14 AS treatment plants from distinct geographical locations (Asia and North America), and operated using different process configurations under different conditions and used to treat different type of sewage [39]. Similarly, Wang et al (2012) identified 60 core genera shared by 14 AS wastewater treatment plants from different geographic locations in China and operated under different conditions (dissolved oxygen, temperature, SRT and MLSS) and treated sewage with different characteristics (i.e. chemical oxygen demand, total nitrogen, total phosphorous, pH and conductivity) [38]. The authors reported that wastewater characteristics had the greatest contribution to the bacterial community variance followed by operational parameters and geographic location. In the current study, the 5 MBRs were selected from the same geographic location, treated predominately municipal

wastewater, were equipped with the same type of membrane (KUBOTA flat-sheet MF membranes) that were operated under the same flux and air-scouring rate (personal communication), and sampled at the same time period (December). Therefore, it was not surprising to observe a large percentage of sequence reads to be shared between the AS samples in the 5 MBRs. Nevertheless, the relative abundances of the shared dominant genera between the AS samples varied, possibly due to variations in wastewater characteristics and/or operational parameters (e.g. SRT, HRT). The fact that the structure of the AS communities differed among the 5 MBRs (Figure 2.1 and Figure 2.4) and the biofilm communities also differed is evidence that the difference in the biofilm community was mainly due to differences in the source communities (i.e. AS); and the local environmental and operational conditions (i.e. deterministic factors) on the membrane selected microorganisms from AS for biofilm formation.

### **Acknowledgments**

This work was sponsored by King Abdullah University of Science and Technology (KAUST). We thank Prof. Regina Lamendella for NMDS analysis (Figure 2.11).

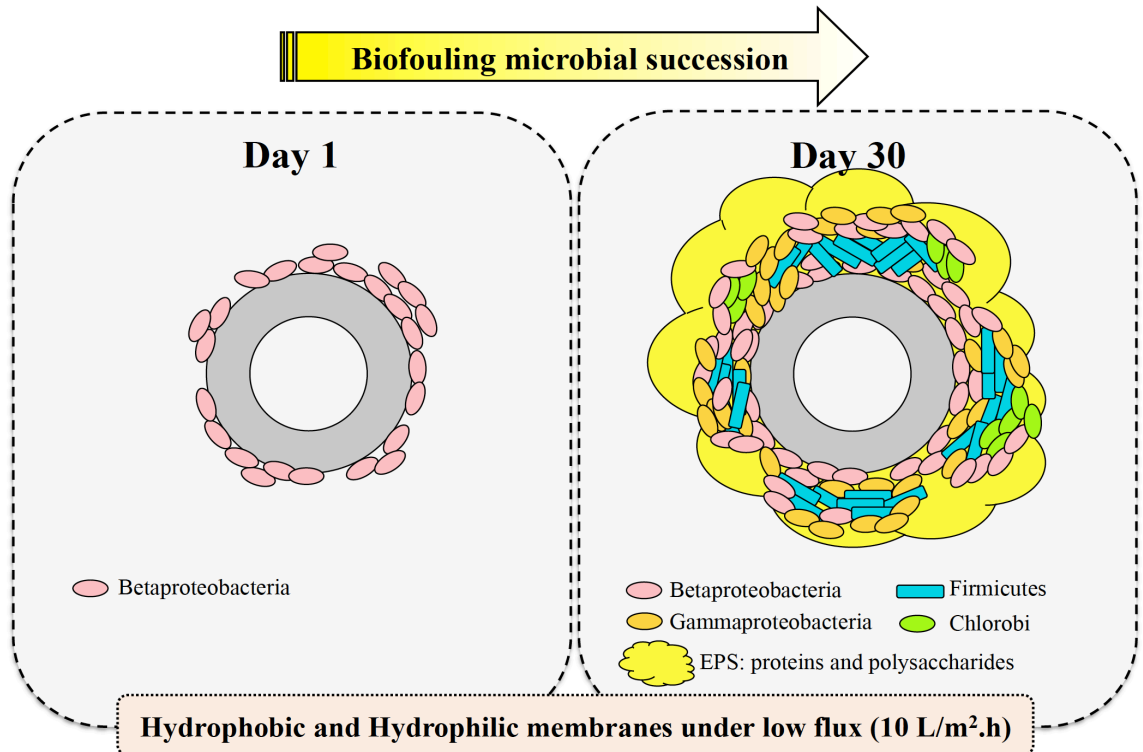
## References

1. Miura, Y., Watanabe, Y., Okabe, S. Membrane biofouling in pilot-scale membrane bioreactors (MBRs) treating municipal wastewater: impact of biofilm formation. **Environ. Sci. Technol.**, v. 41, n. 2, p. 632-638, 2007.
2. Wang, Z., Wu, Z., Tang, S. Extracellular polymeric substances (EPS) properties and their effects on membrane fouling in a submerged membrane bioreactor. **Water Res.**, v. 43, p. 2504-2512, 2009.
3. Liao, B., Bagley, D., Kraemer, H., Leppard, G., Liss, S. A review of biofouling and its control in membrane separation bioreactors. **Water Environ. Res.**, p. 425-436, 2004.
4. Huang, L.N., Wever, H.D., Diels, L. Diverse and distinct bacterial communities induced biofilm fouling in membrane bioreactors operated under different conditions. **Environ. Sci. Technol.**, v. 42, p. 8360-8366, 2008.
5. Malaeb, L., Le-Clech, P., Vrouwenvelder, J.S., Ayoub, G.M., Saikaly, P.E. Do biological based strategies hold promise to biofouling control in MBRs? **Water Res.**, v. 47, n. 15, p. 5447-5463, 2013.
6. Dang, H.Y., Lovell, C.R. Bacterial primary colonization and early succession on surfaces in marine waters as determined by amplified rRNA gene restriction analysis and sequence analysis of 16S rRNA genes. **Appl. Environ. Microbiol.**, v. 66, n. 2, p. 467-475, 2000.
7. Zhang, K., Choi, H., Dionysiou, D., Sorial, G., Oerther, D. Identifying pioneer bacterial species responsible for biofouling membrane bioreactors. **Environ. Microbiol.**, v. 8, n. 3, p. 433-440, 2006.
8. Bereschenko, L.A., Stams, A.J.M., Euverink, G.J.W., van Loosdrecht, M.C.M. Biofilm formation on reverse osmosis membranes is initiated and dominated by *Sphingomonas* spp. **Appl. Environ. Microbiol.**, v. 76, n. 8, p. 2623-2632, 2010.
9. Davey, M.E., O'Toole, O.A. Microbial biofilms. From ecology to molecular genetics. **Microbiol. Mol. Bio. Rev.**, v. 64, p. 847-867, 2000.
10. Costerton, J.W. **The biofilm primer**. [S.l.]: Springer, New York, NY., 2007.
11. Kjelleberg, S., Givskov, M. The biofilm mode of life. **Horizon Biosci.**, p. 5-21, 2007.
12. Jinhua, P., Fukushi, K., Yamamoto, K. Bacterial community structure on membrane surface and characteristics of strains isolated from membrane surface in submerged membrane bioreactor. **Sep. Sci. Technol.**, v. 41, n. 7, p. 1527-1549, 2006.
13. Fontanos, P., Yamamoto, K., Nakajima, F., Fukushi, K. Identification and quantification of the bacterial community on the surface of polymeric membranes at various stages of biofouling using fluorescence in situ hybridization. **Sep. Sci. Technol.**, v. 45, n. 7, p. 904-910, 2010.
14. Lee, S.H., Hong, T.I., Kim, B., Hong, S., Park, H.D. Comparison of bacterial communities of biofilms formed on different membrane surfaces. **World J. Microbiol. Biotechnol.**, v. 30, n. 2, p. 777-782, 2014.
15. Choi, H., Zhang, K., Dionysiou, D.D., Oerther, D.B., Sorial, G.A. Effect of activated sludge properties and membrane operation conditions on fouling characteristics in

- membrane bioreactors. **Chemosphere**, v. 63, p. 1699-1708, 2006.
16. Lim, S.Y., Kim, S., Yeon, K.M., Sang, B.I., Chun, J., Lee, C.H. Correlation between microbial community structure and biofouling in a laboratory scale membrane bioreactor with synthetic wastewater. **Desalination**, v. 287, n. 209-215, 2012.
  17. Piasecka, A., Souffreau, C., Vandepitte, K., Vanysacker, L., Bilad, R., Bie, T., Hellemans, B., Meester, L., Yan, X., Declerck, P., Vankelecom, I. Analysis of the microbial community structure in a membrane bioreactor during initial stages of filtration. **Biofouling**, v. 28, n. 2, p. 225-238, 2012.
  18. Lim, B., Ahn, K., Songprasert, P., Cho, J., Lee, S. Microbial community structure of membrane fouling film in an intermittently and continuously aerated submerged membrane bioreactor treating domestic wastewater. **Water Sci. Technol.**, v. 49, n. 2, p. 255-261, 2004.
  19. Besemer, K., Peter, H., Logue, J.B., Langenheder, S., Lindström, E.S., Tranvik, L.J., Battin, T.J. Unraveling assembly of stream biofilm communities. **The ISME J.**, v. 6, n. 8, p. 1459-1568, 2012.
  20. Caporaso, J.G., Lauber, C.L., Walters, W.A., Berg-Lyons, D., Lozupone, C.A., Turnbaugh, P.J., Fierer, N., Knight, R. Global patterns of 16S rRNA diversity at a depth of millions of sequences per sample. **Proc. Natl. Acad. Sci. USA**, v. 108, n. 4516-4522, 2011.
  21. Tamaki, H., Wright, C.L., Li, X., Lin, Q., Hwang, C., Wang, S., Thimmapuram, J., Kamagata, Y., Liu, W.T. Analysis of 16S rRNA amplicon sequencing options on the Roche/454 next-generation titanium sequencing platform. **Plos One**, v. 6, p. e25263, 2011.
  22. Lu, L., Xing, D., Ren, N. Pyrosequencing reveals highly diverse microbial communities in microbial electrolysis cells involved in enhanced H<sub>2</sub> production from waste activated sludge. **Water Res.**, v. 46, p. 2425-2434, 2012.
  23. Caporaso, J.G., Kuczynski, J., Stombaugh, J., Bittinger, K., Bushman, F.D., Costello, E.K., Fierer, N., Pena, A.G., Goodrich, J.K., Gordon, J.I., Huttley, G.A., Kelley, S.T., Knights, D., Koenig, J.E., Ley, R.E., Lozupone, C.A., McDonald, D., Muegge, B.D., Pirrung, M., Reeder, J., Sevinsky, J.R., Turnbaugh, P.J., Walters, W.A., Widmann, J., Yatsunenkov, T., Zaneveld, J., Knight, R. QIIME allows analysis of high-throughput community sequencing data. **Nature methods.**, v. 7, n. 5, p. 335-336, 2010.
  24. Edgar, R.C. Search and clustering orders of magnitude faster than BLAST. **Bioinformatics.**, v. 26, p. 2460-2461, 2010.
  25. Caporaso, J.G., Bittinger, K., Bushman, F.D., DeSantis, T.Z., Andersen, G.L., Knight, R. PyNAST: a flexible tool for aligning sequences to a template alignment. **Bioinformatics.**, v. 26, n. 2, p. 266-267, 2010.
  26. DeSantis, T.Z., Hugenholtz, P., Larsen, N., Rojas, M., Brodie, E.L., Keller, K., Huber, T., Dalevi, D., Hu, P., Andersen, G.L. Greengenes, a chimera-checked 16S rRNA gene database and workbench compatible with ARB. **Appl. Environ. Microbiol.**, v. 72, n. 7, p. 5069-5072, 2006.
  27. Andrew, D.R., Fitak, R.R., Vega, A.M., Racolta, A., Martinson, V.G., Donstova, K. Abiotic factors shape microbial diversity in Sonoran Desert soils. **Appl. Environ. Microbiol.**, v. 78, n. 21, p. 7527-7537, 2012.

28. Kim, T.S., Jeong, J.Y., Wells, G.F., Park, H.D. General and rare bacterial taxa demonstrating different temporal dynamic patterns in an activated sludge bioreactor. **Appl. Microbiol. Biotechnol.**, v. 97, p. 1755-1765, 2013.
29. Rees, G.N., Baldwin, D.S., Watson, G.O., Perryman, S., Nielsen, D.L. Ordination and significance testing of microbial community composition derived from terminal restriction fragment length polymorphisms: application of multivariate statistics. **Antonie van Leeuwenhoek**, v. 86, p. 339-347, 2004.
30. Ramette, A. Multivariate analyses in microbial ecology. **FEMS Microbiol Ecol**, v. 62, p. 142-160, 2007.
31. Musat, N., Halm, H., Winterholler, B., Hoppe, P., Peduzzi, S., Hillion, F., Horreard, F., Amann, R., Jorgensen, B.B., Kuypers, M.M.M. A single-cell view on the ecophysiology of anaerobic phototrophic bacteria. **Proc. Natl. Acad. Sci. USA.**, v. 105, n. 46, p. 17861-17866, 2008.
32. Zhang, M., Jiang, S., Tanuwidjaja, D., Voutchkov, N., Hoek, E., Cai, B. Composition and variability of biofouling organisms in seawater reverse osmosis desalination plants. **Appl. Environ. Microbiol.**, v. 77, p. 4390-4398, 2011.
33. Wilhelm, L., Singer, G.A., Fasching, C., Battin, T.J., Besemer, K. Microbial biodiversity in glacier-fed streams. **ISME J.**, v. 7, n. 1651-1660, 2013.
34. Besemer, K., Singer, G., Limberger, R., Chlup, A.K., Hochedlinger, G., Hodl, I., Baranyi, C., Battin, T.J. Biophysical controls on community succession in stream biofilms. **Appl. Environ. Microbiol.**, v. 73, p. 4966-4974, 2007.
35. Besemer, K., Singer, G., Hodl, I., Battin, T.J. Bacterial community composition of stream biofilms in spatially variable-flow environments. **Appl. Environ. Microbiol.**, v. 75, p. 7189-7195, 2009.
36. Daims, H., Wagner, M. **Microbial ecology of activated sludge**. [S.l.]: IWA Publishing, London, UK, 2010.
37. Nielsen, P.H., Saunders, A.M., Hansen, A.A., Larsen, P., Nielsen, J.L.. Microbial communities involved in enhanced biological phosphorous removal from wastewater - a model system in environmental biotechnology. **Curr. Opin. Biotechnol.**, v. 23, p. 452-459, 2012.
38. Wang, X., Hu, M., Xia, Y., Wen, X., Ding, K. Pyrosequencing analysis of bacterial diversity in 14 wastewater treatment systems in China. **Appl. Environ. Microbiol.**, v. 78, n. 7042-7047, 2012.
39. Zhang, T., Shao, M., Ye, L. 454 pyrosequencing reveals bacterial diversity of activated sludge from 14 sewage treatment plants. **ISME J.**, v. 6, p. 1137-1147, 2012.

## CHAPTER 3 Microbial Succession and Mature Biofilm Formation on Different Membrane Surfaces Operated Under Low Flux Conditions in a Lab-scale Membrane Bioreactor



Peer reviewed journal article

**Gerald Matar**, Samik Bagchi, Husnul Maab, Wen-Tso Liu, Suzana Nunes, Johannes Vrouwenvelder, Pascal Saikaly (2015). “Microbial Succession and Mature Biofilm Formation on Different Membrane Surfaces Operated Under Low Flux Conditions in a Lab-scale Membrane Bioreactor”. *In preparation*

Abstract, Oral presentation

**G. Matar**, G. Gonzalez-Gil, S. Bagchi, J.S. Vrouwenvelder, S. Nunes, P.E. Saikaly (2015). “Initiation and succession of biofouling communities on hydrophobic and hydrophilic membrane surfaces in a submerged membrane bioreactor.” **250<sup>th</sup> American Chemical Society National Meeting & Exposition**, Boston, MA – USA, August 16-20,2015

Abstract, Oral presentation

**G. Matar**, G. Gonzalez-Gil, S. Bagchi, J.S. Vrouwenvelder, S. Nunes, P.E. Saikaly (2015). “Dynamics and succession of microbial communities on hydrophobic and hydrophilic membrane surfaces in a submerged MBR.” **WEF-EESS ASIA-PACIFIC Wastewater Treatment and Reuse Conference**, Singapore, 28 June–1 July 2015

**ABSTRACT**

Investigating the effect of membrane surface modification on the composition of early colonizers and how they evolve into a mature biofilm has never been addressed in membrane bioreactors. Five different ultrafiltration hollow-fiber membranes having identical nominal pore size (0.1  $\mu\text{m}$ ) but differing in surface hydrophobicity or hydrophilicity were operated simultaneously in the same MBR tank using a flux of 10  $\text{L}/\text{m}^2\cdot\text{h}$ . Identical membrane modules were inserted in the same tank but were operated without permeate flux (0  $\text{L}/\text{m}^2\cdot\text{h}$ ) to investigate the microbial passive adsorption onto different membrane surfaces. Membrane samples and mixed liquor were collected following 1, 10, 20 and 30 d of continuous filtration, and the microbial communities were analyzed with 16S rRNA gene pyrosequencing combined with multivariate statistical analysis. Despite differences in membrane surface chemistry, the hydrophobic or hydrophilic membrane character did not select any specific early bacterial colonizers at the initial stages of filtration, and identical temporal dynamics in the microbial communities were observed on the five different membranes. Pyrosequencing results showed that *Betaproteobacteria* were the most abundant class within the *Proteobacteria* phyla on the five different membranes at days 1 and 10, and *Bacteroidetes* increased in abundance after 10 d of membrane filtration. The relative abundance of *Firmicutes* increased in the biofouling communities at days 20 and 30, possibly due to successional steps that lead to the formation of a mature biofilm. Specific conditions on the membrane surfaces could have recruited the early colonizers from the mixed liquor, which evolved afterwards to form an identical mature biofilm regardless of the membrane surface (i.e.

hydrophobicity, hydrophilicity). Biofilm formation on membrane surfaces could have resulted from natural biofilm formation, initial early colonizers and subsequent development into a mature biofilm.

**Keywords:** membrane biofouling; membrane bioreactor; wastewater treatment; microbial communities; 454-pyrosequencing; hydrophobic; hydrophilic.

### **3.1. Introduction**

Membrane bioreactors (MBR) offer consistent and competent solutions for wastewater treatment and reuse purposes, especially in largely populated cities located away from the seacoast where seawater desalination is not feasible. However, besides membrane channel clogging and membrane screening complications, membrane biofouling remains among the most challenging problem that confronts membrane bioreactors (MBRs) [1], despite the numerous advantages that this technology offers over conventional activated sludge processes (CAS). On the long term, membrane biofouling in MBRs leads to a dramatic increase in the overall operating costs, including an intense escalation in the frequency of chemical and physical cleaning [2, 3] and when irreversible biofouling occurs, membrane modules replacement is inevitable [4].

Biofilm formation, known as biofouling, is a direct result of several successional steps that lead to the development of a mature biofilm. Initially, a conditioning layer composed of polysaccharides [5], proteins [6] and humic substances [7], covers the surface within few minutes. The surface morphology and chemistry affect directly the rate of conditioning layer formation; consequently, it becomes more favorable for the

attachment of pioneer or early colonizers, after they initiate series of physicochemical interactions with the surface [8, 9]. Then, the recruitment of additional microorganisms happens along with cells growth, which all together develop into mushroom-like shapes to provide mechanical durability for the biofilm [10]. These sequential steps have been well investigated in diverse environments, including natural stream rivers [11], marine waters [12, 13], and reverse osmosis [14]. However, studying these successional steps that lead to biofilm formation on membrane surfaces in MBRs is still missing. Moreover, the majority of studies did not characterize the microbial community during early stages of biofilm formation [15, 16, 17, 18, 19], with very few studies that characterized the microbial communities of early colonizers [9, 20, 21].

Several researchers suggested that a better understanding of the microbial composition of early colonizers that initiate biofilm formation on membrane surfaces might assist in the development of better strategies to control biofouling in MBRs [9, 20]. However, only few studies characterized early colonizers in MBRs [9, 20]. On the contrary, the microbial communities of early colonizers that initiate biofilm formation on different artificial surfaces submerged in marine environments have been extensively studied [12, 13, 22, 23, 24, 25, 26]. Also, studies have shown that the composition of early colonizers may be affected by the physicochemical properties of solid surfaces such as surface roughness, hydrophobicity, surface charge, and surface free energy [12, 13, 27, 28].

The effect of physicochemical properties of membrane surfaces in structuring the biofouling microbial community in MBRs is less studied. Lee et al. tested three polymeric microfiltration (MF) flat sheet membranes with varying hydrophobicity;

roughness and surface charge and concluded that surface roughness is an important parameter in shaping the biofouling community [29]. However, they operated their reactor for 15 days in batch and without addition of feeding, and the membranes were operated without filtration. Also, they only characterized the biofouling community at the end of the experiment (day 15). Fontanos et al. reported different microbial community dominance on two polymeric hollow fiber membranes submerged in the same MBR tank [19]. However, in their study they only characterized the bacterial community down to the phyla and proteobacterial class level using fluorescence *in situ* hybridization, and they did not characterize the microbial community during early stages of filtration. Therefore, the objectives of this study were; i) to characterize the community structure and composition of early colonizers that develop on the membrane surfaces of five polymeric ultrafiltration hollow fiber membranes having different hydrophobic and hydrophilic properties, ii) to assess the temporal changes in the biofouling microbial communities on the different membranes; and iii) determine the phylogenetic affiliation of the common bacterial communities that develop on the five membranes. Hydrophobic and hydrophilic membrane modules were operated in parallel in the same MBR tank using a flux of 10 L/m<sup>2</sup>.h, and identical membrane modules were inserted without permeate production to investigate the passive adsorption of microorganisms on different membrane surfaces without the permeate drag force. Membrane samples were collected following 1, 10, 20 and 30 days of continuous filtration, and 20 mL of mixed liquor suspended solids was collected with each membrane sampling event. The microbial community was characterized using high-throughput 16S rRNA gene sequencing combined with multivariate statistical analysis.

## 3.2. Materials and Methods

### 3.2.1. Description of the lab-scale MBR

A lab-scale MBR with a total volume of 20 L was operated using intermittent aeration (30 min aerobic; 30 min anoxic), to achieve simultaneous carbon and nitrogen removal [30]. The operating conditions are summarized in Table 3.1.

**Table 3.1.** Operating conditions of the lab-scale MBR.

	Aerobic phase	Anoxic phase
DO (mg/L)	$8.60 \pm 0.19$	$0.14 \pm 0.07$
pH	$7.80 \pm 0.20$	$7.67 \pm 0.19$
Conductivity (mS)	$3.089 \pm 0.48$	$3.1029 \pm 0.44$
SRT (d)	15	
HRT (h)	12	
Flux (L/m <sup>2</sup> h)	10	
Reactor volume (L)	20	
Aeration cycle	30 min Aerobic / 30 min Anoxic	
Operation	9 min filtration / 1 min relaxation	
MLSS (mg/L)	$3743.58 \pm 311.54$	
MLVSS (mg/L)	$3106.08 \pm 291$	
MLVSS / MLSS	$0.829 \pm 0.035$	
Operating duration (days)	Phase I: 45 d, biomass acclimatization Phase II: 30 d, continuous filtration	

The lab-scale MBR was inoculated with activated sludge collected from a local wastewater treatment plant (Al Ruwais district, Jeddah, K.S.A), and was acclimated to

synthetic wastewater (Table 3.2) for 45 days under continuous filtration mode using commercial ultrafiltration (UF) hollow-fiber membranes (Pall). During acclimation the MBR was operated at a constant flux of 10 L/m<sup>2</sup>.h with a filtration cycle of 9 min followed by 1 min relaxation (no filtration) (Table 3.1). Chemical oxygen demand (COD) and ammonium (NH<sub>4</sub>) were measured in the synthetic wastewater influent and effluent, while nitrate (NO<sub>3</sub>) and nitrite (NO<sub>2</sub>) were measured in the effluent samples only. These measurements were performed using Hach kits (Hach Chemical, USA) according to the manufacturer's protocols.

**Table 3.2.** Synthetic wastewater influent characteristics (in g/L).

<b>Carbon source</b>	
CH <sub>3</sub> COONa.3H <sub>2</sub> O	4.284
<b>Nutrient source</b>	
MgSO <sub>4</sub>	0.216
KCl	0.175
NH <sub>4</sub> Cl	0.236
K <sub>2</sub> HPO <sub>4</sub>	0.091
KH <sub>2</sub> PO <sub>4</sub>	0.035
<b>Trace element solution*</b>	
FeSO <sub>4</sub> .7H <sub>2</sub> O	4.99
CuSO <sub>4</sub> .5H <sub>2</sub> O	1.579
ZnSO <sub>4</sub> .7H <sub>2</sub> O	11
CaCl <sub>2</sub> .2H <sub>2</sub> O	7.35
MnCl <sub>2</sub> .4H <sub>2</sub> O	5.06
CoCl <sub>2</sub> .6H <sub>2</sub> O	1.61
(NH <sub>4</sub> ) <sub>6</sub> Mo <sub>7</sub> O <sub>24</sub> .4H <sub>2</sub> O	1.1
EDTA	50
KOH	3.09

### 3.2.2. Membranes characteristics and sampling frequency

After 45 days of acclimation, five ultrafiltration (UF) hollow-fiber membranes were tested in parallel in the same MBR tank. Four membranes were synthesized in the lab and they were composed of polyoxadiazole (POX), fluorinated polytriazole (PTA), sulfonated polytriazole (SPTA) and sulfonated polysulfone (SPSU), while the fifth tested membrane was a commercial one (COM) provided from PALL corporation (Table 3.3).

**Table 3.3.** Membrane properties and surface characteristics.

Membrane type	Acronym	Membrane properties			Polymer composition and characteristics
		Nominal pore size ( $\mu\text{m}$ )	Contact Angle ( $^{\circ}$ )	Zeta potential (mV)	
Polyoxadiazole	POX	0.1	96.4 $\pm$ 3.2	-28 $\pm$ 1	Very hydrophobic membrane (fluorinated)
Polytriazole	PTA	0.1	85.2 $\pm$ 12.0	-31 $\pm$ 1	Hydrophobic membrane (fluorinated)
Sulfonated Polytriazole	SPTA	0.1	65.4 $\pm$ 7.5	-23 $\pm$ 1	Hydrophilic membrane (sulfonic group)
Sulfonated Polysulfone	SPSU	0.1	54.5 $\pm$ 3.9	-106 $\pm$ 1	Hydrophilic membrane (Sulfonic group)
Commercial Membrane	COM	0.1	n.a.*	n.a.*	Commercial membrane (PVDF)

\*n.a. Not available

The POX and PTA polymers were synthesized and manufactured into hollow fiber membranes following a previously reported procedure [31, 32], and both membranes

were highly hydrophobic due to the fluorinated groups. The SPTA polymer was synthesized according to Ponce et al. [33] and fabricated into a hollow fiber membrane, and polysulfone was sulfonated following a treatment with sulfuric acid and was produced into SPSU hollow fiber membrane. Both SPTA and SPSU membranes owned a hydrophilic character due to the functionalization with sulfonic groups. The four membranes synthesized in the lab were characterized for nominal pore size, contact angle, and surface charge (Table 3.3).

The five membrane modules were constructed following identical procedure, and for each membrane module 12 hollow-fibers were used to achieve a total membrane surface area of 56.5 cm<sup>2</sup> per module. A membrane cassette was designed specifically to contain five different hollow-fiber modules (Figure 3.1), and was submerged into the MBR tank to simultaneously expose different membranes to the same synthetic wastewater and suspended biomass. The five membranes were run in parallel using the same permeate flux of 10 L/m<sup>2</sup>.h, and cycles of 9 min filtration followed by 1 min relaxation (Table 3.1). In addition, identical membrane modules were inserted without permeate production (no flux) to investigate the passive adsorption of microorganisms on different membrane surfaces without the effect of permeate drag force. The membrane modules were run for 1, 10, 20 and 30 d (with and without permeate flux), and membrane modules were sacrificed completely for autopsy and replaced with virgin modules after each run, and 15 mL of mixed liquor suspended solids (MLSS) was collected in parallel to each membrane-sampling event. The trans-membrane pressure was measured with a pressure transducer (68075-32, Cole-Parmer Instrument Company), and recorded using a data acquisition system connected to a computer (LabVIEW, National Instruments).



**Figure 3.1.** Membrane cassette designed to hold simultaneously five different hollow-fiber membrane modules.

### **3.2.3. DNA extraction, PCR amplification and 16S rRNA gene pyrosequencing**

Both DNA and RNA were extracted simultaneously from the membranes and mixed liquor samples using the Mobio PowerBiofilm RNA Isolation kit (MO BIO Laboratories, inc., Carlsbad, CA) with minor modifications, and then the ALLPrep DNA/RNA Mini Kit (Qiagen, Valencia, CA, USA) was used to separate the extracted DNA from RNA according to Ishii et al. [34]. Prior to DNA and RNA extraction of biofilm samples from

membranes, a series of optimization protocols was performed. Initially, the rinsing step of membrane fibers with 1X PBS solution was studied to detect the number of rinsing required to remove the loosely attached bacteria without altering the biofilm forming communities (**Appendix A**). Consequently, the effect of rinsing on the composition and structure of the membrane biofouling communities was investigated for two sets of membranes samples, with rinsing using 1X PBS and without rinsing, as shown in **Appendix A**. For the purpose of this study, the DNA samples were further processed and the RNA samples were stored at  $-80^{\circ}\text{C}$  for future studies. For each membrane-sampling event, total nucleotides were extracted in duplicates from three different fibers that were sacrificed randomly from the membrane modules and cut into small pieces of 1 cm length. The resulting duplicate genomic DNA samples were pooled together as an individual sample, and as a result, a total of 40 membrane samples and four mixed liquor samples were analyzed. The quality (A260/A280) and quantity (A260) of the extracted genomic DNA was determined with a Nanodrop® 1000 spectrophotometer (Thermo Fisher Scientific, Waltham, MA).

For each extracted DNA sample (membrane biofilm and mixed liquor), triplicate PCR reactions was performed in a 25  $\mu\text{L}$  reaction volume using the HotStarTaq Plus Master Mix (QIAGEN, Valencia, CA), 0.25  $\mu\text{M}$  of each primer and 20 ng of template DNA. Bacterial 16S rRNA genes were amplified using the bacteria-specific forward primer 341F (5'-Adaptor A-Barcode-CA Linker- CCTACGGGNGGCWGCAG-3') and reverse primer 805R (5'-Adaptor B-TC Linker- GACTACHVGGGTATCTAATCC-3') [35]. These primers targeted the V4 region of the bacterial 16S rRNA gene. PCR was performed using life technologies veritus thermocycler with the following PCR

conditions: 94°C for 3 minutes, followed by 28 cycles of 94°C for 30 seconds; 53°C for 40 seconds and 72°C for 1 minute; after which a final elongation step at 72°C for 5 minutes was performed. Following PCR, all amplicon products from different samples were mixed in equal concentrations, purified using Agencourt Ampure beads (Agencourt Bioscience Corporation, MA, USA), and pyrosequenced on the Roche 454 FLX Titanium genome sequencer (Roche, Indianapolis, IN) according to the manufacturer's instructions.

#### **3.2.4. Processing of pyrosequencing data**

The 16S rRNA gene amplicons were processed using the QIIME pipeline (Quantitative Insights Into Microbial Ecology v1.7.0) [36]. Initially, all sequences were denoised and filtered for quality check, and then sequence reads were demultiplexed to trim and remove the barcoded primers. All sequence reads that had low quality were removed, including sequences below 200 base pairs (bp) and above 1000 bp, sequences that contained more than 6 ambiguous base pairs and sequences with quality score below 25. Chimera Slayer function as implemented in QIIME was used to identify and remove chimeric sequences.

Sequences were clustered into operational taxonomic units (OTUs) according to the 97% similarity level (3% divergence) using UCLUST [37]. A representative sequence from each OTU was aligned phylogenetically using the PyNAST classifier [38] and assigned to a taxonomic identity using the Greengenes database [39]. The shared OTUs between all biofilm samples collected from day 1 and 30 were visualized using Venn diagram [40]. The distribution of the different bacterial phyla and proteobacterial classes was visualized in a heatmap using R 'vegan scalpel' program.

### **3.2.5. Diversity estimates**

For alpha diversity measurements, both non-phylogeny based metrics (observed OTUs, Shannon diversity index (H) and Chao 1 richness estimator) and phylogeny based metric (phylogenetic diversity (PD<sub>whole</sub>)) were calculated with QIIME at the 3% distance level for each pooled sample using rarefied OTU dataset. Furthermore, dissimilarities between different types of samples were estimated using unweighted UniFrac distance, and the corresponding results were presented using principal coordinate analysis (PCoA). In addition, the beta diversity was measured to assess the dissimilarities between two different samples. Community comparisons between samples was performed with unweighted UniFrac distance (beta diversity) generated in QIIME and visualized by principal coordinate analysis (PCoA) and nonmetric multidimensional scaling (NMDS) using the statistical software PRIMER 6 (version 6.1.13) and PERMANOVA+ add on (version 1.0.3) (PRIMER-E LTD, United Kingdom). To remove inherent heterogeneity of sampling depth, we subsampled the dataset (normalized abundance values) to an even depth of 3,152 sequences across the samples.

## **3.3. Results**

### **3.3.1. Reactor performance and transmembrane pressure measurements**

The concentrations of COD, nitrogen, nitrate and nitrite were measured continuously during both acclimatization and experimental phase (Figure 3.2). The reactor was fed with synthetic wastewater to simulate domestic wastewater with COD concentration of  $404 \pm 8.6$  mg/L COD and  $46 \pm 1.5$  mg/L ammonium. The reactor achieved  $91.93 \pm 2.8$  % COD removal and  $85.85 \pm 6.2$  % nitrogen removal. In the wastewater effluent phase, the

concentrations of Nitrate ( $\text{NO}_3$ ) and Nitrite ( $\text{NO}_2$ ) were  $0.17 \pm 0.09$  and  $0.12 \pm 0.13$  mg/L respectively.

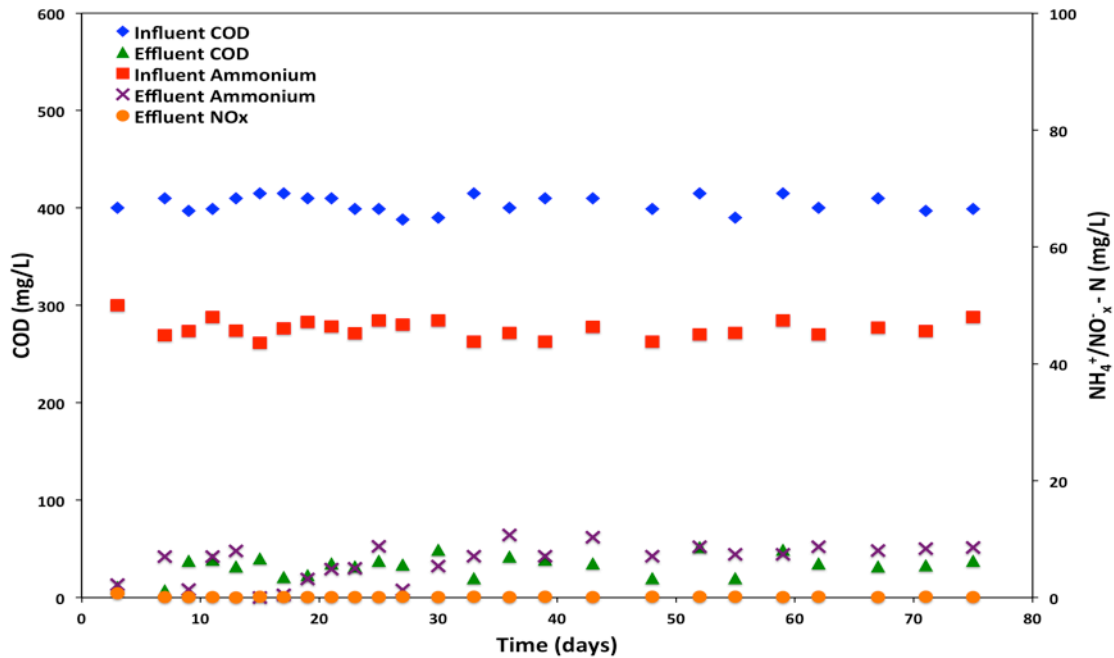


**Figure 3.2.** COD and ammonium concentrations in the synthetic wastewater influent and effluent, and nitrate ( $\text{NO}_3$ ) and nitrite ( $\text{NO}_2$ ) concentrations in the wastewater effluent.

The transmembrane pressure (TMP) was monitored for the five membranes throughout the experiment phase (**Figure 3.3**). For the membranes synthesized in the lab, the TMP of the hydrophobic membranes (POX and PTA) became much higher (reached 80 kPa) than the TMP of hydrophilic membranes (SPTA and SPSU) after one day of filtration. This could be a consequence of the high hydrophobic surface, which favors the adhesion of hydrophobic solutes and leads to a lower effective permeation and higher TMP value (**Figure 3.3**). The commercial membrane showed the lowest TMP during the whole experiment.

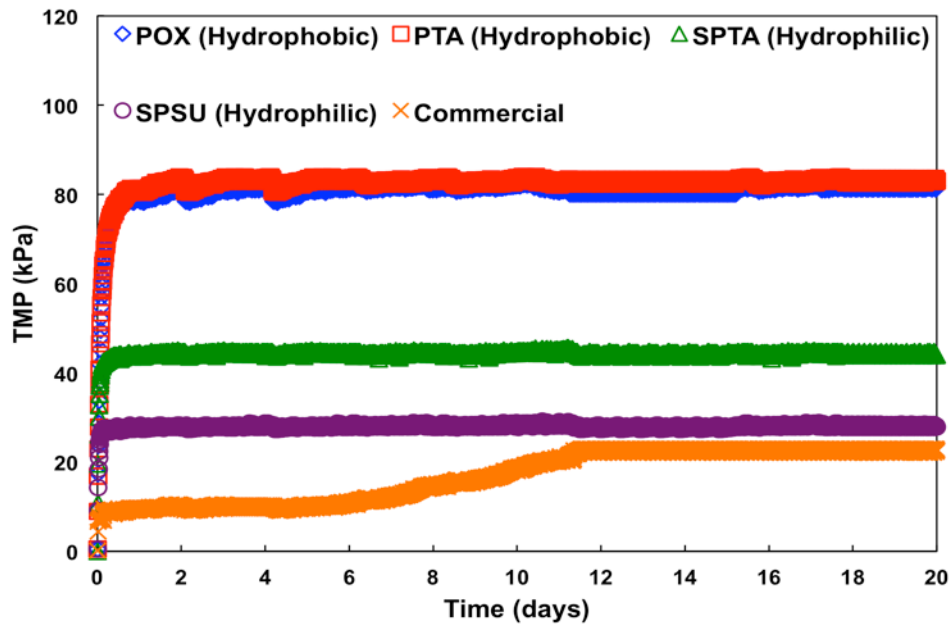


**Figure 3.3.** Transmembrane pressure (TMP) profiles for the five membranes during filtration.

### 3.3.2. Bacterial alpha diversity measures

A total of 366,612 sequence reads were obtained from 40 biofilms and 3 mixed liquor samples, and they were clustered into 43,887 OTUs at 97% similarity level using UCLUST [37]. The mixed liquor sample from day 10 was excluded from the data set since it failed to pass the QA/QC step (very low amplification). Alpha diversity measurements were performed for the different membrane and mixed liquor samples and the results are presented in Table 3.4.

**Table 3.4.** Sequence counts, observed OTUs per sample and alpha diversity measures

Sample Type	Day	Acronym	Sequence counts per Sample	Alpha diversity measures			
				Number of observed OTUs	Richness estimate (Chao 1)	Shannon diversity index (H)	Phylogenetic diversity (PD)
Polyoxadiazole Hydrophobic (Flux)	1	POX.D1	5,674	883	1,802±65	5.93±0.01	65.1±0.55
	10	POX.D10	13,933	1,927	3,622±149	6.51±0.02	127.73±1.15
	20	POX.D20	8,531	1,170	2,379±38	6.51±0.01	100.59±0.27
	30	POX.D30	8,324	1,283	2,808±11	7.05±0.01	109.44±0.18
Polyoxadiazole Hydrophobic (No Flux)	1	POX.D1	6,617	764	1,624±51	4.83±0.01	55.75±0.41
	10	POX.D10	6,820	886	1,780±55	5.27±0.01	72.52±0.61
	20	POX.D20	10,342	905	1,609±8	5.20±0.01	81.14±0.07
	30	POX.D30	7,944	1,063	2,152±59	6.33±0.01	95.7±0.68
Polytriazole Hydrophobic (Flux)	1	PTA.D1	4,618	624	1,243±56	5.19±0.01	49.98±0.64
	10	PTA.D10	10,333	1,195	2,411±5	5.42±0.01	96.53±0.16
	20	PTA.D20	9,769	1,571	3,432±46	7.17±0.01	125.24±0.35
	30	PTA.D30	8,908	1,424	2,890±73	7.16±0.01	117.23±0.77
Polytriazole Hydrophobic (No Flux)	1	PTA.D1	6,266	790	1,631±20	5.24±0.01	62.66±0.22
	10	PTA.D10	9,082	1,272	2,454±54	5.85±0.01	97.05±0.57
	20	PTA.D20	10,378	1,168	1,802±73	5.96±0.01	102.01±0.15
	30	PTA.D30	6,881	945	3,267±65	5.97±0.01	86.36±0.78
Sulfonated Polytriazole Hydrophilic (Flux)	1	SPTA.D1	1,576	256	1,413±46	4.77±0.06	22.49±0.85
	10	SPTA.D10	8,851	1,185	2,174±50	5.87±0.01	93.04±0.27
	20	SPTA.D20	12,276	1,031	1,568±27	4.83±0.02	84.23±0.96
	30	SPTA.D30	8,693	1,446	1,708±44	7.26±0.01	118.86±0.51
Sulfonated Polytriazole Hydrophilic (No Flux)	1	SPTA.D1	5,714	719	1,413±46	5.2±0.01	52.89±0.6
	10	SPTA.D10	7,733	1,078	2,174±50	6.09±0.01	86.34±0.92
	20	SPTA.D20	9,598	849	1,568±27	5.0±0.01	78.69±0.28
	30	SPTA.D30	8,963	887	1,708±44	5.33±0.01	81.42±0.4
Sulfonated Polysulfone Hydrophilic (Flux)	1	SPSU.D1	7,483	861	1,849±46	5.23±0.1	66.9±0.26
	10	SPSU.D10	8,329	1,185	2,338±29	6.52±0.01	91.72±0.22
	20	SPSU.D20	7,729	1,394	2,987±31	7.03±0.01	104.35±0.32
	30	SPSU.D30	10,912	1,355	2,799±44	6.8±0.01	108.18±0.63
Sulfonated Polysulfone Hydrophilic (No Flux)	1	SPSU.D1	9,021	929	1,958±66	5.11±0.01	68.68±0.37
	10	SPSU.D10	7,732	1,149	2,604±69	6.56±0.01	87.94±0.34
	20	SPSU.D20	11,064	1,045	2,046±50	5.34±0.01	89±0.44
	30	SPSU.D30	6,600	932	1,774±45	6.31±0.01	87.26±0.51
Commercial Hydrophilic (Flux)	1	COM.D1	5,420	670	1,431±56	4.95±0.01	53.09±0.44
	10	COM.D10	9,511	1,244	2,666±35	6.53±0.01	101.72±0.32
	20	COM.D20	9,733	1,114	2,122±38	5.79±0.01	92.71±0.46
	30	COM.D30	11,068	1,241	2,324±39	3.08±0.01	100.98±0.5
Commercial Hydrophilic (No Flux)	1	COM.D1	8,211	741	1,545±55	4.57±0.01	53.99±0.6
	10	COM.D10	6,285	812	1,729±19	6.17±0.01	74.54±0.23
	20	COM.D20	9,569	1,105	2,115±31	6.03±0.01	97.81±0.26
	30	COM.D30	10,329	1,183	2,263±5	6.21±0.01	107.45±0.01
Mixed liquor suspended solids	1	MLSS.D1	6,496	821	1,575±38	5.85±0.1	63.75±0.5
	20	MLSS.D20	12,635	830	1,588±35	3.87±0.02	49.58±0.65
	30	MLSS.D30	10,662	838	2,401±97	5.5±0.01	63.94±0.25

Alpha diversity values were the lowest at day 1 for all the membranes tested and increased significantly after 10 days of operation, and remained relatively stable for the majority of the membranes on day 20 and 30. The diversity values across the 40 biofilm samples extracted from the membrane surfaces ranged as follows: observed OTUs (256-1,927), Chao 1 (1,243-3,622), H (3.08-7.05) and PD (22.49-127.73) (Table 3.4). The diversity of the biofilms on the membranes did not seem to change much between days 20 and 30 for most of the membranes (Table 3.4). In addition, the diversity of microbial communities was not significantly different between the hydrophobic and hydrophilic membranes ( $p = 0.1775$ ), and between the membranes operated with and without flux ( $p = 0.0696$ ). On the other hand, the diversity of the mixed liquor was more stable compared to membrane biofilm samples, and it ranged as follows: observed OTUs (821-838), Chao 1 (1,575-2,401), H (3.87-5.85) and PD (49.58-63.94) (Table 3.4).

### **3.3.3. Effect of membrane surface chemistry on the microbial community structure of early colonizers**

Results showed similar composition at the family level of the early colonizers on the five different membranes operated with and without permeate flux, where *Comamonadaceae* was the most abundant family (averaging  $78.6 \pm 3.78\%$ ) detected on all the membranes, followed by *Rhodocyclaceae* ( $10.00 \pm 2.27\%$ ), and *Pseudomonadaceae* ( $4.90 \pm 2.98\%$ ), (Figure 3.4). The composition of the MLSS on day 1 was similar to the early colonizers, and *Comamonadaceae* was the most abundant family (62.2%), followed by *Rhodocyclaceae* (20.3%), and *Pseudomonadaceae* (5.8%) (Figure 3.4).

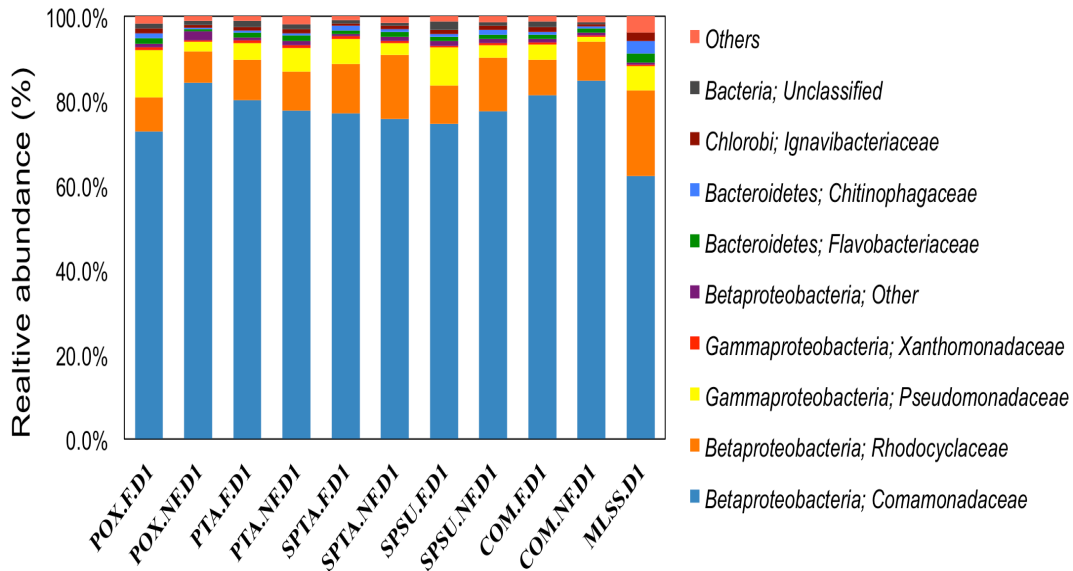


**Figure 3.4.** Classification at the family level of the early colonizers that attached to the hydrophobic and hydrophilic membranes after 1 day of operation, under  $10 \text{ L/m}^2\cdot\text{h}$  flux and without permeate flux. The POX (Polyoxadiazole), PTA (Polytriazole), SPTA (Sulfonated polytriazole), SPSU (Sulfonated polysulfone) and COM (commercial membrane) membranes were operated under  $10 \text{ L/m}^2\cdot\text{h}$  flux (F) and without permeate flux (noF). MLSS correspond to the mixed liquor suspended solids sample, and D1 corresponds to the samples collected at the day 1. Others refer to bacterial family with relative abundance  $< 1\%$ .

A Venn diagram was generated to visualize the shared and unique OTUs for the five different membranes operated with  $10 \text{ L/m}^2\cdot\text{h}$  flux, at day 1 (Figure 3.5). Among a total of 1,563 OTUs only 54 OTUs were shared between the 5 membranes at day 1 and this corresponds to 3.45% (Figure 3.5). In addition, NMDS based on Unweighted Unifrac distance revealed that the microbial communities of primary colonizers, clustered together at day 1 regardless of the membrane type or flux (Figure 3.6).

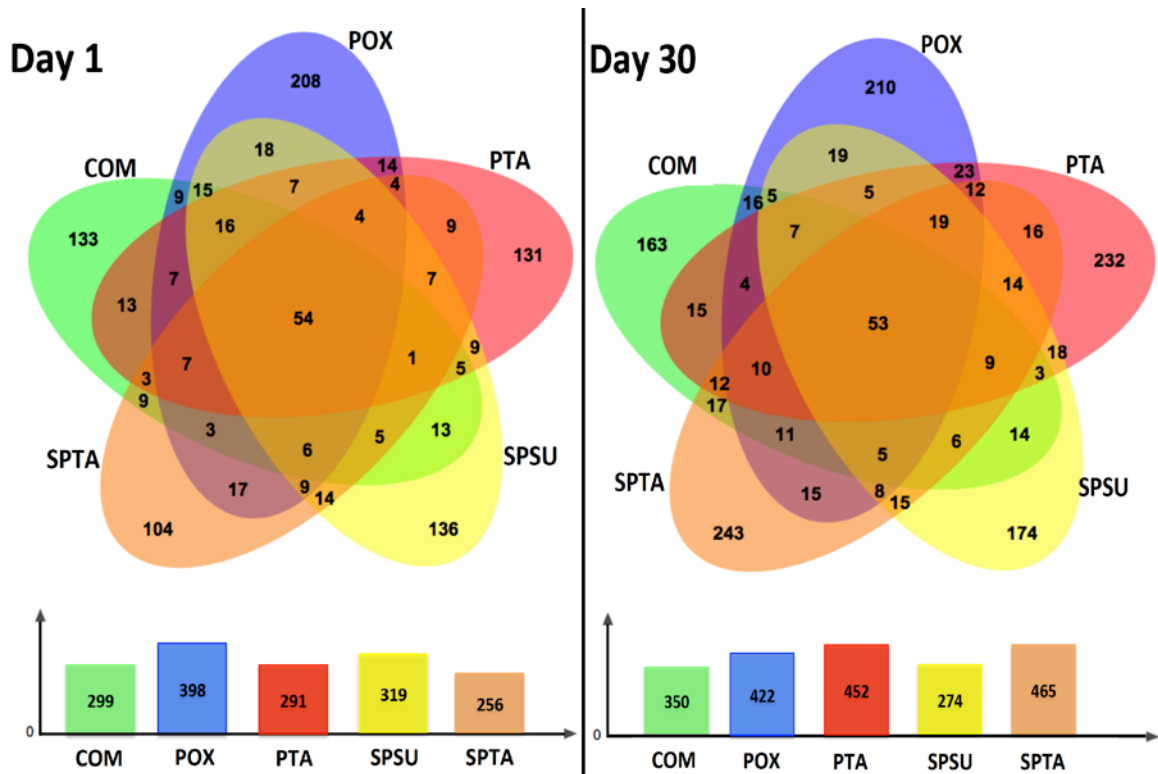


**Figure 3.5.** Venn diagram representing the core shared OTUs between all biofilm samples extracted from the five different membranes operated with  $10 \text{ L/m}^2\cdot\text{h}$  at day 1 (left) and day 30 (right), respectively. The horizontal axis represents the OTUs number corresponding to each membrane type.

The number of shared OTUs and shared sequences within the same membrane operated with ( $10 \text{ L/m}^2\cdot\text{h}$ ) and without ( $0 \text{ L/m}^2\cdot\text{h}$ ) flux are presented in Table 3.5. For the early colonizers (day 1), the percentage of shared OTUs ranged between 18.0% to 22.0%, which corresponded to 81% and 85.0 % of the total number of sequences that were shared between the same membrane type operated with and without flux (Table 3.5).

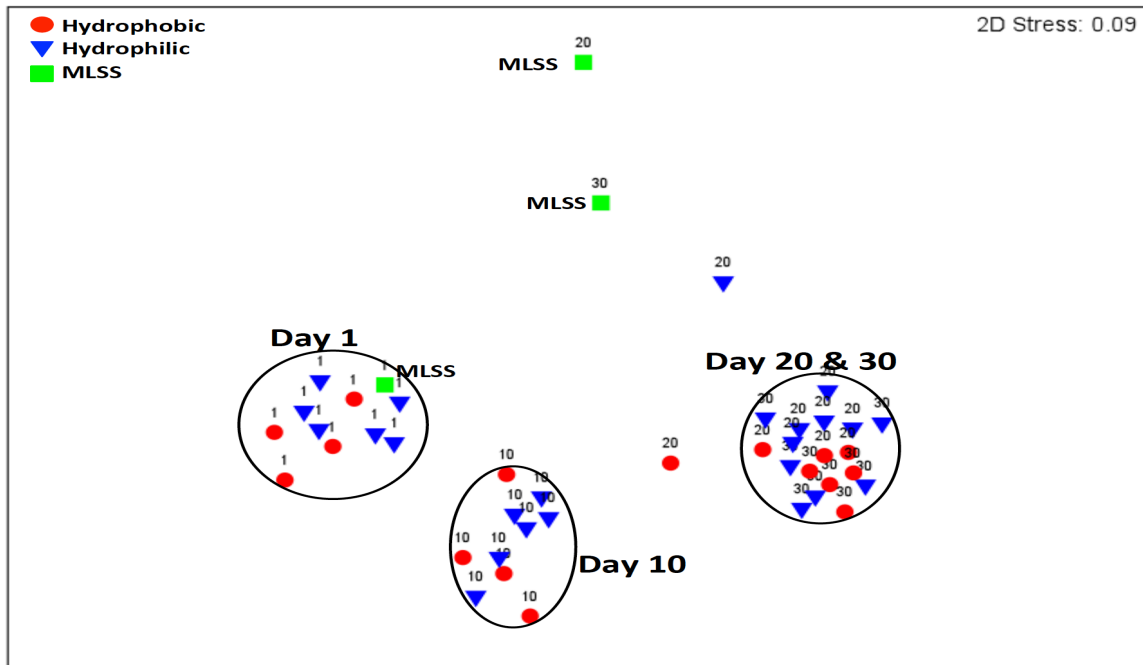


**Figure 3.6.** Non-metric Multi-Dimensional Scaling (NMDS) based on unweighted Unifrac distance for the genomic DNA extracted from the five different membranes operated with a permeate flux of  $10 \text{ L/m}^2\cdot\text{h}$  and without permeate production ( $0 \text{ L/m}^2\cdot\text{h}$ ). The numbers from 1 to 30 correspond to the date of sample collection. Red circles correspond to hydrophobic membranes, blue triangles correspond to hydrophilic membranes, and green squares correspond to MLSS samples. The MLSS sample from day 10 was excluded from the data set because it did not amplify properly.

### 3.3.4. Microbial community succession

Similar temporal changes in the biofilm bacterial community structure was observed for the five different membranes as revealed by NMDS (Figure 3.6). NMDS (Figure 3.6) revealed that the microbial communities clustered into three different clusters according to their percentage of similarity. Biofilm samples from days 1 and 10 formed two different clusters while all biofilm samples from days 20 and 30 clustered into one single group, except for the two outliers from day 20 (Figure 3.6).

**Table 3.5.** Shared OTUs and sequences between membranes operated under flux (10 L/m<sup>2</sup>.h) and no flux (0 L/m<sup>2</sup>.h)

	Shared OTU and Sequences between Flux and No Flux samples*	OTU			Sequences		
		Total	Shared	Shared (%)	Total**	Shared	Shared (%)
Day 1	POX	582	108	18.0	3,152	2,568	81.0
	PTA	501	111	22.0	3,152	2,689	85.0
	SPTA	483	100	20.7	3,152	2,645	83.9
	SPSU	523	106	20.0	3,152	2,643	83.8
	COM	470	101	21.5	3,152	2,728	86.5
Day 10	POX	915	116	12.7	3,152	2,460	78.0
	PTA	867	119	13.7	3,152	2,550	80.9
	SPTA	876	120	13.7	3,152	2,518	79.9
	SPSU	910	130	14.3	3,152	2,506	79.5
	COM	823	109	13.2	3,152	2,517	79.8
Day 20	POX	740	93	12.5	3,152	2,529	80.2
	PTA	925	115	12.4	3,152	2,336	74.1
	SPTA	651	104	16.0	3,152	2,721	86.3
	SPSU	829	84	10.1	3,152	2,342	74.3
	COM	778	102	13.1	3,152	2,511	79.6
Day 30	POX	943	136	14.4	3,152	2,477	78.6
	PTA	989	144	14.5	3,152	2,465	78.2
	SPTA	882	115	13.0	3,152	2,447	77.6
	SPSU	859	106	12.3	3,152	2,462	78.1
	COM	829	102	12.3	3,152	2,460	78.0

\*The shared OTUs and sequences correspond to each pair or samples from the same membrane, operated under flux (10 L/m<sup>2</sup>.h) and no flux (0 L/m<sup>2</sup>.h)

\*\*Total sequences were normalized to 3,152 sequences for all the samples

In addition, the mixed liquor sample from day 1 was closely related to the cluster from day 1, while mixed liquor samples from days 20 and 30 were distant from the common cluster of days 20 and 30. These results propose that the biofilm reached mature phase on the membrane surface after 20 d of filtration (Figure 3.6), and its composition was distinct from the mixed liquor's composition. Similar results were obtained with hierarchical clustering (Figure 3.7) where biofilm samples clustered together according to the sampling day without any clear impact of the membrane surface character

(hydrophobic or hydrophilic), or the imposed operating condition (with flux of 10 L/m<sup>2</sup>.h or without flux 0 L/m<sup>2</sup>.h). All Samples from days 1 and 10 clustered together into two distinct groups, while all biofilm samples from days 20 and 30 assembled together into one separate cluster (Figure 3.7).

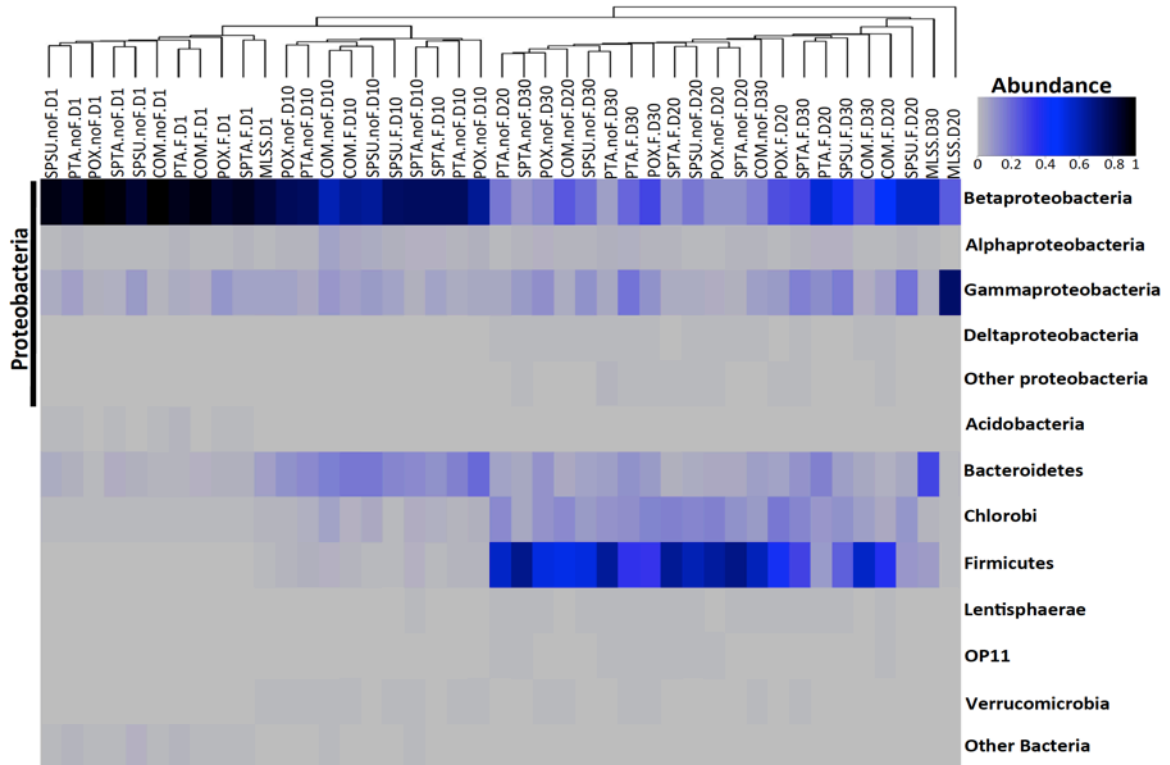


**Figure 3.7.** Heat map distribution of bacterial phyla and proteobacterial classes derived from 40 biofilm and three mixed liquor samples. The color intensity in each cell reflects the abundance of class/phylum in the corresponding sample, light gray corresponds to low abundance and dark blue and black corresponds to higher abundance, respectively. Hierarchical clustering on the top was created using unweighted-pair group method using arithmetic means (UPGMA). POX (Polyoxadiazole), PTA (Polytriazole), SPTA (Sulfonated polytriazole), SPSU (Sulfonated polysulfone) and COM (commercial membrane) membranes were operated under 10 L/m<sup>2</sup>.h flux (F) and without permeate flux (noF). MLSS correspond to the mixed liquor suspended solids sample. Other bacteria refer to phyla with relative abundance < 1%. D1, D10, D20 and D30 refer to sampling days 1, 10, 20 and 30, respectively.

A Heat map was generated to present the relative abundances of bacteria classified at the phyla level and classes that belong to the phylum *Proteobacteria* (Alpha; Beta; Gamma; and *Deltaproteobacteria*) (Figure 3.7). Sequence reads belonging to the class *Betaproteobacteria* were abundant on day 1 and 10. However, their relative abundance decreased on day 20 and 30, and sequence reads belonging to the phylum *Firmicutes* and *Chlorobi* became dominant on day 20 and 30.

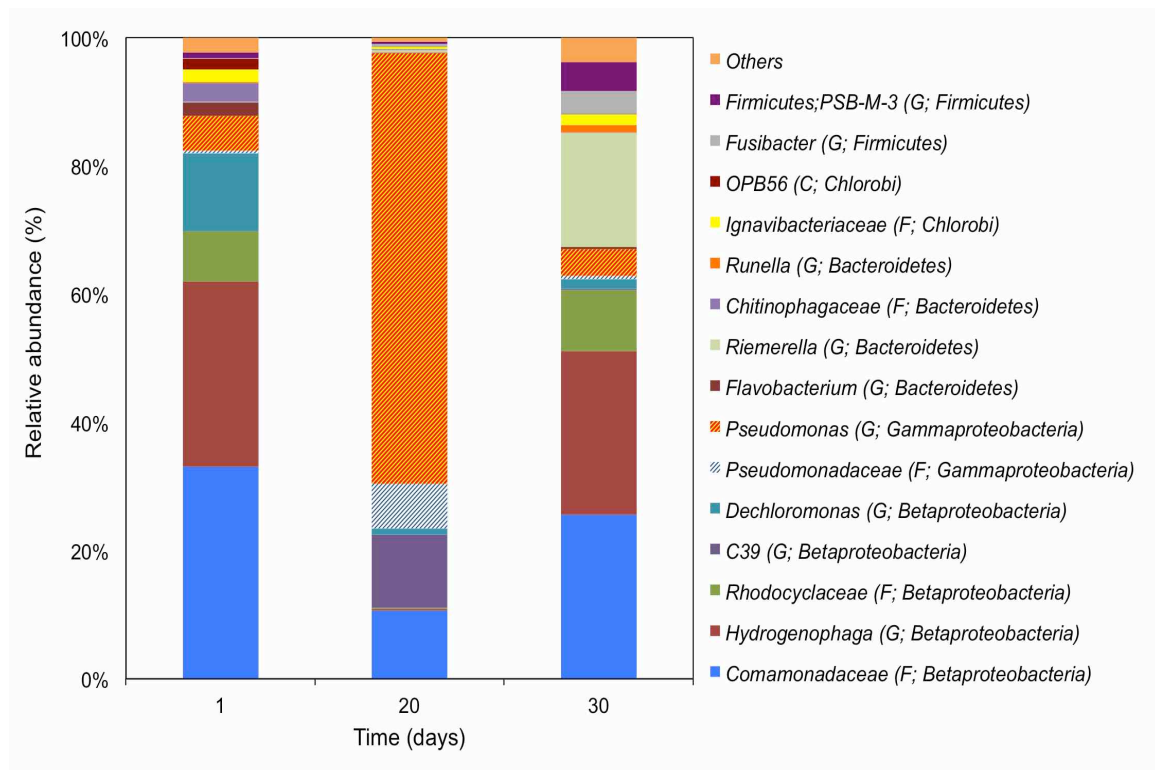


**Figure 3.8.** The relative abundance and phylogenetic classification of the different genera and family detected in the MLSS. The letters F, G and C correspond to family, genus and class, respectively. The corresponding phyla and proteobacterial class is presented in bracket.

On the other hand, the composition of the MLSS evolved differently than the biofilms on the membrane surfaces. The relative abundance and phylogenetic classification of

genera and family in the MLSS showed that at day 1, *Comamonadaceae* was the most abundant family (33.1%) followed by *Rhodocyclaceae* (7.9%) (Figure 3.8). However, at day 20 the relative abundance of family *Comamonadaceae* and *Pseudomonadaceae* decreased and reached 10.6% and 7.0%, respectively (Figure 3.8). On the genus level, the relative abundance of *Pseudomonas* increased at day 20 and reached 67.2%, followed by genus *C39* (11.4%). Then, at day 30 the relative abundance of family *Comamonadaceae* and *Rhodocyclaceae* increased and reached 25.6% and 9.5%, respectively (Figure 3.8). These results suggest that the succession on the membrane surfaces occurred independently from the variations in the composition of MLSS with time.

The phylogenetic classification and relative abundance of the 10 most abundant shared OTUs between the 5 membranes operated at 10 L/m<sup>2</sup>.h flux is presented in Figure 3.9. The family *Comamonadaceae* dominated the composition of the 10 most abundant OTUs at day 1 (65.59%). The relative abundance of the genus *Hydrogenophaga* (class *Betaproteobacteria*) decreased with time from 18.38% at day 1 to 3.96% on day 30, whereas the relative abundance of the genus *Pseudomonas* increased from 5.03% (day 1) to 10.20% (day 30) (Figure 3.9). The genus *Dechloromonas* was only detected on day 1. Interestingly, two genera (*Fusibacter* and *PSB-M-3*) belonging to the phylum *Firmicutes* and one genera (*C39*) belonging to the class *Betaproteobacteria* that were not detected on the membranes on day 1 and 10, became dominant on day 20 and 30. These results highlight clear temporal dynamics in the shared biofouling communities that developed with time on the five different membranes and evolved into a mature biofilm dominated by members belonging to the phylum *Firmicutes* (Figure 3.9).

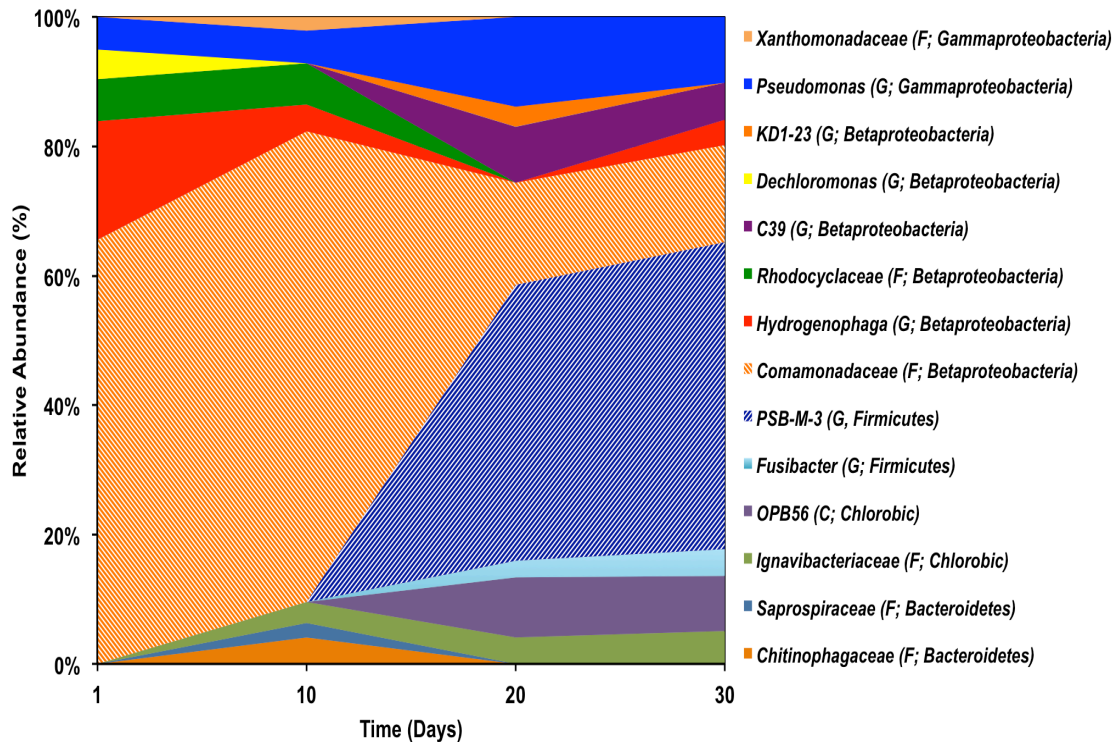


**Figure 3.9.** The relative abundance and phylogenetic classification of the top 10 dominant shared OTUs between the five different membranes operated with 10 L/m<sup>2</sup>.h flux. The letters F, G and C correspond to family, genus and class, respectively. The corresponding phyla and proteobacterial class is presented in bracket.

### 3.3.5. Shared OTUs

The number of shared OTUs and sequences between the same membrane operated with (10 L/m<sup>2</sup>.h) and without (0 L/m<sup>2</sup>.h) flux are presented in Table 3.5. The percentage of shared OTUs was low ranging from 10.1% to 22.0%. However, these shared OTUs comprise a high fraction of the total number of sequences (74.3% -85.0 %; averaging 80.1 ± 3.4%) that were shared between the flux and no flux membranes throughout the experimental period (Table 3.5). By comparing the ratio of the number of reads to the number of OTUs for each membrane type, the shared OTUs correspond to the dominant OTUs (17 to 28 reads per OTU; averaging 23 reads per OTU; Abiotic factors shape

microbial diversity in Sonoran desert soils [41]), whereas the non-shared OTUs correspond to the rare OTUs (averaging 1 read per OTU) [41]. This suggests that those shared OTUs represent the dominant biofouling community in the flux and no flux biofilms.

A Venn diagram was generated to visualize the shared and unique OTUs for the five different membranes operated with 10 L/m<sup>2</sup>.h flux, at days 1 and 30 respectively (Figure 3.5). Of the 1,563 and 1,963 total observed OTUs, only 54 OTUs (3.45%) and 53 OTUs (2.69%) were shared between all the biofilm samples at day 1 and 30 (Figure 3.5). These results suggest that the shared OTUs at day 1 might contribute to the initiation of biofilm formation regardless of the membrane type.

### **3.4. Discussion**

#### **3.4.1. Composition of the early colonizers**

Understanding the successional steps that lead to the formation of a mature biofilm has gained lots of interests in several environments, to develop enhanced antifouling strategies. Many researchers characterized the community structure of early colonizers that attach to solid surfaces submerged in different environments and quickly produce EPS that modify the surfaces' characteristics. For instance, Dang and Lovell assessed the diversity of early colonizers on hydrophobic and hydrophilic surfaces during 24 – 72 h of static adhesion in marine environments, and concluded that materials' physicochemical properties might affect early bacterial attachment and succession [12]. Grasland et al. focused on the surface properties of bacterial cells and studied their interactions with antifouling coatings during 3 – 6 h. They concluded that bacterial surface hydrophilicity

is responsible for the interactions with different surfaces [22]. Briand et al. assessed the diversity and abundance of marine bacterial and microphytobenthic communities that formed on surfaces coated with different materials (biocidal and non biocidal) and immersed in two different coastal locations. Their results confirmed that biofilm formation occurred on all coated samples irrespective of the geographical site or the applied coating material (biocidal-free and biocidal), and the microbial communities displayed significant variations in the richness of the bacterial communities according to biocide-free and biocidal coatings [24]. Membrane surface modification to reduce or potentially delay membrane biofouling has gained a lot of merit. For instance, polymeric membranes were embedded with silver nanoparticles (nAg) [42, 43] that prohibited microbial communities from attaching on membrane surfaces. In addition, Li et al. [44] and Zhang et al. [45] modified the hydrophilic and hydrophobic membrane surface character, and both studies reported a reduction in the attachment of fouling particles on membrane surfaces. However, the effect of these modified surfaces on the composition of early colonizers has not been reported.

Our results showed that the community composition and structure of early colonizers was the same on the 5 different membranes at day 1 (Figure 3.4), and the diversity of the early colonizers (day 1) ranged as follows: observed OTUs (256-929), Chao 1 (1,243-1,958), H (4.57-5.93) and PD (22.49-68.68) (Table 3.4). These results are not in agreement with previous findings reported on modified surfaces inserted in marine environments, which confirmed that modified surfaces affected the composition of early colonizers possibly due to oligotrophic conditions in seawater [12, 22, 24]. In this study, the composition of early colonizers on modified membrane surfaces was similar possibly

due to the conditioning layer that could have formed quickly in a nutrient rich environment such as wastewater. Once conditioned, the initial fouling layer mask the effect of membrane surface and facilitates the attachment of early colonizers [46]. The effect of membrane surface on biofouling formation has been studied during initial stages of membrane biofouling [47]. In addition, Fontanos et al. concluded that the membrane material and configuration affect the microbial community composition and they reported differences in the relative abundances of the biofouling microbial communities according to the membrane type [19]. Furthermore, Lee et al. concluded recently that membrane surface roughness played an important role and affected greatly the distribution of biofouling microbial communities on membranes [29]. However, Fontanos et al. [19] and Lee et al. [29] characterized the composition of the biofilm after 12 and 15 d, without characterizing the composition of early colonizers.

The composition of early colonizers was similar on the five different membranes, yet these membranes exhibited different TMP profiles (**Figure 3.3**). It is possible that membrane modifications affected the cell density without altering the composition of early colonizers. Previously, Camps et al. demonstrated using flow cytometry measurements that the microbial communities displayed high densities on all types of coatings [26]. The relative abundances of microbial communities responsible for biofouling formation varied according to the type of coating, yet it was clear that the microorganisms displayed higher densities on coatings that were biocide-free compared to the remaining other coatings [26]. In a different study on biofouling in MBRs, Miura et al. correlated positively the increase in TMP to the gradual biofilm development on membrane surfaces [15]. In addition, *Betaproteobacteria* contributed to the formation of

mature biofilms and led to irreversible membrane biofouling and an increase in the TMP on polyethylene membrane (PE) [15]. Similarly, Fontanos et al. reported that the relative abundance of *Betaproteobacteria* increased on a polyethylene (PE) membrane when the TMP increased [19]. While characterization of the microbial communities on membrane surfaces could predict the performance of the membranes in terms of TMP behavior, additional parameters like biofilm thickness and density should be considered. Furthermore, future studies that aim to evaluate the effectiveness of membrane modifications to control biofouling should include measurements of cell density using flow cytometry (FCM) to potentially correlate the results with the TMP.

The composition of early colonizers was different from the mixed liquor at day 1 (Figure 3.4). These results oppose previous findings in lab-scale [9, 21] and full-scale (Seattle project, Chapter 2) MBR studies, which reported that the composition of early colonizers was different from the mixed liquor suspended solids. In our previous work (Seattle project), the same type of membrane was used but the composition of the wastewater was different according to different full-scale MBR plant, while in the current study five different membranes were tested in parallel using the same conditions (flux of 10 L/m<sup>2</sup>.h). In this study, it is possible that the successional steps that changed the composition of biofouling communities afterwards happened at slower pace compared to previously reported findings by Zhang et al. (4 h), Piasecka et al. (1 d) and in the Seattle project (5 h) [9, 21]. Furthermore, at later stages (20 and 30 d) the community composition in the MLSS and biofilms on the five membranes were distinct and this is in line with previous studies that showed differences between the community in the MLSS and the well established mature biofilm [15, 17, 19]. On the other hand, Huang et al.

compared the biofouling communities of identical membranes operated under 15 and 30 L/m<sup>2</sup>.h and different SRTs (8 and 30 d) and concluded that the imposed membrane flux affected the community structure and composition of biofouling microorganisms. The low-flux (i.e. 15 L/m<sup>2</sup>.h) biofilm communities from two MBRs operated at different SRTs were related. In contrast, distinct biofilm communities developed on the high-flux MBRs operated at different SRTs. Also, the microbial communities were significantly different between the same SRT MBRs operated at different fluxes [17]. The authors explained this difference in the results between the low and high-flux to the strong convective force that transports bacterial cells towards the membrane surface at higher permeate flux. The results reported by Huang et al. (2008) could explain why our results failed to detect any remarkable differences in the composition of biofouling microbial communities between membranes operated with (10 L/m<sup>2</sup>.h) and without flux (0 L/m<sup>2</sup>.h) (Figure 3.4). The imposed permeate flux of 10 L/m<sup>2</sup>.h could be considered low, and might have accumulated microbial communities similar to the no flux membranes.

Despite tremendous efforts focused on characterizing the biofouling communities in MBRs, a universal conclusion on the MBR operating conditions that could shape the composition of early colonizers is still missing. Previously, Huang et al. confirmed the effect of membrane flux on shaping the biofouling microbial communities [48], and Miura et al. showed that air-scouring rate affects the composition of membrane biofilms in MBRs [15]. However, both studies did not investigate the effect of these operating conditions on the composition of early colonizers. Lee et al. confirmed that membrane surface roughness is a more important parameter in shaping the membrane biofouling community compared to hydrophobic or hydrophilic surface character [29]. Still, their

results were concluded following 15 d of static adsorption of bacterial communities on membrane surfaces. In our previous work (Seattle project), the wastewater composition together with membrane operating conditions shaped the composition of early colonizers (chapter 2). On the other hand, Bereschenko et al. confirmed that *Sphingomonas* spp are responsible for the initiation of biofilm formation and subsequent development into a mature biofilm in reverse osmosis membranes [14]. In marine environments, specific microorganisms were identified as dominant colonizers on different materials inserted in the sea. For instance, Dang and Lovell (2000) identified *Roseobacter* genus (subdivision of *Alphaproteobacteria*) as the dominant and rapid colonizers of surfaces in coastal environments after 24 - 72 h of incubation [12]. Similarly, Elifantz et al. identified *Roseobacter* genus as the dominant biofouling group forming on glass coupons and accounted for 25% of the community [25]. Compared to biofilm formation on membranes in MBRs, it seems that early colonizers are more complex and variable than expected.

### **3.4.2. Successional steps towards a mature biofilm**

Bacterial attachment onto the five hydrophilic and hydrophobic membranes occurred under passive adsorption (i.e. no flux) and active (i.e. filtration mode) conditions [46]. The composition and structure of biofilm communities responsible for membrane biofouling were very similar, without clear distinction between the membranes operated with or without permeate flux (Figure 3.4; Figure 3.7 and Figure 3.9). In addition, successional biofouling steps that included growth and development of early colonizers into identical mature biofilm occurred on the five different membranes under flux and no flux conditions (Figure 3.7 and Figure 3.9). Throughout the 30 d sampling period, the

bacterial diversity of the MLSS was relatively stable (Table 3.4) whereas, the biofilm diversity increased significantly on day 10 for the five membranes (Table 3.4). Previously, Jackson et al. suggested that species diversity increases within the biofilm during successional steps [49]. Initially, early species responsible for biofilm formation assemble randomly on surfaces, and then competition shapes the overall species diversity at mid-stages of biofilm development. Finally, species diversity increases when the biofilm matures, following the development of a complex three-dimensional architecture that provides habitats for bacterial growth [49].

The comparison between the biofouling forming communities on the five membranes and the composition of the MLSS suggest that successional steps within the biofilms occurred on both flux and no flux membranes, independently from the MLSS. This process could be the result of natural biofilm colonization on membrane surfaces and consequential development into a mature biofilm potentially due to the low selected flux (10 L/m<sup>2</sup>.h). Huang et al. compared the community composition of membrane biofouling at two different fluxes of 15 and 30 L/m<sup>2</sup>.h, and showed that the biofouling communities were identical for the low flux (15 L/m<sup>2</sup>.h) independently from the sludge ages. Their conclusion highlighted that the membrane biofilm formation seemed to be the result of a natural process of initial colonization and subsequent biofilm development [17]. The same scenario could have happened in our study for the membranes operated with a low flux of 10 L/m<sup>2</sup>.h and without flux.

While biofilm developed and matured on membrane surfaces, the community composition successively shifted with time. Initially, the class *Betaproteobacteria* was the most abundant bacterial group at day 1 on the membrane surfaces, and on days 20 and

30 *Firmicutes* became the most dominant phylum, followed by *Betaproteobacteria* and *Gammaproteobacteria* (Figure 3.7). Interestingly these biofouling communities evolved differently than the MLSS (Figure 3.8). At day 1 the community structure of the MLSS was similar to the biofilm communities (early colonizers), but they became distinct from each other's after 30 days (Figure 3.8). These observations could suggest that the successional changes in the biofouling communities on the membranes were not affected by variations in the source community (MLSS community).

Compared to other bacterial groups, *Betaproteobacteria* class from the phylum *Proteobacteria* has been distinguished previously by its ability to attach easily onto surfaces during initial biofilm formation and could dominate biofilm succession in stream rivers [50]. Miura et al. found that *Betaproteobacteria* increased in the abundance of the membrane biofouling community composition after they increased the aeration flow rate and performed membrane cleaning [15]. Their results confirmed a direct role of the aeration flow rate in shaping the community structure and highlighted an important role of *Betaproteobacteria* in the development of mature membrane biofilm [15]. Besmer et al. confirmed in their study that the flow velocity affected directly the succession of biofilm community composition and explained that this phenomenon shifted from predominantly stochastic to deterministic processes [11]. In this study, the successional steps that formed a mature biofilm on the five different membranes occurred naturally. The membranes featured identical nominal pore size, were operated using a constant flux of 10 L/m<sup>2</sup>.h and were exposed simultaneously to the same source community (MLSS). The only difference was the hydrophobic and hydrophilic surface character, which failed to affect the composition of early colonizers or mature biofilms.

Phylum *Firmicutes* dominated the composition of the membrane biofilms after 20 and 30 days (Figure 3.7), on the five different membranes. It is possible that anoxic zones formed within the biofilm following succession and development into a mature biofilm with time. In addition, our reactor was operated under intermittent aeration, which could have favored the development of this anaerobic phylum. *Firmicutes* were identified as the dominant biofouling communities on membrane coupled with anaerobic sludge blanket bioreactor [51]. Gao et al. detected low abundances of *Firmicutes* in the membrane biofouling layer, which remained dominant in the MLSS of an anaerobic membrane bioreactor [52].

*Hydrogenophaga* is an autotrophic H<sub>2</sub>-oxidizing bacteria [53] and was the dominant genus at days 1 and 10 (Figure 3.9). *Hydrogenophaga* belongs to the *Betaproteobacteria* class and was previously found to play an important role in denitrification, and its relative abundance increased in wastewater treatment process based on denitrification [54]. The imposed operating conditions to achieve denitrification enriched the sludge with *Hydrogenophaga* its relative abundance was 28.9% at day 1 (Figure 3.8). It is possible that genus *Hydrogenophaga* found a niche on the surfaces of the five different membranes and accounted for 18.38% of 10 dominant shared OTUs (Figure 3.9).

*Iganvibacteriaceae* has an adaptable metabolism that allows it of organoheterotrophy under both oxic and anoxic condition [55]. Our lab-scale MBR was operated under intermittent aeration with cycles of 30 min aeration followed by 30 min anoxic, to achieve simultaneous carbon and nitrogen removal. This genus started to appear on all membrane surfaces after 10 d of filtration and persisted in the biofilm at day 30 with a relative abundance of 5.13% (Figure 3.9). Similarly, Zhu et al. reported that

*Ignavibacteria* was more enriched in the biofilm (2.74%) compared with the mixed liquor (0.78%) [56]. Likewise, genus *PSB-M-3* dominated the biofouling communities after 20 and 30 d of filtration, and reached 42.59 and 47.53% respectively (Figure 3.9). Genus *PSB-M-3* belongs to phylum *Firmicutes*, which were the dominant phylum after 20 and 30 d in the membrane biofilms. These anaerobic genera might have created micro-niches within the biofilm on the different membrane surfaces.

### **3.5. Conclusion**

In this study, the sequential steps were studied with regards to the formation of mature biofilm on different hydrophobic and hydrophilic membranes inserted in the same membrane bioreactor. Our results showed that the composition of the early colonizers was identical for the five different membranes, and the sequential steps that lead to the formation of a mature biofilm happened on all membranes. It seems that the imposed low flux of 10 L/m<sup>2</sup>.h did not create a strong selective pressure that affected the composition of the microbial communities. Specific conditions on the membrane surfaces could have selected specific early colonizers predominantly *Betaproteobacteria*, and they evolved afterwards into a mature biofilm composed of Gammaproteobacteria and Firmicutes, regardless of the membrane surface (i.e. hydrophobicity, hydrophilicity). Biofilm formation on membrane surfaces could have resulted from natural biofilm formation, initial early colonizers and subsequent development into a mature biofilm.

### **Acknowledgments**

This work was sponsored by King Abdullah University of Science and Technology (KAUST).

## References

1. Judd, S. The status of industrial and municipal effluent treatment with membrane bioreactor technology. **Chem. Eng. J.**, 2015.
2. Malaeb, L., Le-Clech, P., Vrouwenvelder, J.S., Ayoub, G.M., Saikaly, P.E. Do biological-based strategies hold promise to biofouling control in MBRs? **Water Res.**, v. 47, n. 15, p. 5447-5463, 2013.
3. Vanysacker, L., Boerjan, B., Declerck, P., Vankelecom, I.F. Biofouling ecology as a means to better understand membrane biofouling. **Appl. Microbiol. Biotechnol.**, v. 98, n. 19, p. 8047-8072, 2014.
4. Le-Clech, P., Chen, V. Fane, T.A. Fouling in membrane bioreactors used in wastewater treatment. **J. Membr. Sci.**, v. 284, n. 1, p. 17-53, 2006.
5. Garg, A., Jain, A., Bhosle, N.B. Chemical characterization of a marine conditioning film. **Intern. Biodeter. & Biodeg.**, v. 63, n. 1, p. 7-11, 2009.
6. Ng, T.C.A., Ng, H.Y. Characterisation of initial fouling in aerobic submerged membrane bioreactors in relation to physico-chemical characteristics under different flux conditions. **Water Res.**, v. 44, n. 7, p. 2336-2348, 2010.
7. Khan, M.T., de O. Manes, C.-L., Aubry, C., Gutierrez, L., Croue, J.P. Kinetic study of seawater reverse osmosis membrane fouling. **Environ. Sci. Technol.**, v. 47, n. 19, p. 10884-10894, 2013.
8. Tansel, B., Sager, J., Garland, J., Xu, S., Levine, L., Bisbee, P. Deposition of extracellular polymeric substances (EPS) and microtopographical changes on membrane surfaces during intermittent filtration conditions. **J. Membr. Sci.**, v. 285, n. 1, p. 225-231, 2006.
9. Zhang, K., Choi, H., Dionysiou, D.D., Sorial, G.A., Oerther, D.B. Identifying pioneer bacterial species responsible for biofouling membrane bioreactors. **Environ. Microbiol.**, v. 8, n. 3, p. 433-440, 2006.
10. Flemming, H.-C., Wingender, J. The biofilm matrix. **Nature reviews Microbiology**, v. 8, n. 9, p. 623-633, 2010.
11. Besemer, K., Peter, H., Logue, J.B., Langenheder, S., Lindström, E.S., Tranvik, L.J., Battin, T.J. Unraveling assembly of stream biofilm communities. **ISME J.**, v. 6, n. 8, p. 1459-1568, 2012.
12. Dang, H., Lovell, C.R. Bacterial primary colonization and early succession on surfaces in marine waters as determined by amplified rRNA gene restriction analysis and sequence analysis of 16S rRNA genes. **Appl. Environ. Microbiol.**, v. 66, n. 2, p. 467-475, 2000.
13. Lee, J. W., Nam, J. H., Kim, Y. H., Lee, D.H. Bacterial communities in the initial stage of marine biofilm formation on artificial surfaces. **The journal of microbiology.**, v. 46, n. 2, p. 147-182, 2008.
14. Bereschenko, L., Stams, A., Euverink, G., Van Loosdrecht, M. Biofilm formation on reverse osmosis membranes is initiated and dominated by *Sphingomonas* spp. **Appl. Environ. Microbiol.**, v. 76, n. 8, p. 2623-2632, 2010.

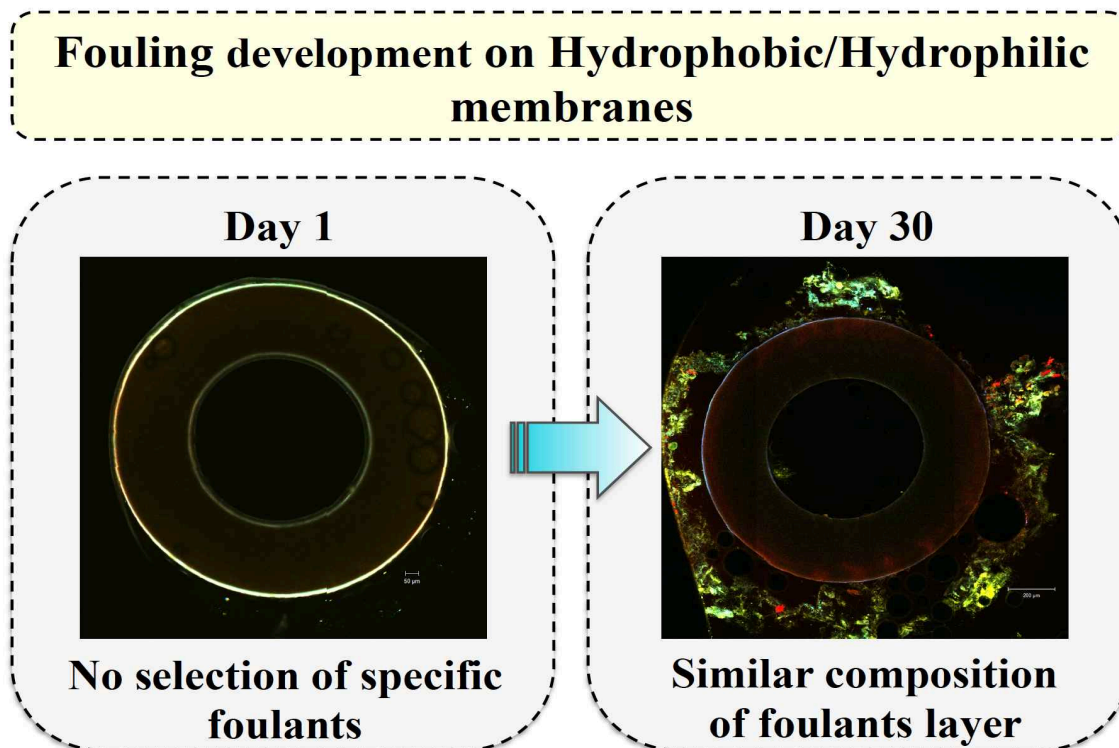
15. Miura, Y., Watanabe, Y., Okabe, S. Membrane biofouling in pilot-scale membrane bioreactors (MBRs) treating municipal wastewater: impact of biofilm formation. **Environ. Sci. Technol.**, v. 41, n. 2, p. 632-638, 2007.
16. Ma, J., Wang, Z., Yang, Y., Mei, X., Wu, Z. Correlating microbial community structure and composition with aeration intensity in submerged membrane bioreactors by 454 high-throughput pyrosequencing. **Water Res.**, v. 47, n. 2, p. 859-869, 2013.
17. Huang, L.-N., De Wever, H., Diels, L. Diverse and distinct bacterial communities induced biofilm fouling in membrane bioreactors operated under different conditions. **Environ. Sci. Technol.**, v. 42, n. 22, p. 8360-8366, 2008.
18. Lim, S., Kim, S., Yeon, K.M., Sang, B.I., Chun, J., Lee, C.H. Correlation between microbial community structure and biofouling in a laboratory scale membrane bioreactor with synthetic wastewater. **Desalination**, v. 287, n. 209-215, 2012.
19. Fontanos, P., Yamamoto, K., Nakajima, F., Fukushi, K. Identification and quantification of the bacterial community on the surface of polymeric membranes at various stages of biofouling using fluorescence in situ hybridization. **Sep. Sci. Technol.**, v. 45, n. 7, p. 904-910, 2010.
20. Vanysacker, L., Declerck, P., Bilad, M. Vankelecom, I. Biofouling on microfiltration membranes in MBRs: role of membrane type and microbial community. **J. Membr. Sci.**, v. 453, p. 394-401, 2014.
21. Piasecka, A., Souffreau, C., Vandepitte, K., Vanysacker, L., Bilad, R.M., De Bie, T., Hellemans, B., De Meester, L., Yan, X., Declerck, P. Analysis of the microbial community structure in a membrane bioreactor during initial stages of filtration. **Biofouling**, v. 28, n. 2, p. 225-238, 2012.
22. Grasland, B., Mitalane, J., Briandet, R., Quemener, E., Meylheuc, T., Linossier, I., Vallee-Rehel, K., Haras, D. Bacterial biofilm in seawater: cell surface properties of early-attached marine bacteria. **Biofouling**, v. 19, n. 5, p. 307-313, 2003.
23. Siboni, N., Lidor, M., Kramarsky-Winter, E., Kushmaro, A. Conditioning of membrane and initial biofilm formation on ceramics tiles in the marine environment. **FEMS Microbiol. Lett.**, v. 274, p. 24-29, 2007.
24. Briand, J.F., Djeridi, I., Jamet, D., Coupé, S., Bressy, C., Molmeret, M., Le Berre, B., Rimet, F., Bouchez, A., Blache, Y. Pioneer marine biofilms on artificial surfaces including antifouling coatings immersed in two contrasting French Mediterranean coast sites. **Biofouling**, v. 28, n. 5, p. 453-463, 2012.
25. Elifantz, H., Horn, G., Ayon, M., Cohen, Y., Minz, D. Rhodobacteraceae are the key members of the microbial community of the initial biofilm formed in Eastern Mediterranean coastal seawater. **FEMS microbiol. Ecol.**, v. 85, n. 2, p. 348-357, 2013.
26. Camps, M., Barani, A., Gregori, G., Bouchez, A., Le Berre, B., Bressy, C., Blache, Y., Briand, J.F. Antifouling coatings influence both abundance and community structure of colonizing biofilms: a case study in the Northwestern Mediterranean sea. **Appl. Environ. Microbiol.**, v. 80, n. 16, p. 4821-4831, 2014.
27. Jones, P.R., Cottrell, M.T., Kirchman, D.L., Dexter, S.C. Bacterial Community Structure of Biofilms on Artificial Surfaces in an Estuar. **Microbiol Ecology**, v. 53, n. 1, p. 153-162, 2007.

28. Kim, L., Pagaling, E., Zuo, Y.Z., Yan, T. Impact of Substratum Surface on Microbial Community Structure and Treatment Performance in Biological Aerated Filters. **Appl. Environ. Microbiol.**, v. 80, n. 1, p. 177-183, 2014.
29. Lee, S.H., Hong, T.I., Kim, B., Hong, S., Park, H.D. Comparison of bacterial communities of biofilms formed on different membrane surfaces. **World J. Microbiol. Biotechnol.**, v. 30, n. 2, p. 777-782, 2014.
30. Wang, Y.K., Sheng, G.P., Ni, B.J., Li, W.W., Zeng, R.J., Wang, Y.Q., Shi, B.J., Yu, H.Q. Simultaneous carbon and nitrogen removals in membrane bioreactor with mesh filter: An experimental and modeling approach. **Cehm. Eng. Sci.**, v. 95, p. 78-84, 2013.
31. Maab, H., Al Saadi, A., Francis, L., Livazovic, S., Ghaffour, N., Amy, G.L., Nunes, S.P. Polyazole hollow fiber membranes for direct contact membrane distillation. **Ind. Eng. Chem. Res.**, v. 52, n. 31, p. 10425-10429, 2013.
32. Maab, H., Francis, L., Al Saadi, A., Aubry, C., Ghaffour, N., Amy, G., Nunes, S.P. Synthesis and fabrication of nanostructured hydrophobic polyazole membranes for low-energy water recovery. **J. Membr. Sci.**, v. 423, p. 11-19, 2012.
33. Ponce, M.L., Gomes, D., Nunes, S.P. One-post of high molecular weight sulfonated poly (oxadiazole-triazole) copolymers for proton conductive membranes. **J. Membr. Sci.**, v. 319, n. 1, p. 14-22, 2008.
34. Ishii, S.i., Suzuki, S., Norden-Krichmar, T.M., Tenney, A., Chain, P.S., Scholz, M.B., Nealon, K.H., Bretschger, O. A novel metatranscriptomic approach to identify gene expression dynamics during extracellular electron transfer. **Nature communications.**, v. 4, p. 1601, 2013.
35. Klindworth, A., Pruesse, E., Schweer, T., Peplies, J., Quast, C., Horn, M., Glöckner, F.O. Evaluation of general 16S ribosomal RNA gene PCR primers for classical and next-generation sequencing-based diversity studies. **Nucleic acids research.**, 2012.
36. Caporaso, J.G., Kuczynski, J., Stombaugh, J., Bittinger, K., Bushman, F.D., Costello, E.K., Fierer, N., Pena, A.G., Goodrich, J.K., Gordon, J.I. QIIME allows analysis of high-throughput community sequencing data. **Nature methods.**, v. 7, n. 5, p. 335-336, 2010.
37. Edgar, R.C. Search and clustering orders of magnitude faster than BLAST. **Bioinformatics.**, v. 26, p. 2460-2461, 2010.
38. Caporaso, J.G., Bittinger, K., Bushman, F.D., DeSantis, T.Z., Andersen, G.L., Knight, R. PyNAST: a flexible tool for aligning sequences to a template alignment. **Bioinformatics.**, v. 26, n. 2, p. 266-267, 2010.
39. DeSantis, T.Z., Hugenholtz, P., Larsen, N., Rojas, M., Brodie, E.L., Keller, K., Huber, T., Dalevi, D., Hu, P., Andersen, G.L. Greengenes, a chimera-checked 16S rRNA gene database and workbench compatible with ARB. **Appl. Environ. Microbiol.**, v. 72, n. 7, p. 5069-5072, 2006.
40. Bardou, P., Mariette, J., Escudié, F., Djemiel, C., Klopp, C. Jvenn: an interactive Venn diagram viewer. **BMC bioinformatics**, v. 15, n. 1, p. 293, 2014.
41. Andrew, D.R., Fitak, R.R., Munguia-Vega, A., Racolta, A., Martinson, V.G., Dontsova, K. Abiotic factors shape microbial diversity in Sonoran Desert soils. **Appl.**

- Environ. Microbiol.**, v. 78, n. 21, p. 7527-7537, 2012.
42. Zodrow, K., Brunet, L., Mahendra, S., Li, D., Zhang, A., Li, Q., Alvarez, P.J. Polysulfone ultrafiltration membranes impregnated with silver nanoparticles show improved biofouling resistance and virus removal. **Water Res.**, v. 43, n. 3, p. 715-723, 2009.
  43. Tang, L., Livi, K.J., Chen, K.L. Polysulfone membranes modified with bioinspired polydopamine and silver nanoparticles formed in situ to mitigate biofouling. **Environ. Sci. Technol. Letters.**, v. 2, n. 3, p. 59-65, 2015.
  44. Li, W., Zhou, J., Gu, J.S., Yu, H.Y. Fouling control in a submerged membrane-bioreactor by the membrane surface modification. **J Appl. Polymer Sci.**, v. 115, n. 4, p. 2302-2309, 2010.
  45. Zhang, M., Liao, B.Q, Zhou, X., He, Y., Hong, H., Lin, H. Chen, J. Effects of hydrophilicity/hydrophobicity of membrane on membrane fouling in a submerged membrane bioreactor. **Bioresour. Technol.**, v. 175, p. 59-67, 2015.
  46. Drioli, E., Giorno, L. **Membrane operations: innovative separations and transformations.** [S.l.]: Wiley-VCH, 2009.
  47. Pasmore, M., Todd, P., Smith, S., Baker, D., Silverstein, J., Coons, D., Bowman, C.N. Effects of ultrafiltration membrane surface properties on *Pseudomonas aeruginosa* biofilm initiation for the purpose of reducing biofouling. **J. Membr. Sci.**, v. 194, n. 1, p. 15-32, 2001.
  48. Huang, J., Wang, Z., Zhu, C., Ma, J., Zhang, X., Wu, Z. Identification of microbial communities in open and closed circuit bioelectrochemical MBRs by high-throughput 454 pyrosequencing. **PLoS one**, v. 9, p. 93842, 2014.
  49. Jackson, C.R., Churchill, P.F., Roden, E.E. Successional changes in bacterial assemblage structure during epilithic biofilm development. **Ecology.**, v. 82, n. 2, p. 555-566, 2001.
  50. Araya, R., Tani, K., Takagi, T., Yamaguchi, N., Nasu, M M. Bacterial activity and community composition in stream water and biofilm from an urban river determined by fluorescent in situ hybridization and DGGE analysis. **FEMS Microbiol. Ecol.**, v. 43, n. 1, p. 111-119, 2003.
  51. Calderón, K., Rodelas, B., Cabirol, N., González-.López, J., Noyola, A. Analysis of microbial communities developed on the fouling layers of a membrane coupled anaerobic bioreactor applied to wastewater treatment. **Biores. Technol.**, v. 102, n. 7, p. 4618-4627, 2011.
  52. Gao, D.W., Zhang, T., Tang, C.Y.Y., Wu, W.M., Wong, C.Y., Lee, Y.H., Yeh, D.H., Criddle, C.S. Membrane fouling in an anaerobic membrane bioreactor: Differences in relative abundance of bacterial species in the membrane foulant layer and in suspension. **J. Membr. Sci.**, v. 364, n. 1, p. 331-338, 2010.
  53. Yoon, K.S., Sakai, Y., Tsukada, N., Fujisawa, K., Nishihara, H. Purification and biochemical characterization of a membrane-bound [NiFe]-hydrogenase from a hydrogen-oxidizing, lithotrophic bacterium, *Hydrogenophaga* sp. **FEMS Microbiol. Letters**, v. 290, n. 1, p. 114-120, 2009.
  54. Hoshino, T., Terahara, T., Tsuneda, S., Hirata, A., Inamori, Y. Molecular analysis of

- microbial population transition associated with the start of denitrification in a wastewater treatment process. **J. Appl. Microbiol.**, v. 99, n. 5, p. 1165-1175, 2005.
55. Liu, Z., Frigaard, N.U., Vogl, K., Lino, T., Ohkuma, M., Overmann, J., Bryant, D.A. Complete genome of *Ignavibacterium album*, a metabolically versatile, flagellated, facultative anaerobe from the phylum Chlorobi. **Frontiers in Microbiol.**, v. 3, 2012.
56. Zhu, X., Tian, J., Liu, C., Chen, L. Composition and dynamics of microbial community in a zeolite biofilter-membrane bioreactor treating coking wastewater. **Appl. Microbiol. Biotechnol.**, v. 97, n. 19, p. 8767-8775, 2013.
57. Kämpfer, P., Schulze, R., Jäckel, U., Malik, K.A., Amann, R., Spring, S. *Hydrogenophaga defluvii* sp. nov. and *Hydrogenophaga atypica* sp. nov., isolated from activated sludge. **Intern. J. Syst. Evol. Microbiol.**, v. 55, n. 1, p. 341-344, 2005.
58. Gao, D., Fu, Y., Ren, N. Tracing biofouling to the structure of the microbial community and its metabolic products: A study of the three-stage MBR process. **Water Res.**, v. 47, n. 17, p. 6680-6690, 2013.
59. Guo, X., Miao, Y., Wu, B., Ye, L., Yu, H., Liu, S., Zhang, X.X. Correlation between microbial community structure and biofouling as determined by analysis of microbial community dynamics. **Biores. Technol.**, v. 197, p. 99-105, 2015.

## CHAPTER 4 Temporal Changes in Extracellular Polymeric Substances on Hydrophobic and Hydrophilic Membrane Surfaces in a Submerged Membrane Bioreactor



Peer reviewed journal article

**Gerald Matar**, Graciela Gonzalez-Gil, Husnul Maab, Suzana Nunes, Pierre Le-Clech, Johannes Vrouwenvelder, Pascal Saikaly (2015). “Temporal Changes in Extracellular Polymeric Substances on Hydrophobic and Hydrophilic Membrane Surfaces in a Submerged Membrane Bioreactor.” *Submitted to Water Research*

Abstract, oral presentation

**G. Matar**, G. Gonzales-Gil, H. Maab, S. Nunes, J.S. Vrouwenvelder, P.E. Saikaly (2015). “Evolution and accumulation of organic foulants on hydrophobic and hydrophilic membrane surfaces in a submerged membrane bioreactor.” **International Water Association: NOM 6 IWA Specialist Conference on Natural Organic Matter in Water**, Malmö, Sweden, September 7-10, 2015

**ABSTRACT**

Membrane surface hydrophilic modification has always been considered to mitigating biofouling in membrane bioreactors (MBRs). Four hollow-fiber ultrafiltration membranes (pore sizes  $\sim 0.1 \mu\text{m}$ ) differing only in hydrophobic or hydrophilic surface characteristics were operated at a permeate flux of  $10 \text{ L/m}^2\cdot\text{h}$  in the same lab-scale MBR fed with synthetic wastewater. In addition, identical membrane modules without permeate production ( $0 \text{ L/m}^2\cdot\text{h}$ ) were operated in the same lab-scale MBR. Membrane modules were autopsied after 1, 10, 20 and 30 days of MBR operation, and total extracellular polymeric substances (EPS) accumulated on the membranes were extracted and characterized in detail using several analytical tools, including conventional colorimetric tests (Lowry and Dubois), liquid chromatography with organic carbon detection (LC-OCD), fluorescence excitation - emission matrices (FEEM), fourier transform infrared (FTIR) and confocal laser scanning microscope (CLSM). The transmembrane pressure (TMP) quickly stabilized with higher values for the hydrophobic membranes than hydrophilic ones. The sulfonated polysulfone (SPSU) membrane had the highest negatively charged membrane surface, accumulated the least amount of foulants and displayed the lowest TMP. The same type of organic foulants developed with time on the four membranes and the composition of biopolymers shifted from protein dominance at early stages of filtration (day 1) towards polysaccharides dominance during later stages of MBR filtration. Nonmetric multidimensional scaling of LC-OCD data showed that biofilm samples clustered according to the sampling event (time) regardless of the membrane surface chemistry (hydrophobic or hydrophilic) or operating mode (with or without permeate flux). These results suggest that EPS composition may not be the

dominant parameter for evaluating membrane performance and possibly other parameters such as biofilm thickness; porosity, compactness and structure should be considered in future studies for evaluating the development and impact of biofouling on membrane performance.

**Keywords:** wastewater treatment; water reuse, hydrophobicity, hydrophilicity, membrane bioreactor, membrane biofouling.

#### **4.1. Introduction**

Membrane bioreactors (MBRs) are gaining worldwide merit as a promising solution for wastewater treatment and reuse, offering several advantages over conventional activated sludge systems, especially a smaller footprint, a better effluent quality [1], and an improved disinfection capability [2]. However, membrane biofouling in MBRs remains one of the most problematic challenges that result into a dramatic decrease in the quantity and quality of permeate flux production, and a sharp increase in the energy demand and trans-membrane pressure (TMP) [3, 4]. In addition, when severe and irreversible biofouling occurs, the premature replacement of membrane modules becomes inevitable, escalating the overall MBR operation costs [5].

Biofouling has been considered as the “Achilles heel” of membrane systems [6], and several control strategies have been proposed to reduce biofouling in MBRs including physical and chemical cleaning, membrane surface modification (e.g. charge, hydrophobicity, roughness), and biological-based antifouling strategies (e.g. quorum quenching, enzymatic disruption, energy uncoupling) [7]. Among these strategies,

membrane surface modification to reduce biofouling has attracted a lot of attention, not only in MBRs, but in reverse osmosis (RO) systems and membrane spacers as well [8, 9, 10]. In particular, increasing the membrane surface hydrophilicity allows for an efficient initial surface wetting and a higher initial permeate flux; however, the long-term effectiveness of hydrophilic surfaces in reducing biofouling is still debatable. For instance, ultrafiltration (UF) and nanofiltration (NF) membranes coated with polydopamine (PDA) increased the hydrophilicity of the membrane surface and reduced bacterial attachment during short-term filtration (one hour). However, PDA lost its hydrophilic character after ten days of filtration and became ineffective in reducing bacterial adhesion [11]. Moreover, polysulfone (PS) membranes with silver nanoparticles (nAg) reduced bacterial attachment on membrane surfaces and demonstrated a potential antimicrobial activity due to the toxicity of the silver nano-particles [12, 13] were performed in flow-cell filtration systems and used commercial organic foulants or model microorganisms, which are not representative for the membrane biofouling phenomenon in MBRs.

Extracellular polymeric substances (EPS) have been recognized as the main fouling components in MBRs and contribute to membrane biofouling phenomenon, which leads to a fast and sharp increase in TMP [14, 15]. The complexity of the EPS matrix, composed of polysaccharides, proteins, humic acids and metal ions [15], increases the difficulty of understanding the interactions between different EPS components and the membrane surface. Previously, the increase in the membrane fouling resistance was correlated to higher protein concentrations on the membrane and resulted in a dramatic rise in the TMP [16]. On the other hand, another study reported that the polysaccharide

fraction of the EPS and soluble microbial products (SMP) was responsible for membrane biofouling and created sharper TMP increase when compared with the protein fraction [17, 18]. Although several studies characterized the EPS components responsible for biofouling on different membrane surfaces [14, 15, 16], a fundamental understanding on the temporal dynamics of EPS components according to modified membrane surfaces is still lacking.

Therefore, the objective of this study was to assess the role of membrane hydrophilicity and surface chemical composition on biofouling and EPS composition and temporal dynamics in long-term experiments using a lab-scale MBR. Membrane modules corresponding to different membrane types (hydrophobic or hydrophilic) were operated in parallel in the same MBR tank, and membrane samples were collected following 1, 10, 20 and 30 days of continuous filtration. In parallel, additional modules were inserted without permeate production, to compare the effect of membrane surface selection against the permeate drag force. To the best of our knowledge, this is the first study that monitored the temporal dynamics of the EPS biofouling layer that developed on different membrane types, and extensively characterized the EPS fractions using several analytical and microscopic tools.

## **4.2. Materials and Methods**

### **4.2.1. Membranes manufacture and characteristics**

Four UF hollow-fiber membranes were synthesized in the lab, composed of fluorinated polyoxadiazole (POX), fluorinated polytriazole (PTA), sulfonated polytriazole (SPTA) and sulfonated polysulfone (SPSU) (Table 4.1). The POX and PTA polymers were

synthesized and manufactured into hollow fiber membranes, following a previously reported procedure [19, 20]. SPTA was synthesized using a procedure previously reported by Ponce et al. [21] and manufactured into hollow fibers. Polysulfone was sulfonated by treatment with sulfuric acid before the SPSU hollow fiber manufacture. POX and PTA hollow fiber membranes are highly hydrophobic due to fluorinated groups. SPTA and SPSU are hydrophilic due to the functionalization with sulfonic groups.

**Table 4.1.** Membrane properties and polymer composition

Membrane type	Acronym	Membrane properties				Polymer composition and characteristics
		Pore size ( $\mu\text{m}$ )	Contact Angle ( $^{\circ}$ )	Zeta potential (mV) <sup>a</sup>	$R_m$ ( $\text{m}^{-1}$ ) <sup>b</sup>	
Polyoxadiazole	POX	0.1	96.4 $\pm$ 3.2	-28 $\pm$ 1	17 $\times$ 10 <sup>12</sup>	Very hydrophobic (fluorinated)
Polytriazole	PTA	0.1	85.2 $\pm$ 12.0	-31 $\pm$ 1	16.5 $\times$ 10 <sup>12</sup>	Hydrophobic (fluorinated)
Sulfonated Polytriazole	SPTA	0.1	65.4 $\pm$ 7.5	-23 $\pm$ 1	12.2 $\times$ 10 <sup>12</sup>	Hydrophilic (sulfonic group)
Sulfonated Polysulfone	SPSU	0.1	54.5 $\pm$ 3.9	-106 $\pm$ 1	9.1 $\times$ 10 <sup>12</sup>	Hydrophilic (sulfonic group)

<sup>a</sup>Zeta potential measured using 10 mM NaCl as ionic solution, and presented for pH 7.5

<sup>b</sup>Intrinsic membrane resistance measure with deionized water

#### 4.2.2. Lab-scale MBR construction and operation

A lab-scale MBR was constructed and operated under intermittent aeration (30 min aerobic; 30 min anoxic) (Figure 4.1), to achieve simultaneous carbon and nitrogen

removal [22] (**Appendix B**). The dissolved oxygen (DO) was 6 mg/L during the aerobic phase. The MBR was operated at a solid retention time (SRT) of 15 d and a hydraulic retention time (HRT) of 12 h. The lab-scale MBR was fed with synthetic wastewater (Table 4.2) and was inoculated with activated sludge collected from a local wastewater treatment plant (Al Ruwais district, Jeddah, K.S.A).

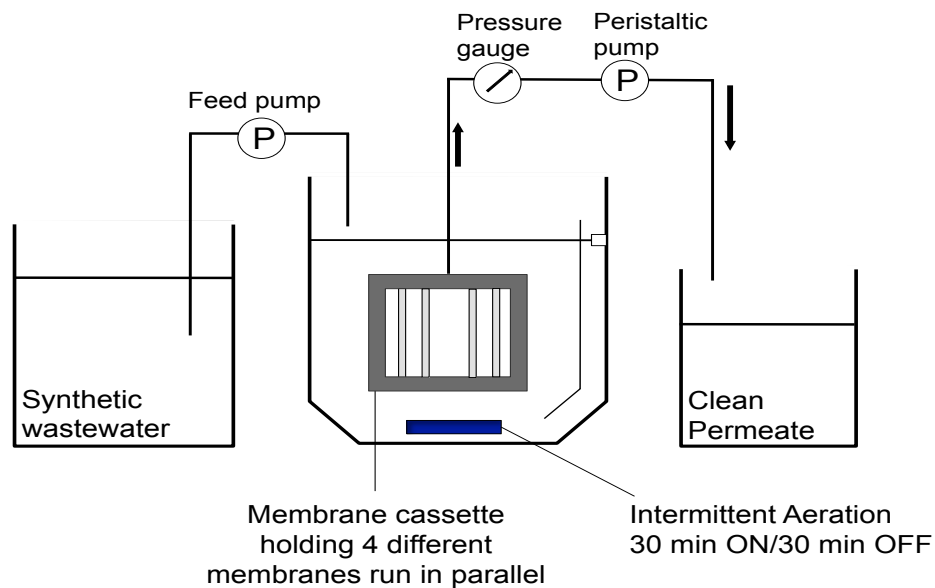


**Figure 4.1.** Schematic of the lab-scale membrane bioreactor (MBR).

The activated sludge was acclimated to the synthetic wastewater for 45 days under continuous filtration mode using commercial ultrafiltration (UF) hollow-fiber membranes (Pall) before experiments were initiated with the four different UF hollow-fiber membranes synthesized in the lab. During the acclimation period, the MBR was maintained at a constant permeate flux of  $10 \text{ L/m}^2\cdot\text{h}$ , which is closely similar to the

design flux in municipal wastewater treatment [23], with a filtration cycle of 9 min followed by 1 min relaxation (no filtration).

**Table 4.2.** Synthetic wastewater influent characteristics (in g/L).

<b>Carbon source</b>	
CH <sub>3</sub> COONa.3H <sub>2</sub> O	4.284
<b>Nutrient source</b>	
MgSO <sub>4</sub>	0.216
KCl	0.175
NH <sub>4</sub> Cl	0.236
K <sub>2</sub> HPO <sub>4</sub>	0.091
KH <sub>2</sub> PO <sub>4</sub>	0.035
<b>Trace element solution*</b>	
FeSO <sub>4</sub> .7H <sub>2</sub> O	4.99
CuSO <sub>4</sub> .5H <sub>2</sub> O	1.579
ZnSO <sub>4</sub> .7H <sub>2</sub> O	11
CaCl <sub>2</sub> .2H <sub>2</sub> O	7.35
MnCl <sub>2</sub> .4H <sub>2</sub> O	5.06
CoCl <sub>2</sub> .6H <sub>2</sub> O	1.61
(NH <sub>4</sub> ) <sub>6</sub> Mo <sub>7</sub> O <sub>24</sub> .4H <sub>2</sub> O	1.1
EDTA	50
KOH	3.09

\*1 ml of trace element solution was added 1 liter of carbon and nutrient source

Four membrane modules corresponding to the four different membranes were constructed following identical procedure, and 12 hollow-fibers were used to achieve a total membrane surface area of 56.5 cm<sup>2</sup> per module. A membrane cassette that holds the four modules was inserted in the MBR tank, and the four modules were run in parallel using the same permeate flux of 10 L/m<sup>2</sup>.h, with cycles of 9 min filtration followed by 1

min relaxation. In parallel, a similar membrane cassette that holds identical hollow-fiber modules were inserted in the MBR tank without permeate production ( $0 \text{ L/m}^2\cdot\text{h}$ ), to compare the effect of the membrane surface chemistry with the permeate drag force. All membrane modules (flux and no flux) were run for 1, 10, 20 and 30 d, and membrane modules were sacrificed completely for membrane autopsy and replaced with virgin modules after each run. Lastly, 15 mL of mixed liquor suspended solids (MLSS) was collected from the MBR tank at each sampling event. The TMP for all the membranes operated at  $10 \text{ L/m}^2\cdot\text{h}$  was measured using a pressure transducer (68075-32, Cole-Parmer Instrument Company), and recorded using a data acquisition system (LabVIEW, National Instruments) connected to a computer.

#### **4.2.3. EPS extraction**

In this study, total EPS solutions refer to the soluble microbial products (SMPs) or soluble EPS and the non-soluble fraction of the EPS. For each extraction, two fibers (10 cm length each) from the same module were sacrificed, and total EPS were extracted according to Gonzalez-Gil et al., with minor modifications [24]. Briefly, membrane fibers were cut into small pieces of 1 cm length and placed in a falcon tube. Then, 15 mL of 0.1 M NaCl (prepared in milliQ water) were added and samples were vortexed at high speed for 45 min, to achieve complete biofilm detachment. Next, 6 mL of 0.4 M NaOH was added to the EPS solution, followed by a heating phase at  $60^\circ\text{C}$  for 30 min. Finally, the EPS solutions were centrifuged at  $12,000g$  for 20 min at  $4^\circ\text{C}$ , to remove remaining bacterial cells. The extraction of EPS from hollow-fiber membranes was optimized as presented in **Appendix E**.

#### **4.2.4. Analysis of the EPS solution**

##### **4.2.4.1. Liquid chromatography with organic carbon detection**

A Shimadzu TOC-Vesh Analyzer was used to measure the total dissolved organic carbon (TOC) of EPS solutions, then a liquid chromatography with organic carbon detection model 8 (LC-OCD) (DOC-LABOR, Germany) [25] equipped with a size exclusion chromatography was used to separate the EPS fractions according to their molecular weight. The ChromCALC® software, compatible with the LC-OCD was used to integrate the resulting peak areas of different EPS fractions and convert them into carbon concentrations (mg/L) [25]. For each sample, the injection volume was 1000  $\mu$ L and the analysis time was 130 min [26].

##### **4.2.4.2. Fluorescence excitation – emission matrices**

A Fluoro Max-4 spectrofluorometer (Horiba Scientific, Japan) was used to measure the fluorescence excitation - emission matrices (FEEM) of the EPS solutions. EEM matrixes were collected with excitation and emission wavelengths that ranged from 200 to 600 nm and from 200 to 400 nm, respectively. The emission integration time was fixed at 1 s and both excitation and emission bandwidths were adjusted to 5 nm [26], and the EEM signals were corrected using blank subtraction process [27].

##### **4.2.4.3. Fourier transform infrared spectroscopy**

Membrane dialysis was performed according to [28] to remove remaining salts and NaOH from the EPS solutions, then the EPS solutions were lyophilized to obtain dried foulant material, and 100 mg of dried foulant material was mixed with 100 mg of potassium bromide salt (KBr) and pressed into KBr pellets [28]. Finally, fourier

transform infrared (FTIR) spectroscopy with an attenuated total reflection (PerkinElmer, USA) was used to obtain the FTIR spectra of the lyophilized EPS material.

#### 4.2.4.4. Proteins and polysaccharides quantification

Proteins and polysaccharides in the EPS samples were quantified using the Lowry method [29] with the bovine serum albumin as standards, and the phenol-sulphuric method [30] with glucose as standards, respectively.

#### 4.2.5. Confocal laser scanning microscopy

Membrane fibers were cut into small pieces of 1 cm length and the biofilms were stained with SYTO 9 for 30 min in the dark, to visualize the spatial distribution of the bacterial cells. Then, membrane samples were rinsed with 1× phosphate buffer saline (PBS) solution to remove excess dye, and were incubated for 30 min in the dark, with a mixture of Sypro Orange, Con A Alexa and WGA Alexa, to target the total proteins,  $\alpha$ -Man polysaccharides and  $\beta$ -GlcNAc polysaccharides, respectively (Table 4.3). Finally, membrane fibers were rinsed with 1× PBS to remove excess dye.

**Table 4.3.** Characteristics of the dyes used to label different EPS components for the CLSM study.

Label	Excitation/Emission	Targets	Assigned color	Concentration
SYTO 9	488/500 nm	Bacterial cells	Blue	2.5 $\mu$ M
Sypro Orange	470/570 nm	Proteins	Green	5.0 $\mu$ g/mL
Con-A Alexa 633	633/647 nm	$\alpha$ -Man; $\alpha$ -Glu Polysaccharides	Red	10 $\mu$ g/mL
WGA Alexa 633	633/647 nm	$\beta$ -GlcNAc; NeuNAc Polysaccharides	Yellow	10 $\mu$ g/mL

The membrane samples were then embedded with Jung Tissue Freezing medium. Then, membrane pieces were finely cut in transverse direction, into 20  $\mu\text{m}$  thick slices using a Cryostat CM 3050 E (Leica Biosystems), at  $-20^{\circ}\text{C}$ . Triplicate slices were performed for each membrane sample. Cryosection slices were mounted on microscope glass slides and covered with a cover slip, and examined immediately using LSM710 confocal laser scanning microscope (Zeiss, Germany). On average, triplicate images were taken for each sample using a 20 x -magnification lens.

#### **4.2.6. Statistical analysis**

Multivariate statistical analysis was used to identify the agglomerative trends of different membranes with regards to EPS fractions [31]. Non-metric multidimensional scaling (NMDS) based on Bray-Curtis distances was created to visualize differences in the EPS samples extracted from the different membrane surfaces. EPS fractions were characterized using LC-OCD and then normalized and Hellinger transformed as recommended for Bray-Curtis distances.

A principal component analysis (PCA) biplot was generated to visualize ordination space distances, between different membrane surfaces and the abundances of EPS fractions measured by LC-OCD. EPS fractions were normalized and Hellinger transformed as recommended for Euclidian distance based ordinations such as PCA [32]. All analyses were conducted using RStudio [33] with the package Vegan [34], respectively.

### 4.3. Results

#### 4.3.1. TMP measurements

The TMP was monitored for the four different membranes during the experiment (Figure 4.2). A series of characterization was performed for the virgin membranes before starting the experiment, as shown in Appendix C. Although all membranes featured similar pore size (Table 4.1), the TMP of the hydrophobic membranes (POX and PTA) after one day of filtration became much higher (reached 80 kPa) than the TMP of hydrophilic membranes (SPTA and SPSU). This could be a consequence of the high hydrophobicity, which favors the adhesion of hydrophobic solutes, leading to a lower effective permeation (higher TMP value). In addition, the SPSU membrane exhibited lower TMP compared with the SPTA membrane (Figure 4.2).

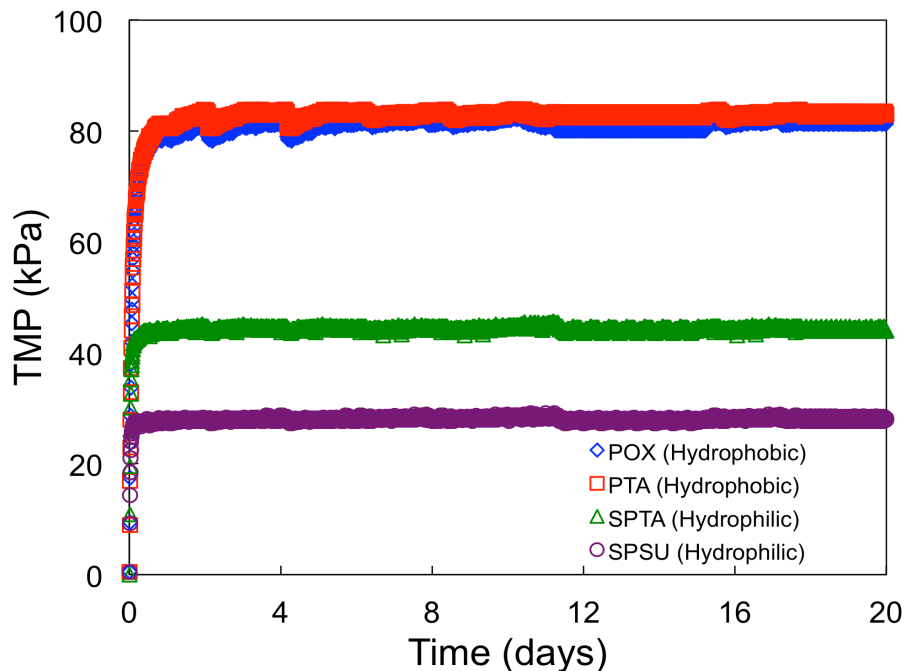


**Figure 4.2.** Transmembrane pressure (TMP) profiles for the four membranes during filtration (with permeate production).

The SPSU membrane surface was characterized with the lowest contact angle (higher hydrophilicity) and most negative charge (-106 mV) (Table 4.1), and displayed the lowest intrinsic membrane resistance ( $R_m$ ) measured with deionized water compared with the remaining three other membranes.  $R_m$  values are summarized in the following order: POX ( $17 \times 10^{12} \text{ m}^{-1}$ ) > PTA ( $16.5 \times 10^{12} \text{ m}^{-1}$ ) > SPTA ( $12.2 \times 10^{12} \text{ m}^{-1}$ ) > SPSU ( $9.1 \times 10^{12} \text{ m}^{-1}$ ), which correlate well with the membrane's surface relative hydrophobicity (Table 4.1). The TMP was quickly established (after 2 hr for hydrophilic and 5 hr for hydrophobic membranes), and the stabilized TMP values can be summarized in the following series: POX  $\approx$  PTA  $\gg$  SPTA > SPSU, which clearly correlate with the contact angle measurements of the four membranes: POX ( $96.4^\circ$ ) > PTA ( $85.2^\circ$ ) > SPTA ( $65.4^\circ$ ) > SPSU ( $54.5^\circ$ ) (Table 4.1).

#### **4.3.2. Characterisation of the initial fouling layer**

The initial fouling layer that developed on the membrane surfaces after 1 day of filtration was analyzed using FTIR for the membranes operated with permeate flux (Figure 4.3). The results revealed that all membranes accumulated an identical fingerprint profile, composed mainly of protein-like substances. Peaks related to amide ( $1640 \text{ cm}^{-1}$ ,  $1560 \text{ cm}^{-1}$ , and  $1414 \text{ cm}^{-1}$ ) were detected on the surfaces of the four different membranes (Figure 4.3), and contributed along with other accumulated organics to masking the specific functional groups of the virgin membrane surfaces (**Appendix C**). Similar results were observed with the membranes operated without flux (Figure 4.4).

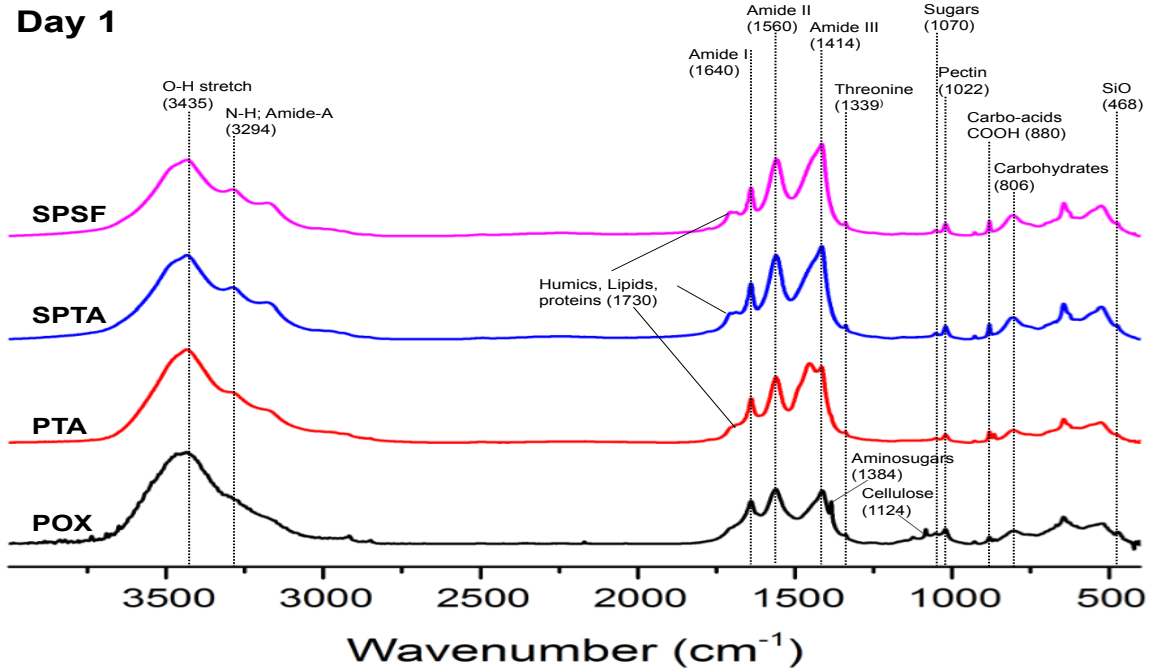


**Figure 4.3.** Fourier transform infrared (FTIR) spectroscopic analysis of the foulant material extracted from the four different membrane surfaces during early stages of filtration, operated with  $10 \text{ L/m}^2 \cdot \text{h}$  permeate production (1 day).

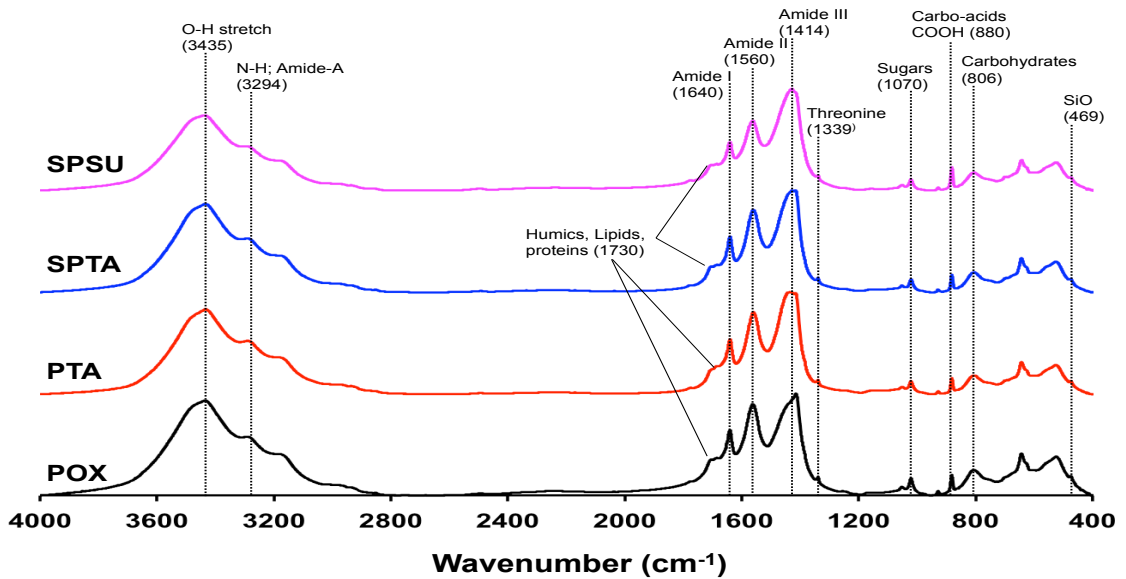


**Figure 4.4.** FTIR spectroscopic analysis of the foulant material extracted from the four different membrane surfaces inserted in the membrane tank, without permeate flux after 1 day of MBR operation.

In addition, the proteins and polysaccharides concentrations in the EPS samples were quantified using standard colorimetric methods, and results showed that proteins were more abundant than polysaccharides at day 1 for the four membranes operated with 10 L/m<sup>2</sup>.h (Figure 4.5 - A), suggesting that the initial conditioning fouling layer was composed predominantly of proteins. The SPSU membrane accumulated significantly lower amounts of organic foulants ( $p < 0.05$ ), compared to the remaining three other membranes (Figure 4.5 - B).

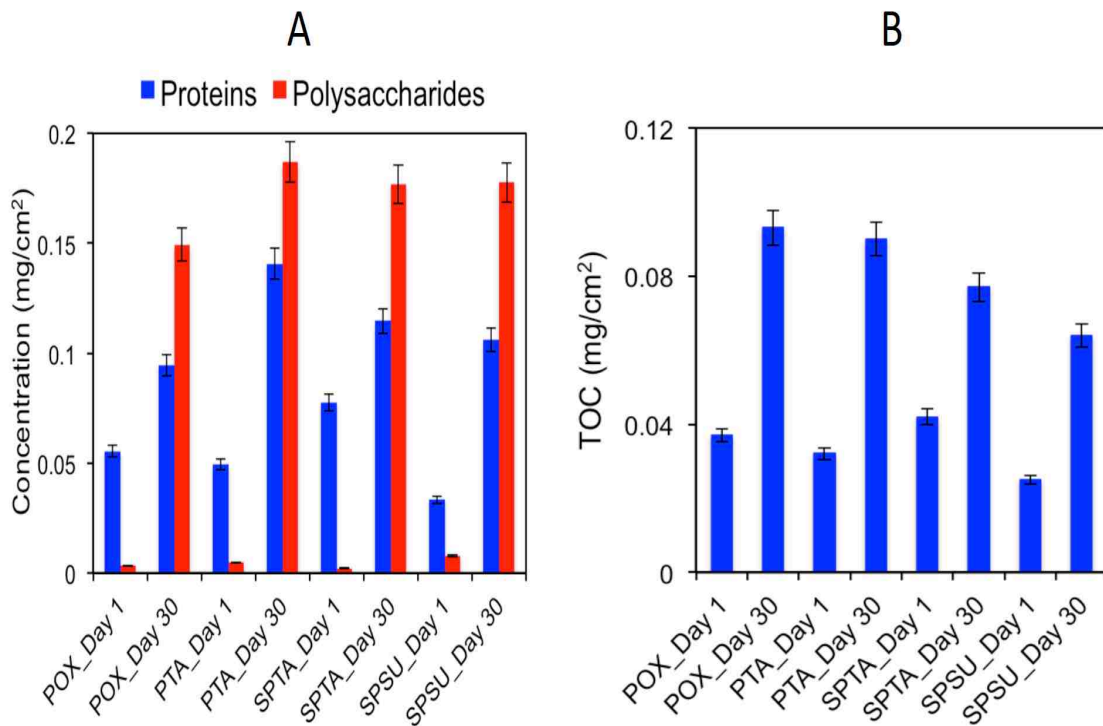


**Figure 4.5.** Concentrations of proteins and polysaccharides in the extracellular polymeric substances (EPS) samples extracted from the four membrane surfaces on day 1 and 30, and quantified using colorimetric methods (Lowry et al., 1951; Dubois et al., 1956) (A); and TOC concentrations (mg/cm<sup>2</sup>) accumulated on the four different membranes operated in continuous mode for 1 and 30 days (B).

### 4.3.3 Temporal changes in fouling characteristics

#### 4.3.3.1. LC-OCD

The LC-OCD chromatograms of the four membranes operated with  $10 \text{ L/m}^2\cdot\text{h}$  permeate flux evolved similarly with time (Figure 4.6), and the difference in accumulation of organic foulants in the four membranes was not large, but it can be seen for instance that in days 1 and 10 the accumulation of neutral biopolymers, humic substances and other medium molecular weight building blocks was lower in SPSU membranes compared to the other membranes (POX, PTA and SPTA) (Figure 4.7), which might explain the lower TMP values for SPSU.

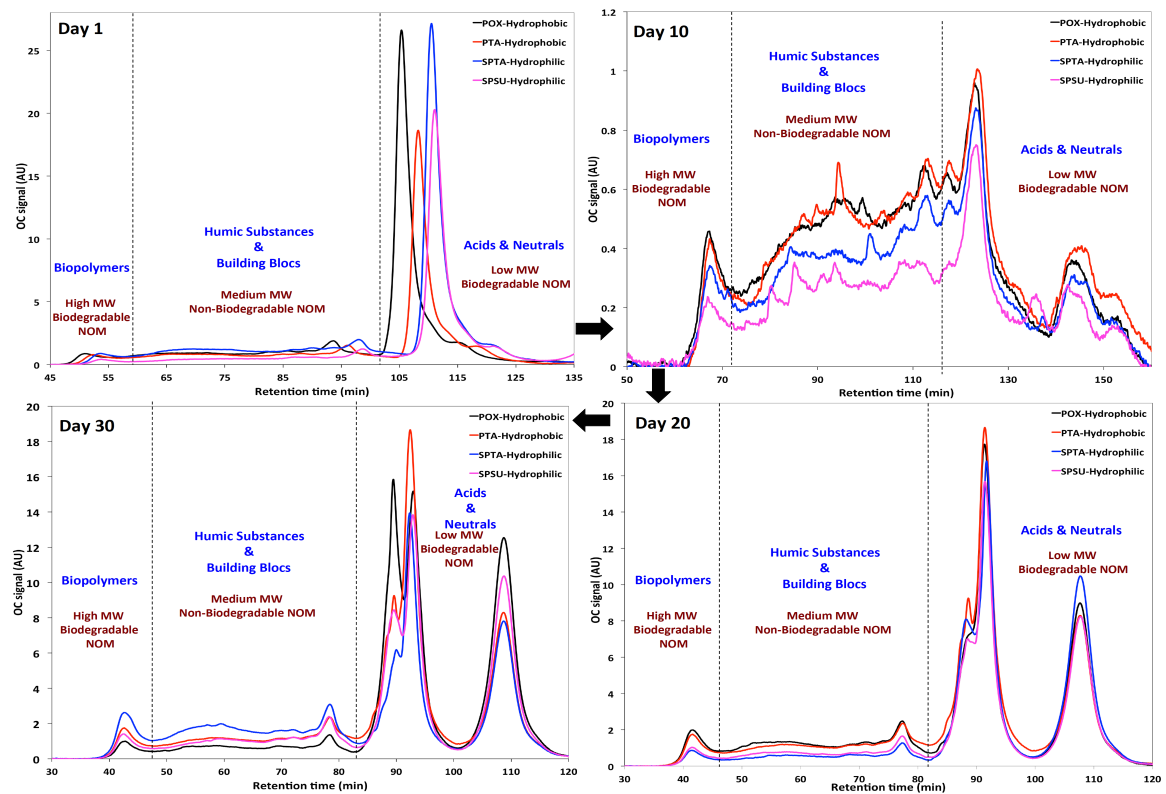


**Figure 4.6.** Evolution of the relative abundance of different organic fractions extracted from the surfaces of four different membranes operated with  $10 \text{ L/m}^2\cdot\text{h}$  permeate flux, and analyzed using LC-OCD over a 30 d MBR operation. The black arrows correspond to the chronological order of the membrane sample collection.

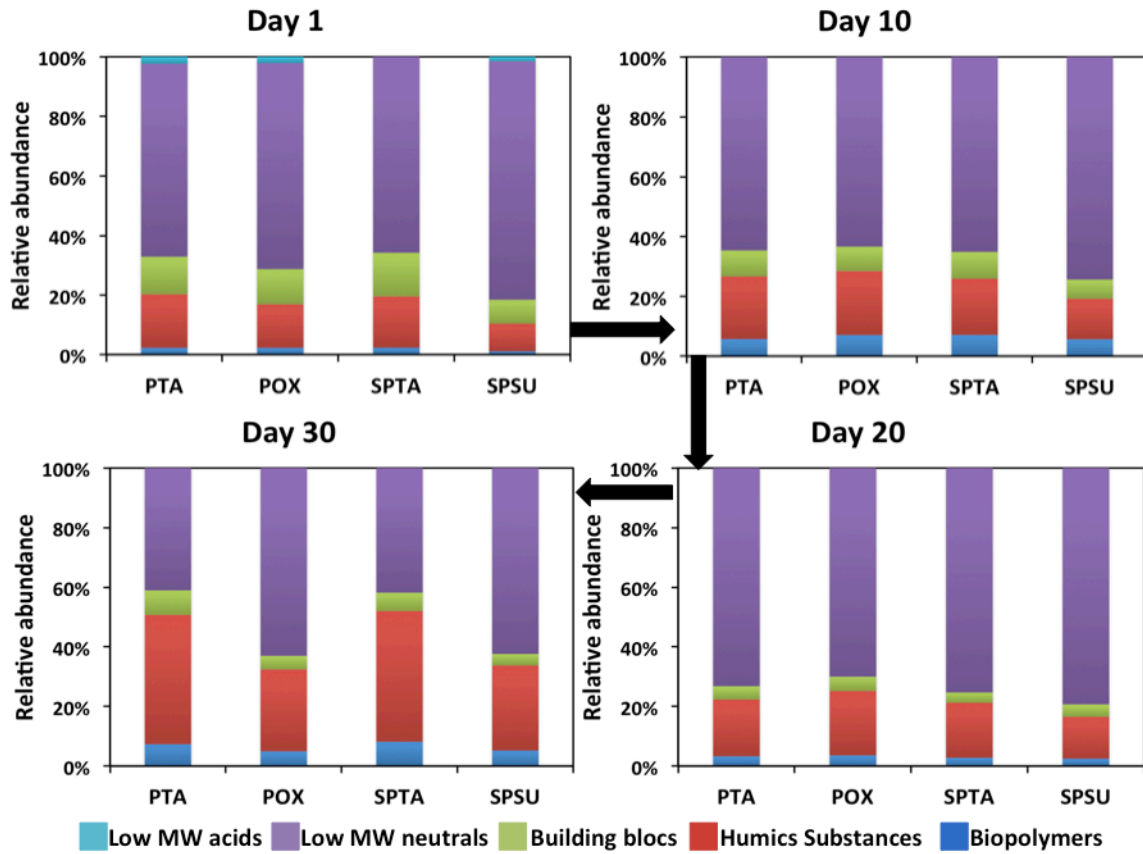


**Figure 4.7.** Temporal dynamics of organic foulants extracted from the surfaces of four different membranes operated with 10 L/m<sup>2</sup>.h permeate flux, and analyzed using liquid chromatography with organic carbon detection (LC-OCD). The black arrows correspond to the chronological order of the membrane sample collection.

Finally, the amount of humic substances that accumulated on the membranes almost doubled between day 20 and 30 for all the membranes, and when comparing the four membranes at the final stage of filtration, PTA and SPTA membranes slightly accumulated more humics than POX and SPSU respectively (Figure 4.5. - A and B). The membranes operated without permeate flux behaved similarly.

NMDS analysis showed that EPS samples clustered together according to the day of sampling, regardless of the membrane surface characteristic (hydrophobic or hydrophilic), and no clear differences were observed between membranes that undergo



A biplot was generated based on the LC-OCD data with the different samples represented by blue circles (day 1) and red circles (day 30) and the gray arrows correspond to the variables (i.e. the different EPS components) (Figure 4.9).

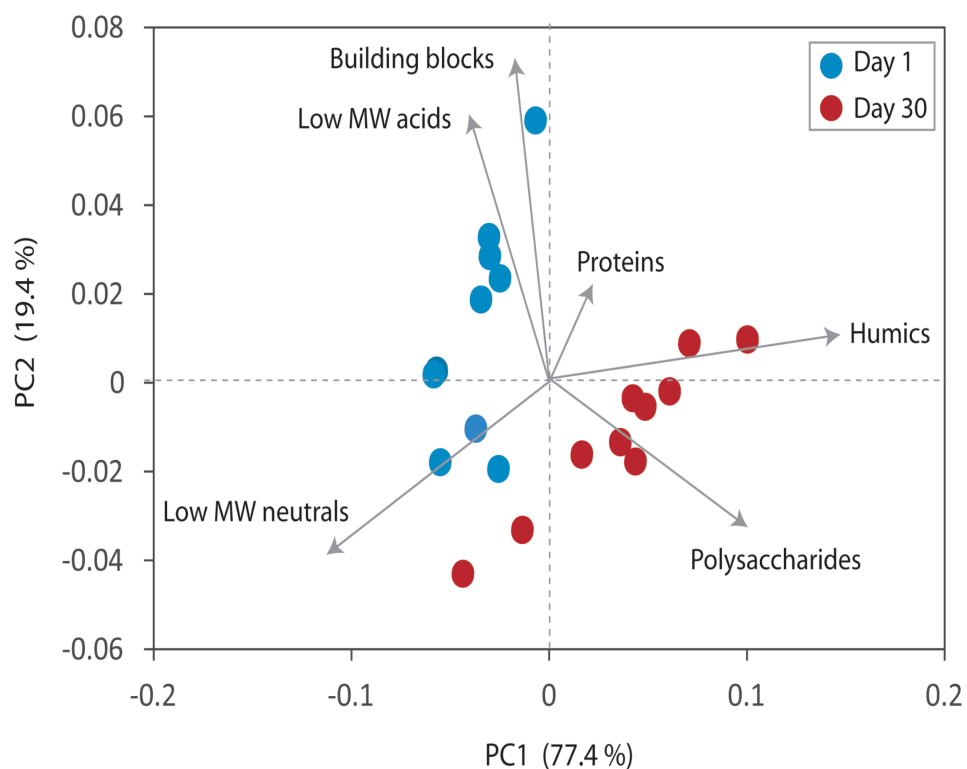


**Figure 4.9.** Biplot of the EPS solution, extracted from the different membrane surfaces. Blue circles and red circles correspond to samples from day 1 and day 30, respectively. The gray arrows point towards different EPS fractions, and PC1 (component 1) and PC2 (component 2) explain 77.4% and 19.5% of the variance between samples, respectively.

The EPS samples extracted from the membrane surfaces (combining flux and no flux data) at day 1 occupied the two left quadrants (blue circles), while the majority of the samples extracted from day 30 were located in the two right quadrants (red circles) (Figure 4.9). The EPS structure shifted from proteins-like substances, low molecular weight acids and building blocs after day 1 of filtration, towards polysaccharides-like

substances, humics and low molecular weight neutrals after 30 days of filtration (Figure 4.9). In addition, the proteins and polysaccharides quantification showed that, the protein production continued to increase in the EPS samples (Figure 4.5), however the polysaccharides fraction became more abundant after 30 days of filtration.

#### 4.3.3.2. FEEM

The excitation and emission profiles were measured for the EPS samples of the different membranes operated with  $10 \text{ L/m}^2 \cdot \text{h}$  permeate flux using a spectrofluorometer, and their dynamics was monitored over time (Figure 4.10).

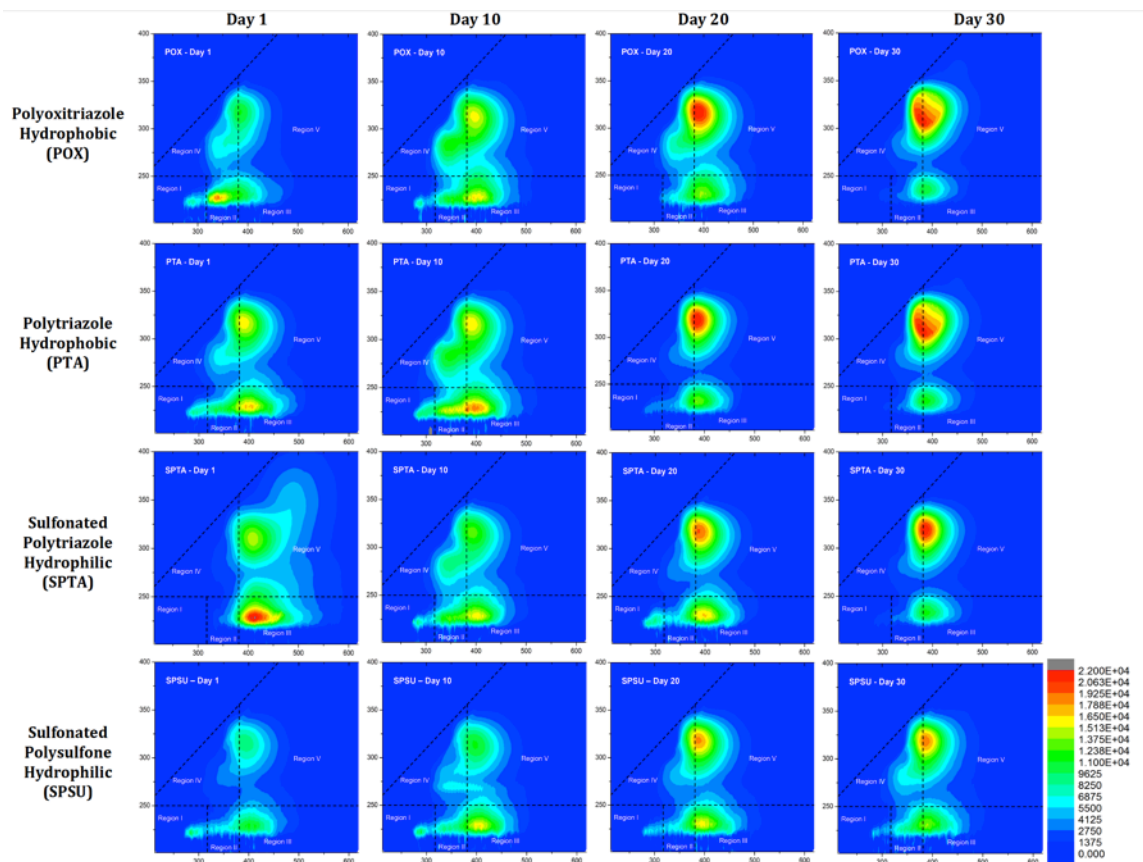


**Figure 4.10.** Evolution of 3D Fluorescence Excitation Emission (FEEM) diagrams for four different membranes operated with permeate production for 1, 10, 20 and 30 days.

The EPS from the four membranes evolved similarly in composition and exhibited a reproducible pattern. Initially at day 1, low intensity peaks related to aromatic proteins were detected in regions I and II, and peaks related to fulvic acid-like material were detected in region III on all membrane surfaces, with SPTA membrane displaying the highest signal. High intensity peaks corresponding to humic acid-like material were detected in region V for all membranes samples at day 30 (Figure 4.10) [27]. Even though the intensities of the detected peaks corresponding to various organics were different, the same signals were identified on all the membranes. This could suggest that following the development of a biofouling layer on the membranes, the hydrophobic or hydrophilic membrane surface loses its characteristic, and the different membranes accumulated identical EPS fractions.

#### **4.3.4. Visualization of the biofilm architecture**

The buildup of the protein and polysaccharide fractions of the EPS on the four different membrane surfaces operated with 10 L/m<sup>2</sup>.h permeate flux was monitored with CLSM imaging (Figure 4.11). Imaging results confirmed LC-OCD and FEEM results, where the four different membranes behaved similarly (Figure 4.11). Also, the conditioning layer after day 1 was composed mainly of proteins, which shifted towards polysaccharides-like substances after 30 days of continuous filtration. In addition, the thickness of the biofouling layer that developed on the four membranes continued to increase with time; whereas initially a thin layer covered the membranes at day 1, and at the end of the experiment, a thick and uniform biofouling layer was formed (100 µm) (Figure 4.11).

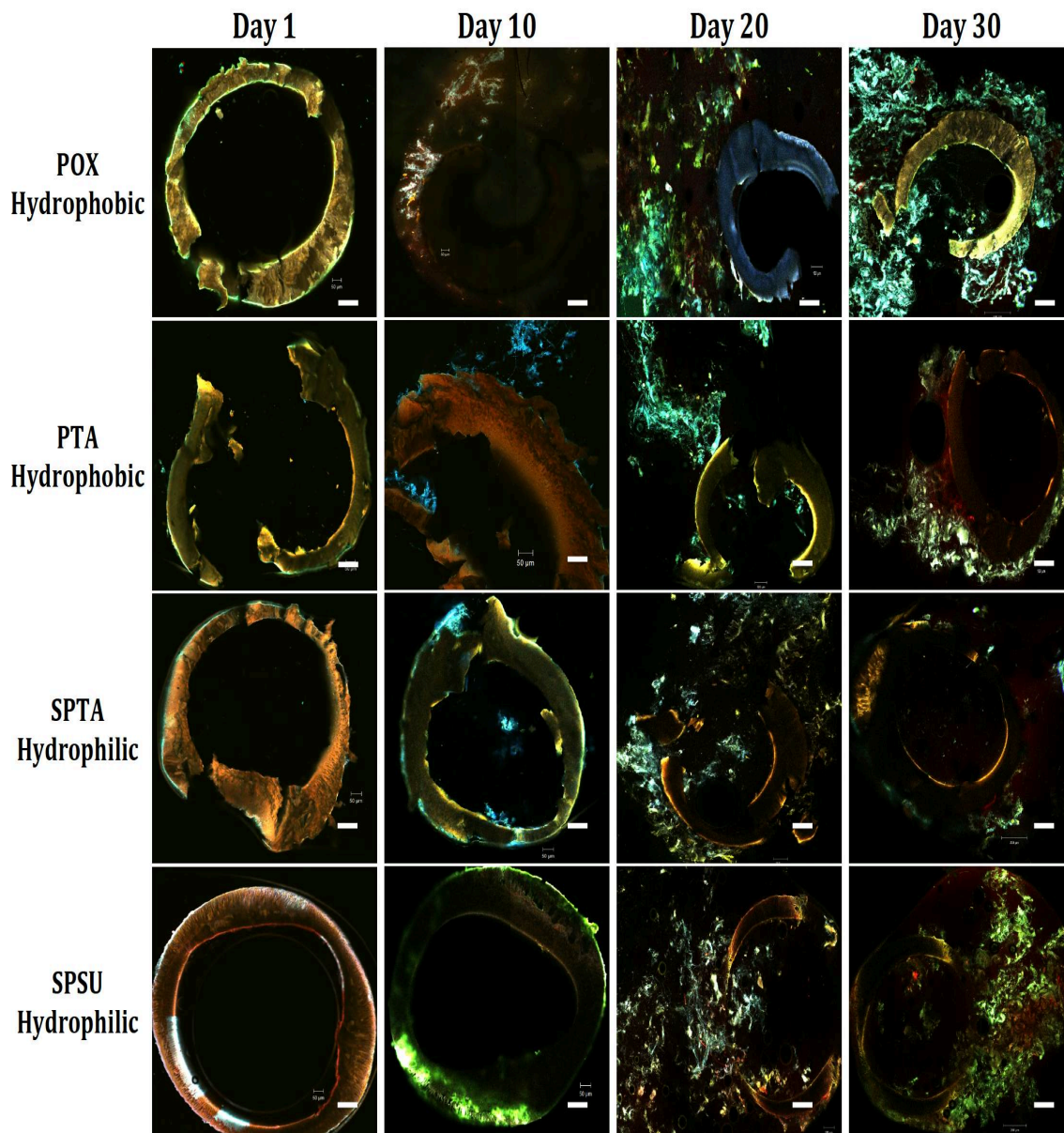


**Figure 4.11.** Confocal laser scanning microscopy (CLSM) images showing the evolution of different EPS fractions accumulated on the four membrane surfaces. Total cells, proteins and  $\alpha$ - and  $\beta$ -Polysaccharides were stained with their corresponding dyes (**Table 4.3**). The scale bar length corresponds to 50  $\mu\text{m}$ .

## 4.4 Discussion

### 4.4.1. Effect of surface hydrophilicity and charge on biofouling

In this study, we measured the contact angle for the four ultrafiltration membranes as an estimate of hydrophilicity (Table 4.1). Despite the fact that contact angle measurement remains an approximate test method to determine surface hydrophilicity [35], results showed differences among the four tested membranes, with SPSU membrane having the lowest contact angle value ( $54.5^\circ$ ) and the highest hydrophilicity. Highly hydrophobic POX and PTA hollow-fiber membranes distinguished themselves from hydrophilic SPTA and SPSU membranes as far as TMP is concerned. Hydrophobic membranes had higher TMP values than hydrophilic ones throughout the experiment.

The influence of hydrophilicity and surface chemistry on biofouling has been demonstrated by many research groups, justifying for instance with the fact that a layer of absorbed water molecules on hydrophilic surfaces, reduces the adhesion of foulants on membrane surfaces [36]. However, fouling behavior in long-term filtration of membranes in MBRs, as reported in this work, are much less dependent on hydrophilicity. This supports previous observations by other groups [11] who coated UF and NF membranes and feed spacers with polydopamine to increase their hydrophilic surface character, and their fouling tendency were tested under continuous filtration mode during 10 days [11]. Their results also showed that biofilm developed on the modified membranes independently of the hydrophilic surface character. In this study, the hydrophilic SPSU membranes accumulated lower amounts of EPS compared with other more hydrophobic membranes (Figure 4.10) potentially due to the highly negative surface charge (Table 4.1). The influence of the surface zeta potential on interactions with foulants particles for

other membrane surfaces has been reported by Zhang et al. as being even more important than hydrophilicity [37]. Similarly, Qu et al. showed that membrane's negative surface charge increased the electrostatic repulsion with the organic matter and reduced their adherence on membrane surfaces [38]. Therefore, designing membranes with high zeta potential could alleviate membrane fouling in MBRs, but the long-term effectiveness of high zeta potential membrane surfaces in reducing biofouling still requires further investigations.

#### **4.4.2. Dynamics of the EPS deposition on different membrane surfaces**

Studying the temporal dynamics of EPS and how their components evolve with time when the biofilm matures according to different membrane surfaces could be essential to establish a better understanding of the membrane biofouling phenomenon in submerged MBRs, especially that these studies are still lacking in MBRs compared with RO and NF membrane systems [39, 40, 41]. The development of the fouling layer on RO membranes was investigated in a bench-scale RO system over two weeks [41], and their results showed that carbohydrate materials increased with time after 14 d, but the amounts of proteins remained stable. Dreszer et al found during 4 d biofilm development studies that the biofilm contained more proteins than polysaccharides [40], which was in agreement with our findings following similar short membrane operation time. The evolution of microbial communities and their EPS products on NF membranes were monitored over 24 d, and findings revealed that the accumulation of EPS on NF membranes was initiated by polysaccharides (after 8 hours), and contributed to permeate flux decline [39].

All the aforementioned studies used colorimetric and/or microscopic techniques to characterize EPS that developed on the membrane surface. Conventional colorimetric

analytical tests, such as Lowry [29] and Dubois [30] are applied to quantify proteins and polysaccharides fractions in the MBR fouling layer, respectively. However, these colorimetric tests remain non-exclusive since nitrate or nitrites can potentially affect the Dubois results, and since the Lowry test can respond to humic substances [42]. Instead, several other chemical analytical techniques such as LC-OCD, FEEM and FTIR are currently being used to characterize EPS on membrane surfaces [7, 43]. LC-OCD is based on size exclusion chromatography and is applied to characterize biopolymers (proteins and carbohydrates), humics and low molecular weight molecules (acids and neutrals) in MBR fouling layer, membrane permeate and sludge supernatant [43]. On the other hand, FEEM allows detection of aromatic proteins, humic acid-like substances, fulvic acid-like substances and SMP [27, 44]. FTIR allows detecting the functional groups of membrane foulants, such as polysaccharides, proteins, amino acids and humic-like substances [43].

In the current study, conventional colorimetric tests (Lowry and Dubois), LC-OCD, FEEM, FTIR, and CLSM were applied to monitor the temporal dynamics of EPS on four different membranes. The initial fouling layer was predominantly composed of proteins based on the Lowry method (Figure 4.5) and CLSM images (Figure 4.11). At later stages polysaccharides became dominant based on Dubois method (Figure 4.5) and CLMS (Figure 4.11). FTIR results showed a very low peak at  $1070\text{ cm}^{-1}$  corresponding to sugars at day 1 (Figure 4.3 and Figure 4.4), and that confirmed the low concentration of polysaccharides obtained using colorimetric methods. On the other hand, LC-OCD analysis showed low molecular weight neutrals were dominant at day 1 and their relative abundance decreased with time with the concomitant increase in the relative abundance

of humic substances and biopolymers (Figure 4.7 and Figure 4.9). FEEM diagrams at day 30 showed the dominance of humic substances (Figure 4.10) and are in coherence with the results obtained by LC-OCD. It is clear from these results that a combination of complementary analytical tools is required to get a better insight on the composition and type of foulants selected on membrane surfaces.

Irrespective of the analytical technique used to characterize foulants, the same organic foulants were observed on the surfaces of the four different membranes regardless of membrane surface characteristic (Figure 4.3; Figure 4.7 and Figure 4.10) or mode of operation (10 vs. 0 L/m<sup>2</sup>.h). Also, the same temporal dynamics in EPS composition was observed on the four different membranes (Figure 4.8). The only remarkable difference between the four membranes was the TOC concentration (Figure 4.5 - B). The amount of foulants that amassed on the SPSU membrane at the initial (day 1) and final stages of filtration (day 30), were significantly lower than the three other membranes (Figure 4.5 - B), possibly due to the very high negatively charged membrane surface (Table 4.1). Collectively, these results suggest that other parameters such as biofilm thickness, porosity, compactness and structure should be considered in future studies for evaluating membrane performance and effectiveness of membrane surface modifications. For example, recent studies showed that membrane operational conditions such as the imposed permeate flux caused variations in the compactness, morphology and thickness of the biofilm on the membrane, which lead to losses in the membrane system's performance and an increase in the TMP [45, 46].

Despite the fact that membrane surface chemistry might contribute to selecting the conditioning fouling layer during early stages of filtration, this fouling selection becomes

of reduced importance since the membrane loses its intrinsic affinity following the accumulation and development of a mature fouling layer. The results presented in this study suggest that the conditioning fouling layer might have developed quickly on the membrane surface and masked its intrinsic characteristic after one day of filtration, where the four membranes showed similar composition of EPS. Therefore, studies on membrane surface modifications should be performed under MBR mode for extended durations, to evaluate their effectiveness in reducing or delaying MBR fouling and membrane performance.

A recent study investigated the effect of organic nutrient load on biofouling of spiral wound nanofiltration, reverse osmosis and forward osmosis membrane systems [47]. Their results showed that the organic nutrient load dictated the accumulation of biomass on membrane surfaces and feed spacers, and the impact of accumulated biomass on membrane performance was reduced when adopting lower crossflow velocity combined with a modified geometry feed spacer [47]. Future studies that focus on controlling membrane biofouling should include strategies to reduce the impact of accumulated biofilm on membrane performance and potentially applying advanced cleaning strategies [48, 49, 50] that are simple and cost-effective, to reduce the overall membrane operating costs. For such studies, a suite of tools for non-destructive in-situ analysis of fouling is available, such as optical coherence tomography [45, 46, 52, 51] and nuclear magnetic resonance imaging [53, 54, 55].

#### **4.4.3. Effect of permeate production on membrane biofouling**

Operating membranes systems at sub-critical permeate flux values has been considered as an alternative approach to reduce membrane biofouling, and several studies confirmed

that biofilm formation occurs even at low permeate flux. Despite operating the MBR at sub-critical flux values defined between 30 and 40 L/m<sup>2</sup>.h, membrane fouling occurred progressively and contributed to the gradual increase in transmembrane pressure [56]. Similar results were observed in an MBR operated at much lower flux ranging between 10 and 18 L/m<sup>2</sup>.h, and concluded that membrane fouling in an MBR is unavoidable even at low flux rates, yet it changes considerably when the critical flux is reached [57]. Likewise, the imposed permeate flux (10 L/m<sup>2</sup>.h) did not affect the pressure drop increase in NF or RO membranes; neither did it impact the membrane biofouling rate, consequently the critical flux concept was not applicable [58, 59].

Despite the very low flux of 10 L/m<sup>2</sup>.h, membrane biofouling was unavoidable, and the accumulation of microorganisms and their EPS products increased with time, on the surfaces of the four hollow-fiber membranes (Figure 4.11). EPS attachment onto the four different membranes occurred under passive adsorption (i.e. no flux) and active (i.e. filtration mode) conditions, as described previously [60]. The rate of passive bacterial adsorption on the membrane surface is expected to be different from those obtained during filtration. During initial membrane contact with the mixed liquor components (filtration or not), SMP interact with the membrane surface on which specific foulants adsorb depending on its hydrophobicity. Once the membrane is covered, additional SMP and EPS products interact with the organic-covered membrane and its intrinsic characteristics do not affect the fouling rate any further. Recently, hydrophilic fractions of natural organic matter composed of biopolymers (proteins and polysaccharides), resulted into irreversible fouling of different membranes after only 13 h of filtration [61]. Our results showed that identical relative abundances of EPS fractions accumulated on

the four different membranes using LC-OCD analysis (Figure 4.7), and similar accumulation of EPS fractions occurred on the membranes without flux ( $0 \text{ L/m}^2\cdot\text{h}$ ). However, subsequent biofouling steps that include attachment of pioneer microorganisms and their growth into a mature biofilm happened eventually on the four membranes under flux and no flux conditions. Studying these modified membranes under sub-critical flux was not the main objective of this work, yet biofilm formation happened on all the membranes, regardless of the chemical characteristics of the membrane surface or the imposed permeate flux.

#### **4.5. Conclusion**

This is the first study that adopted several analytical tools to characterize the temporal dynamics of EPS, on four polymeric ultrafiltration membranes differing in hydrophobic and hydrophilic character, tested in parallel in the same membrane bioreactor tank.

The main outcomes can be summarized as follows:

- (1) The intrinsic membrane characteristics does not seem to impact long term membrane fouling, yet it might contribute to the initial transmembrane pressure value that was established within couple of hours after filtration.
- (2) Despite clear differences in the transmembrane pressure measurements, the different surface characteristics of the membranes did not affect the selection of specific foulants at the initial stages of filtration (day 1).
- (3) Hydrophilic sulfonated polysulfone membrane accumulated the lowest amounts of foulants and developed the lowest transmembrane pressure compared with the other four membranes, potentially due to the high negative surface charge.

- (4) The same temporal changes in EPS were observed on the surfaces of all the membranes tested.
- (5) The combination of analytical tools provided a comprehensive analysis of the accumulated foulants selected on membrane surfaces in the lab-scale MBR.

A potential alternative explanation for the impact of accumulated biomass on transmembrane pressure was discussed, involving the thickness, biofilm compactness (density) and spatial structure including *in-situ* non-destructive methods for characterization such as optical coherence tomography and NMR.

### **Acknowledgements**

This work was sponsored by King Abdullah University of Science and Technology (KAUST).

## References

1. Santos, A., Ma, W., Judd, S.J. Membrane bioreactors: two decades of research and implementation. **Desalination**, v. 273, n. 1, p. 148-154, 2011.
2. Vanysacker, L., Boerjan, B., Declerck, P., Vankelecom, I.F. Biofouling ecology as a means to better understand membrane fouling. **Appl. Microbiol. Biotechnol.**, v. 98, n. 10, p. 8047-8072, 2014.
3. Meng, F., Chae, S.R., Drews, A., Kraume, M., Shin, H.S., Yang, F. Recent advances in membrane bioreactors (MBRs): membrane fouling and membrane material. **Water Res.**, v. 43, n. 6, p. 1489-1512, 2009.
4. Gao, D.W., Wen, Z.D., Li, B., Liang, H. Microbial community structure characteristics associated membrane fouling in A/O-MBR system. **Bioresour. Technol.**, v. 154, p. 87-93, 2014.
5. Verrecht, B., Maere, T., Nopens, I., Breplos, C., Judd, S. The cost of a large-scale hollow fiber MBR. **Water Res.**, v. 44, n. 18, p. 5274-5283, 2010.
6. Flemming, H.C., Schaule, G., Griebe, T., Schmitt, J., Tamachkiarowa, A. Biofouling – The Achilles heel of membrane processes. **Desalination**, v. 113, n. 2, p. 215-225, 1997.
7. Malaeb, L., Le-Clech, P., Vrouwenvelder, J.S., Ayoub, G.M., Saikaly, P.E. Do biological-based strategies hold promise to biofouling control in MBRs? **Water Res.**, v. 47, n. 15, p. 5447-5463, 2013.
8. Yang, H.L., Chun-Te Lin, J., Huang, C. Application of nanosilver surface modification to RO membrane and spacer for mitigating biofouling in seawater desalination. **Water Res.**, v. 43, n. 15, p. 3777-3786, 2009.
9. Araújo, P., Miller, D., Correia, P., Van Loosdrecht, M., Kruithof, J., Freeman, B., Paul, D., Vrouwenvelder, J. Impact of feed spacer and membrane modification by hydrophilic, bactericidal and biocidal coating on biofouling control. **Desalination**, v. 295, p. 1-10, 2012.
10. Nikolaeva, D., Langner, C., Ghanem, A., Rehim, M.A., Voit, B., Meier-Haack, J. Hydrogel surface modification of reverse osmosis membranes. **J. Membr. Sci.**, v. 476, p. 264-276, 2015.
11. Miller, D.J., Araújo, P.A., Correia, P.B., Ramsey, M.M., Kruithof, J.C., Van Loosdrecht, M.C., Freeman, B.D., Paul, D.R., Whiteley, M., Vrouwenvelder, J.S. Short-term adhesion and long-term biofouling testing of polydopamine and poly(ethyleneglycol) surface modifications of membranes and feed spacers for biofouling control. **Water Res.**, v. 46, n. 12, p. 3737-3753, 2012.
12. Zodrow, K., Brunet, L., Mahendra, S., Li, D., Zhang, A., Li, Q., Alvarez, P.J. Polysulfone ultrafiltration membranes impregnated with silver nanoparticles show improved biofouling resistance and virus removal. **Water Res.**, v. 43, n. 3, p. 715-723, 2009.
13. Tang, L., Livi, K.J., Chen, K.L. Polysulfone membranes modified with bioinspired polydopamine and silver nanoparticles formed in situ to mitigate biofouling. **Environ. Sci. Technol. Letters.**, v. 2, n. 3, p. 59-65, 2015.

14. Kimura, K., Tanaka, I., Nishimura, S.I., Miyoshi, R., Miyoshi, T., Watanabe, Y. Further examination of polysaccharides causing membrane fouling in membrane bioreactor (MBRs): Application of lectin affinity chromatography and MALDI-TOF/MS. **Water Res.**, v. 46, n. 17, p. 5725-5734, 2012.
15. Gao, D., Fu, Y., Ren, N. Tracing biofouling to the structure of the microbial community and its metabolic products: A study of the three-stage MBR process. **Water Res.**, v. 47, n. 17, p. 6680-6690, 2013.
16. Ng, T.C.A., Ng, H.Y. Characterisation of initial fouling in aerobic submerged membrane bioreactors in relation to physico-chemical characteristics under different flux conditions. **Water Res.**, v. 44, n. 7, p. 2336-2348, 2010.
17. Kimura, K., Hane, Y., Watanabe, Y., Amy, G., Ohkuma, N. Irreversible membrane fouling during ultrafiltration of surface water. **Water Res.**, v. 38, n. 14, p. 3431-3441, 2004.
18. Jarusutthirak, C., Amy, G. Role of soluble microbial products (SMP) in membrane fouling and flux decline. **Environ. Sci. Technol.**, v. 40, n. 3, p. 969-974, 2006.
19. Maab, H., Al-Saadi, A., Francis, L., Livazovic, S., Ghaffour, N., Amy, G.L., Nunes, S.P. Synthesis and fabrication of nanostructured hydrophobic polyazole membranes for low-energy water recovery. **J. Membr. Sci.**, v. 423, p. 11-19, 2012.
20. Maab, H., Francis, L., Al-Saadi, A., Aubry, C., Ghaffour, N., Amy, G., Nunes, S.P. Polyazole hollow fiber membranes for direct contact membrane distillation. **Ind. Eng. Chem. Res.**, v. 52, n. 31, p. 10425-10429, 2013.
21. Ponce, M.L., Gomes, D., Nunes, S.P. One-step of high molecular weight sulfonated poly (oxadiazole-triazole) copolymers for proton conductive membranes. **J. Membr. Sci.**, v. 319, n. 1, p. 14-22, 2008.
22. Wang, Y.K., Sheng, G.P., Ni, B.J., Li, W.W., Zeng, R.J., Wang, Y.Q., Shi, B.J., Yu, H. Q. Simultaneous carbon and nitrogen removals in membrane bioreactor with mesh filter: An experimental and modeling approach. **Cehm. Eng. Sci.**, v. 95, p. 78-84, 2013.
23. Judd, S. The status of industrial and municipal effluent treatment with membrane bioreactor technology. **Chem. Eng. J.**, 2015.
24. Gonzalez-Gil, G., Thomas, L., Emwas, A., Lens, P., Saikaly, P. NMR and MALDI-TOF MS based characterization of exopolysaccharides in anaerobic microbial aggregates from full-scale reactors. **Sci. Rep.**, v. 5, p. 14316, 2015.
25. Huber, S.A., Balz, A., Albert, M., Pronk, W. Characterisation of aquatic humic and non-humic matter with size-exclusion chromatography-organic carbon detection organic nitrogen detection (LC-OCD-OND). **Water Res.**, v. 45, n. 2, p. 879-885, 2011.
26. Wang, Y., Le Roux, J., Zhang, T., Croue, J.P. Formation of brominated disinfection byproducts from natural organic matter isolates and model compounds in a sulfate radical-based oxidation process. **J. Membr. Sci.**, v. 48, n. 24, p. 14534-14542, 2014.
27. Murphy, K.R., Butler, K.D., Spencer, R.G., Stedmon, C.A., Boehme, J.R., Aiken, G.R. Measurement of dissolved organic matter fluorescence in aquatic environments: an interlaboratory comparison. **Environ. Sci. Technol.**, v. 44, n. 24, p. 9405-9412,

- 2010.
28. Khan, M.T., Busch, M., Molina V.G., Emwas, A.H., Aubry, C., Croue, J.P. How different is the composition of the fouling layer of wastewater reuse and seawater desalination RO membranes? **Water Res.**, v. 59, p. 271-282, 2014.
  29. Lowry, O.H., Rosebrough, N.J., Farr, A.L., Randall, R.J. with the Folin phenol reagent. Protein measurement. **J. Biol. Chem.**, v. 193, n. 1, p. 265-275, 1951.
  30. Dubois, M., Gilles, K.A., Hamilton, J.K., Rebers, P., Smith, F. Colorimetric method for determination of sugars and related substances. **Anal. Chem.**, v. 28, n. 3, p. 350-356, 1956.
  31. Varmuza, K., Filzmoser, P. Introduction to multivariate statistical analysis in chemometrics. CRC Press, Boca Raton, FL, USA., 2009.
  32. Legendre, P., Gallagher, E.D. Ecologically meaningful transformation for ordination of species data. **Oecologia**, v. 129, n. 2, p. 271-280, 2001.
  33. RStudio. RStudio: Integrated development environment for R (Version 0.98.501) [Computer Software]. Available from <http://www.rstudio.org/> Boston, MA., 2012.
  34. Oksanen, J., Blanchet, G., Kindt, R., Legendre, P., Minchin, P.R., O'Hara, B., Simpson, G.L., Solymos, P., Stevens, M.H.H., Wagner, H. Vegan: Community ecology package. R package version (2.0-8) <http://CRAN.R-project.org/package=vegan>., 2013.
  35. Subhi, N., Verliefde, A.R., Chen, V., Le-Clech, P. Assessment of physicochemical interactions in hollow fiber ultrafiltration membrane by contact angle analysis. **J. Membr. Sci.**, v. 403, n. 2012, p. 32-40, 2012.
  36. Elimelech, M., Phillip, W.A. The future of seawater desalination energy, technology, and the environment. **Science**, v. 333, n. 6043, p. 712-717, 2011.
  37. Zhang, M., Liao, B.Q., Zhou, X., He, Y., Hong, H., Lin, H., Chen, J. Effects of hydrophilicity/hydrophobicity of membrane on membrane fouling in a submerged membrane bioreactor. **Bioresour. Technol.**, v. 175, p. 59-67, 2015.
  38. Qu, F., Liang, H., Wang, Z., Wang, H., Li, G. Ultrafiltration membrane fouling by extracellular organic matters (EOM) of *Microcystis Aeruginosa* in stationary phase: Influence of interfacial characteristics of foulants and fouling mechanisms. **Water Res.**, v. 46, n. 5, p. 1490-1500, 2012.
  39. Ivnitsky, H., Katz, I., Minz, D., Volvovic, G., Shimoni, E., Kesselman, E., Semiart, R., Dosoretz, C.G., Bacterial community composition and structure of biofilms developing on nanofiltration membranes applied to wastewater treatment. **Water Res.**, v. 41, n. 17, p. 3924-3935, 2007.
  40. Dreszer, C., Wexler, A.D., Drusová, S., Overdijk, T., Zwijnenburg, A., Flemming, H.C., Kruijthof, J.C., Vrouwenvelder, J.C. In-situ biofilm characterization in membrane systems using optical coherence tomography: formation, structure, detachment and impact of flux change. **Water Res.**, v. 67, p. 243-254, 2014.
  41. Farias, E.L., Howe, K.J., Thomson, B.M. Spatial and temporal evolution of organic foulant layers on reverse osmosis membranes in wastewater reuse applications. **Water Res.**, v. 58, p. 102-110, 2014.
  42. Drews, A. Membrane fouling in membrane bioreactors-characterisation,

- contradictions, cause and cures. **J. Membr. Sci.**, v. 363, n. 1, p. 1-28, 2010.
43. Meng, F., Liao, B., Liang, S., Yang, F., Zhang, H., Song, L. Morphological visualization, componential characterization and microbiological identification of membrane fouling in membrane bioreactor (MBRs). **J. Membr. Sci.**, v. 361, n. 1, p. 1-14, 2010.
  44. Bridgemna, J., Bieroza, M., Baker, A. The application of fluorescence spectroscopy to organic matter characterisation in drinking water treatment. **Rev. Environ. Sci. Biotechnol.**, v. 10, n. 3, p. 277-290, 2011.
  45. Dreszer, C., Flemming, H.C., Zwijnenburg, A., Kruithof, J., Vrouwenvelder, J. Impact of biofilm accumulation on transmembrane and feed channel pressure drop: Effects of crossflow velocity, feed spacer and biodegradable nutrient. **Water Res.**, v. 50, p. 200-211, 2014.
  46. Valladares Linares, R., Wexler, A.D., Bucs, Sz.S., Dreszer, C., Zwijnenburg, A., Flemming, H. -C, Kruithof, J.C., Vrouwenvelder, J.C. Compaction and relaxation of biofilms. **Desal. Water Treat.**, p. 1-13, 2015.
  47. Bucs, Sz. S., Valladares Linares, R., Van Loosdrecht, M.C.M., Kruithof, J.C., Vrouwenvelder, J.S. Impact of organic nutrient load on biomass accumulation and pressure drop increase in membrane systems. **Water Res.**, v. 67, p. 227-242, 2014.
  48. Cornelissen, E.R., Vrouwenvelder, J.S., Heijman, S.G.J., Viallefont, X.D., Van Der Kooij, D., Wessels, L.P. Periodic air/water cleaning for control of biofouling in spiral wound membrane elements. **J. Membr. Sci.**, v. 287, n. 1, p. 94-101, 2007.
  49. Vrouwenvelder, J.S., Buitter, J., Riviere, M., Van der Meer, W.G.J., Van Loosdrecht, M.C.M., Kruithof, J.C. Impact of flow regime on pressure drop increase and biomass accumulation and morphology in membrane systems. **Water Res.**, v. 44, n. 3, p. 689-702, 2010.
  50. Van Loosdrecht, M.C.M., Bereschenko, L.A., Radu, A.I., Kruithof, J.C., Picioreanu, C., Johns, M.L., Vrouwenvelder, J.S. New approaches to characterizing and understanding biofouling of spiral wound membrane systems. **Water Sci. Technol.** , v. 66, n. 1, p. 88-94, 2012.
  51. Derlon, N., Peter-Varbanets, M., Scheidegger, A., Pronk, W., Morgenroth, E. Predation influences the structure of biofilm developed on ultrafiltration membranes. **Water Res.**, v. 46, n. 10, p. 3323-3333, 2012.
  52. West, S., Wagner, M., Engelke, C., Horn, H. Optical coherence tomography for the in situ three-dimensional visualization and quantification of feed spacer channel fouling in reverse osmosis membrane modules. **J. Membr. Sci.** , v. 498, p. 345-352, 2016.
  53. Graf von der Schulenburg, D.A., Vrouwenvelder, J.S., Creber, S.A., van Loosdrecht, M.C.M., Gladden, L.F., Johns, M.L. Nuclear Magnetic Resonance microscopy studies of membrane biofouling. **J. Membr. Sci.**, v. 323, n. 1, p. 37-44, 2008.
  54. Creber, S.A., Pintelon, T.R.R., Schulenburg, D.A.W.G., Vrouwenvelder, J.S., van Loosdrecht, M.C.M., Johns, M.L. Magnetic resonance imaging and 3D simulation studies of biofilm accumulation and cleaning on reverse osmosis membranes. **Food and Bioproducts Processing**, v. 88, n. 4, p. 401-408, 2010.
  55. Creber, S.A., Vrouwenvelder, J.S., Van Loosdrecht, M.C.M., Johns, M.L. Chemical

- cleaning of biofouling in reverse osmosis membranes evaluated using magnetic resonance imaging. **J. Membr. Sci.**, v. 362, n. 1-2, p. 202-210, 2010.
56. Ognier, S., Wisniewski, C., Grasmick, A. Membrane bioreactor fouling in sub-critical filtration conditions: a local critical flux concept. **J. Membr. Sci.**, v. 229, n. 1, p. 171-177, 2004.
57. Le-Clech, P., Jefferson, B., Chang, I.S., Judd, S.J. Critical flux determination by the flux-step method in a submerged membrane bioreactor. **J. Membr. Sci.**, v. 227, n. 1, p. 81-93, 2003.
58. Vrouwenvelder, J., Van Paassen, J., Van Agtmaal, J., Van Loosdrecht, M., Kruithof, J., 2009a. A critical flux to avoid biofouling of spiral wound nanofiltration and reverse osmosis membranes: fact or fiction? **J. Membr. Sci.**, v. 326, n. 1, p. 36-44, 2009.
59. Vrouwenvelder, J., Von Der Schulenburg, D.G., Kruithof, J., Johns, M., Van Loosdrecht, M.C.M. Biofouling of spiral wound nanofiltration and reverse osmosis membranes: a feed spacer problem. **Water Res.**, v. 43, n. 3, p. 583-594, 2009.
60. Drioli, E., Giorno, L. **Membrane operations: innovative separations and transformations**. [S.l.]: Wiley-VCH, 2009.
61. Yamamura, H., Okimoto, K., Kimura, K., Watanabe, Y. Hydrophilic fraction of natural organic matter causing irreversible fouling of microfiltration and ultrafiltration membranes. **Water Res.**, v. 54, p. 123-136, 2014.

## CHAPTER 5 CONCLUSION

### 5.1. General conclusions

Membrane bioreactors (MBRs) offer alternative and promising solutions for wastewater treatment and reuse, as a potential strategy to address water scarcity issues. Besides screening blockage and membrane pore clogging, membrane fouling, especially biofouling, remains a burden for MBR treatment installations and plants operators. This phenomenon is unavoidable since it involves direct interactions between complex microbial communities and membrane surfaces.

The imposed operating conditions in MBRs (i.e. sludge retention time, aeration intensity, permeate flux, wastewater type, nutrient load) directly affect the composition of microbial communities in the mixed liquor, which ultimately affect the rate of membrane biofouling. In chapter 2, a study was conducted on five full-scale MBR treatment plants equipped with the same type of membrane modules and treating different domestic wastewater. The microbial communities responsible for early and mature membrane biofouling were characterized, and samples from the mixed liquor were collected in parallel. Our results showed that the sessile (membrane biofilm) and planktonic (mixed liquor) bacterial communities were distinct from each. These results are in agreement with previous findings in other studies conducted on lab-scale MBR systems. The microbial communities from each MBR plant (mixed liquor biomass, early and mature biofilm) clustered separately, possibly due to differences in the operating conditions (i.e. SRT, HRT) that affected the microbial source community. Pyrosequencing results

revealed that *Proteobacteria* was the dominant phylum in the five MBR plants, while phylum *Bacteroidetes* were highly abundant in only two MBR plants and *Chloroflexi* was found in high abundance in only one MBR plant. Statistical analysis confirmed that both early and mature biofouling communities differed significantly from random assemblages from the mixed liquor ( $P < 0.001$  for each MBR), indicating that biofouling communities were unlikely to immigrate randomly from the suspended community, and they did not reflect the community in the mixed liquor. It seems that local conditions on the membrane surface selected for specific biofouling species from the source community. According to the results obtained from the full-scale study in chapter 2, investigating the effect of membrane surface properties on the composition of biofouling communities was suggested.

In chapter 3, a lab-scale MBR treating synthetic wastewater was used to determine the fouling propensity of hollow-fiber membranes having different surface chemistry, during 30 d filtration experiments. Similarly to the full-scale results, the membrane biofouling and the mixed liquor communities were distinct. Biofouling communities were characterized on hydrophobic and hydrophilic membranes, tested in parallel with and without permeate flux in the same MBR tank. Our results showed that the permeate drag force did not affect the composition of biofouling communities, and the microbial communities that adsorbed passively (without flux) and actively (with 10 L/m<sup>2</sup>.h permeate flux) were identical. Despite differences in membrane surface chemistry, the hydrophobic or hydrophilic membrane character did not select any specific early bacterial colonizers at the initial stages of filtration. Pyrosequencing results showed that *Betaproteobacteria* were the most abundant class within the phylum *Proteobacteria* on

the five different membranes at days 1, and the relative abundance of *Firmicutes* increased in the biofouling communities at days 20 and 30, possibly due to successional steps that lead to the formation of a mature biofilm. Specific conditions on the membrane surfaces could have recruited the early colonizers from the mixed liquor, which evolved afterwards to form an identical mature biofilm regardless of the membrane surface (i.e. hydrophobicity, hydrophilicity). Biofilm formation on membrane surfaces could have been the result of a natural biofilm formation, initial early colonizers and subsequent development into a mature biofilm. In addition, the hydrophobic/hydrophilic membrane character did not select any specific early bacterial colonizers at the initial stages of filtration, and identical temporal dynamics in the communities were observed on the five different membranes. Pyrosequencing results showed that *Betaproteobacteria* were the most abundant class within the *Proteobacteria* phyla on the five different membranes at days 1 and 10, and *Bacteroidetes* increased in abundance after 10 d of membrane filtration. The relative abundance of *Firmicutes* increased in the biofouling communities at days 20 and 30, potentially due to successional steps that lead to the formation of a mature biofilm. It is possible that specific conditions on the membrane surfaces allowed the recruitment of early colonizers from the mixed liquor, which evolved afterwards to form an identical mature biofilm regardless of the membrane surface properties.

Several past research studies on MBR biofouling have concluded that extracellular polymeric substances (EPS) are primarily responsible for membrane pore clogging, cake layer formation and loss in membranes' permeability. However, very few studies have examined the effect of modified membrane surfaces in selecting different EPS fractions and how these different EPS fractions change in composition with time. In chapter 4 we

investigated this knowledge gap by testing four different hydrophobic and hydrophilic hollow-fiber membranes, with and without permeate flux, for 30 d of continuous filtration in a lab-scale MBR treating synthetic wastewater. Several chemical analytical tools were used to characterize the composition of EPS at different stages of filtration (1, 10, 20 and 30 d). Our results showed that the same temporal changes in EPS composition were observed on the surfaces of the four different membranes. The results observed in chapter 3 (microbial communities) and chapter 4 (EPS foulants) followed a similar trend: i) different membrane surface chemistry did not select any specific early bacterial colonizers or EPS fractions after 1 d of filtration, and ii) identical temporal dynamics were observed regardless of membrane surface properties. The intrinsic membrane characteristics might have affected the initial transmembrane pressure (TMP) value that was established within couple of hours of filtration, but did not seem to impact the long-term membrane fouling propensity. When comparing the four different lab-made membranes, hydrophilic sulfonated polysulfone (SPSU) had the most negatively charged surface, accumulated the smallest amounts of foulants and exhibited the lowest TMP value after 30 d of filtration. The aforementioned results suggest that membrane surface does not affect the composition of EPS. Therefore, we propose to thoroughly investigate the thickness, compactness (density) and spatial architecture of biofilms by using *in-situ* non-destructive methods for biofilm characterization, such as optical coherence tomography (OCT) and nuclear magnetic resonance spectroscopy (NMR). A graphical schematic that summarizes the complex interactions between biological parameters, membrane biofilm attachment and growth, and membrane performance is proposed in Figure 5.1.

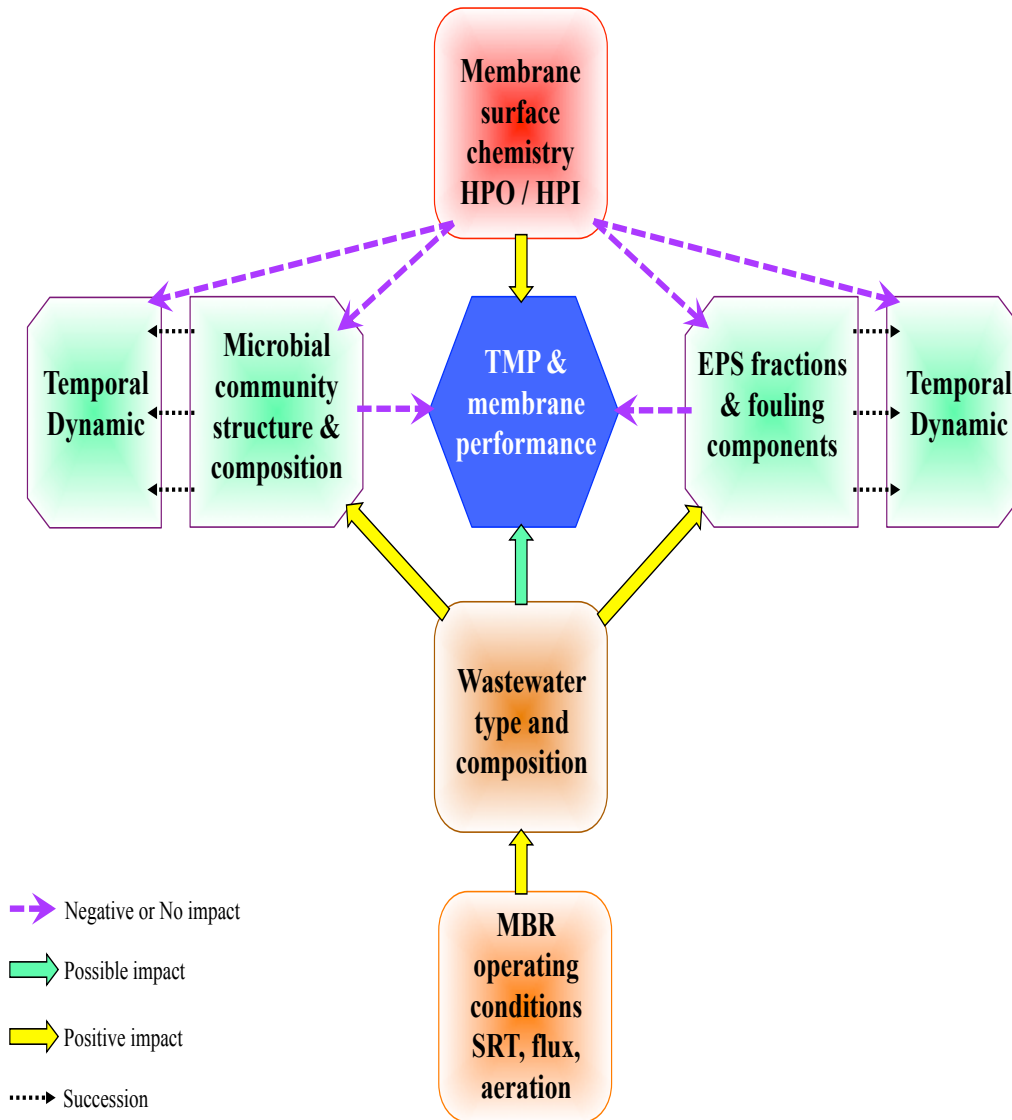


**Figure 5.1.** Inter-relationship between membrane biofouling in MBRs and the studied parameters that could affect the rate of this phenomenon.

## 5.2. Proposed approaches for future studies on MBR biofouling

The following approaches could be considered in future studies on MBR biofouling:

- Membrane surface modification has gained broad interests as a solution to control fouling and to improve system performance, especially including reverse osmosis,

nanofiltration and ultrafiltration membranes. Notwithstanding the significance of surface modification on the initial biofouling steps during early stages of filtration, the modified surface becomes secondary once the conditioning layer covers the membrane. Consequently, the membranes' surface characteristics are expected to lose their significance following the development of a mature fouling layer after extended filtration events. Therefore, it would be important to test the fouling propensity of modified membranes during extended durations, to evaluate their effectiveness in reducing or delaying MBR fouling.

- For reverse osmosis membranes, the measurement of silt density index (SDI) has been universally recognized in desalination applications as a parameter that can predict the fouling propensity of reverse osmosis feed water. In MBRs, the Delft Filtration Characterisation method (DFCm) has been normalized to assess the filterability of the MBR sludge. Alternatively, the critical-flux approach could determine a sustainable permeate flux below which the membrane fouling rate could remain relatively low. A combination of both approaches could enhance the performance of MBR systems in terms of delaying or reducing the occurrence of membrane biofouling
- Furthermore, a unified methodology that uses state-of-the-art analytical equipment's to characterize the foulants on membrane surface should be considered. While colorimetric tests such as Dubois and Lowry methods are important to quantify the polysaccharides and proteins fractions in the EPS fouling layer, other approaches should be considered to analyze different EPS fractions. Alternative analytical instruments could thoroughly identify different components of polysaccharides and

proteins, such as solid-state  $^{13}\text{C}$  NMR spectroscopy, elemental analysis with inductively coupled plasma optical emission spectroscopy (ICP-OES) and pyrolysis gas-chromatography mass spectroscopy (Pyro GC-MS).

- In the past decades, multiple approaches have been proposed to mitigate the occurrence of membrane biofouling, including membrane surface modification, addition of chemicals to increase the flocs sizes, periodic membrane backwashing, operating the system at sub-critical flux, and application of quorum quenching bacteria. These aforementioned approaches concluded their work following short filtration experiments, which does not necessarily predict the long-term membrane's performance. An integrated strategy to reduce or delay biofouling in MBRs should combine membrane cleaning and backwashing, increasing the membrane's surface hydrophilicity, and optimizing MBR operating conditions.

## **Appendix A - Effect of rinsing on the structure and composition of biofouling communities in MBRs.**

Several researchers investigated the prerequisite of rinsing the biofilm on the membrane with 1X phosphate-buffered saline (PBS) solution, prior to DNA extraction to differentiate between the loosely attached bacteria and the biofilm forming species. The objectives of this optimization study were to i) identify the rinsing frequency required to achieve a plateau in cell counts and ii) to investigate the effect of rinsing on the biofouling community structure and composition. Five different membranes were tested in the same MBR tank and membrane fibers were sacrificed after 24 h. Prior to DNA extraction, membrane samples were rinsed by consequently dipping the fiber in a falcon tube that contains 1X PBS solution. These solutions that contain the detached microbial communities were used to measure the number of cells using an Accuri C6 flow cytometer equipped with a 50 mW laser. Each measurement was repeated in triplicates.

Figure A.1. shows a decrease in the average cell count per membrane fiber, following each repetitive rinsing frequency. All membrane samples reached a plateau in cell counts after three times membrane rinsing with 1X PBS solution (Figure A.1.).

Consequently, the effect of rinsing frequency on the microbial community structure was investigated. A new batch of membrane modules was prepared and modules were run for 24 h before removing them from the MBR tank. The sacrificed membrane samples were separated into two categories: triplicate fibers were rinsed three times with 1X PBS (rinsing) prior to DNA extraction, and triplicate samples were kept without rinsing and DNA was extracted immediately after sample collection (no rinsing).

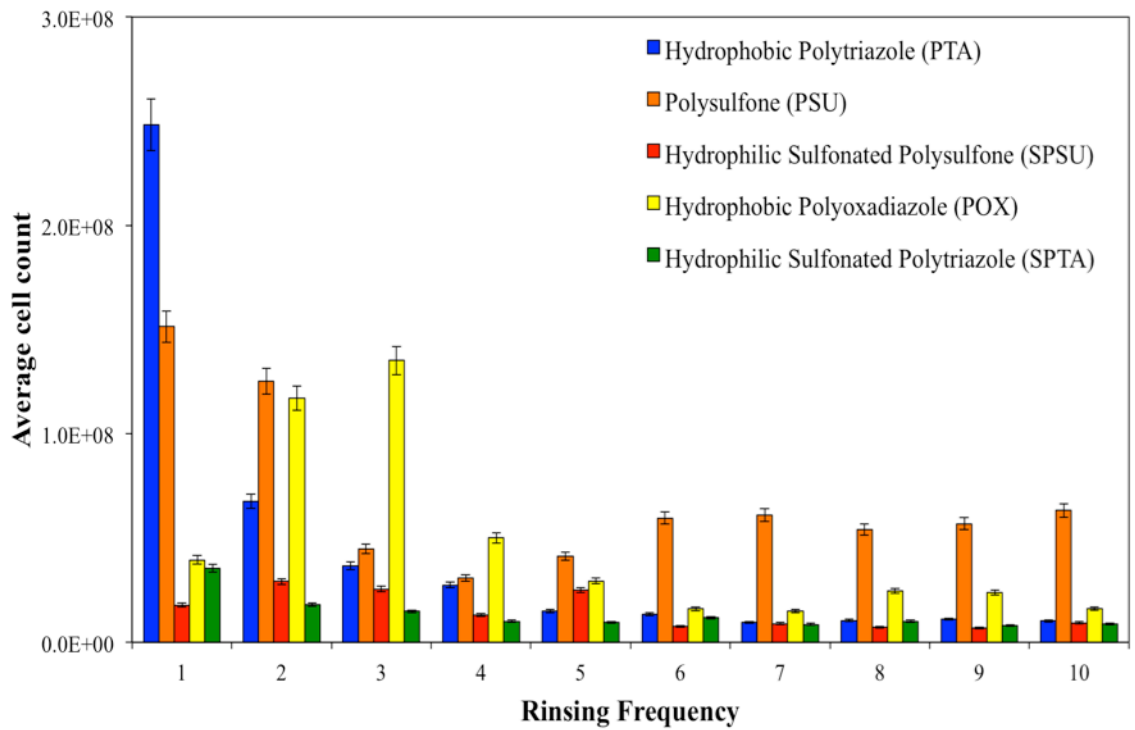


**Figure A.1.** Average cell count per rinsing for the five different hollow-fiber membranes.

Figure A.2. revealed similar composition of the biofouling communities for the different membrane categories (with and without rinsing), and *Epsilonproteobacteria* dominated the biofouling communities, followed by *Gammaproteobacteria* and *Betaproteobacteria*.

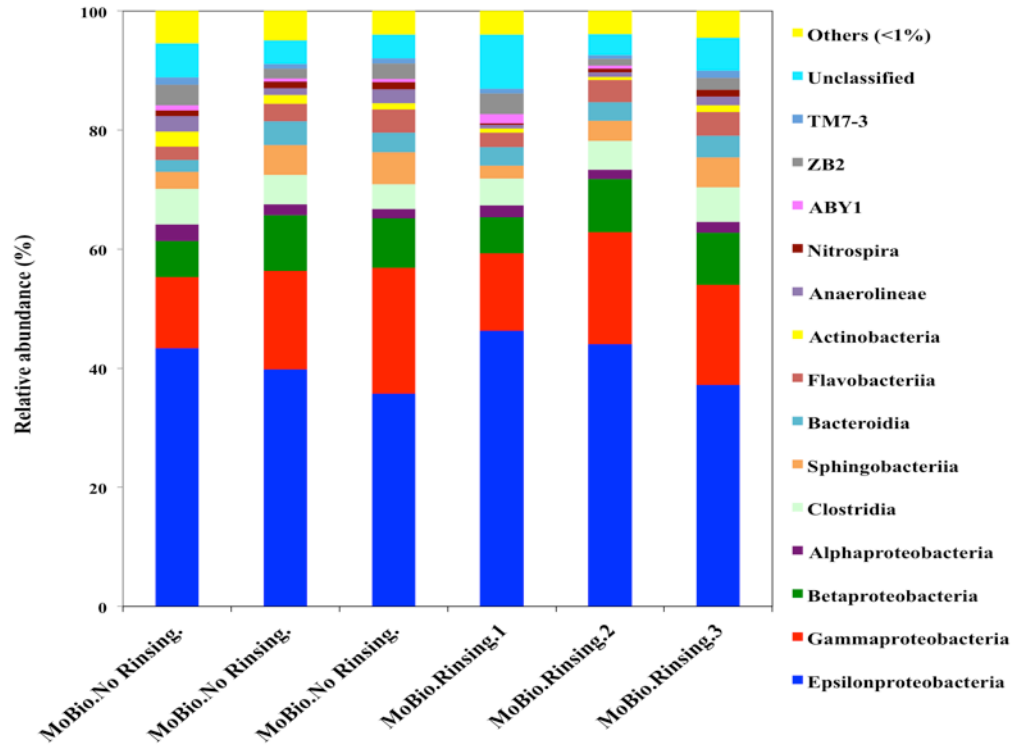


**Figure A.2.** Classification at the class level of the microbial communities extracted from membrane samples, with and without rinsing.

### Appendix B - Lab-scale MBR routine measurements, COD and Nutrients removal.

The lab-scale MBR was designed and operated for simultaneous COD and nutrients removal, and was inoculated with real sludge collected from the return activated sludge basin from a local wastewater treatment plant in Jeddah - KSA. The MBR was run for sludge acclimatization for 45 d and fed with synthetic wastewater. The concentrations of mixed liquor suspended solids (MLSS) and mixed liquor volatiles suspended solids (MLVSS) were monitored continuously and reached  $3743.5 \pm 311.5$  mg/L and  $3106 \pm 291$  mg/L, respectively (Figure B.1.).

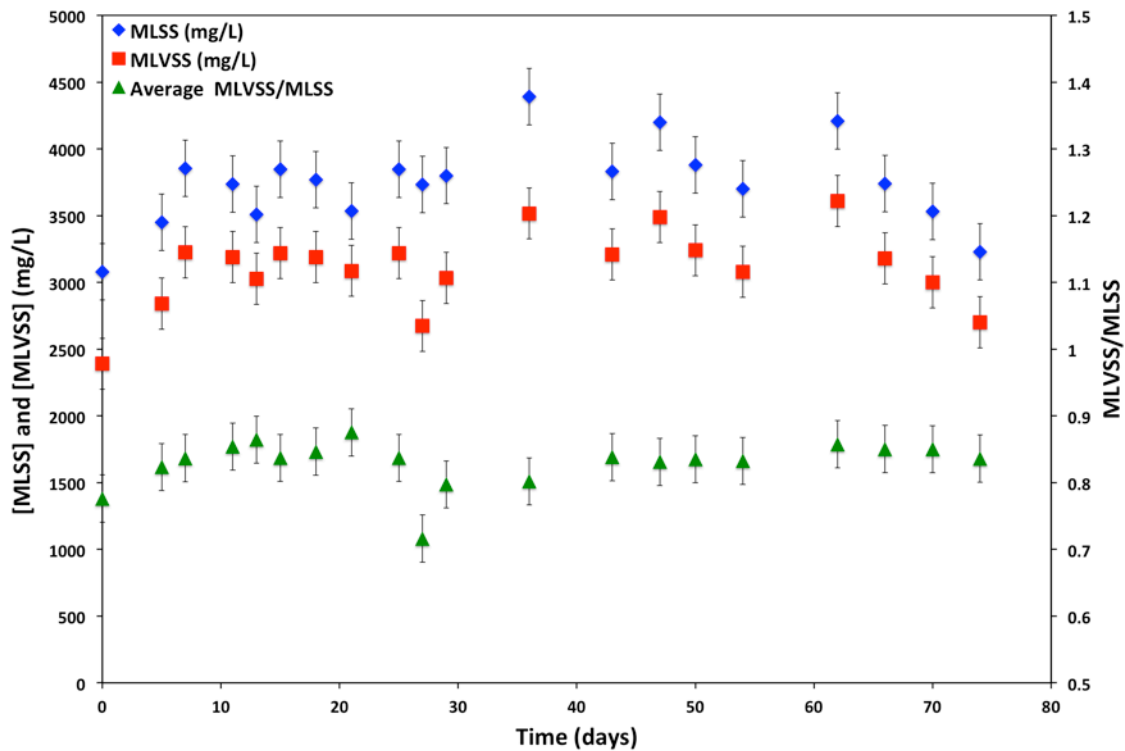


**Figure B.1.** Mixed liquor suspended solids (MLSS) and mixed liquor volatiles suspended solids (MLVSS) concentrations measured during acclimatization and experimental phase.

Likewise, daily measurements were conducted during aerobic and anoxic phases to monitor the dissolved oxygen concentration, pH and conductivity (Figure B.2). On average, the pH was  $7.8\pm 0.2$  and  $7.67\pm 0.19$ , while the conductivity in the mixed liquor was  $3.08\pm 0.4$  mS and  $3.1\pm 0.4$  mS during aerobic and anoxic phases, respectively. The concentration of dissolved oxygen was  $8.6\pm 0.1$  mg/L during the aerobic phase.

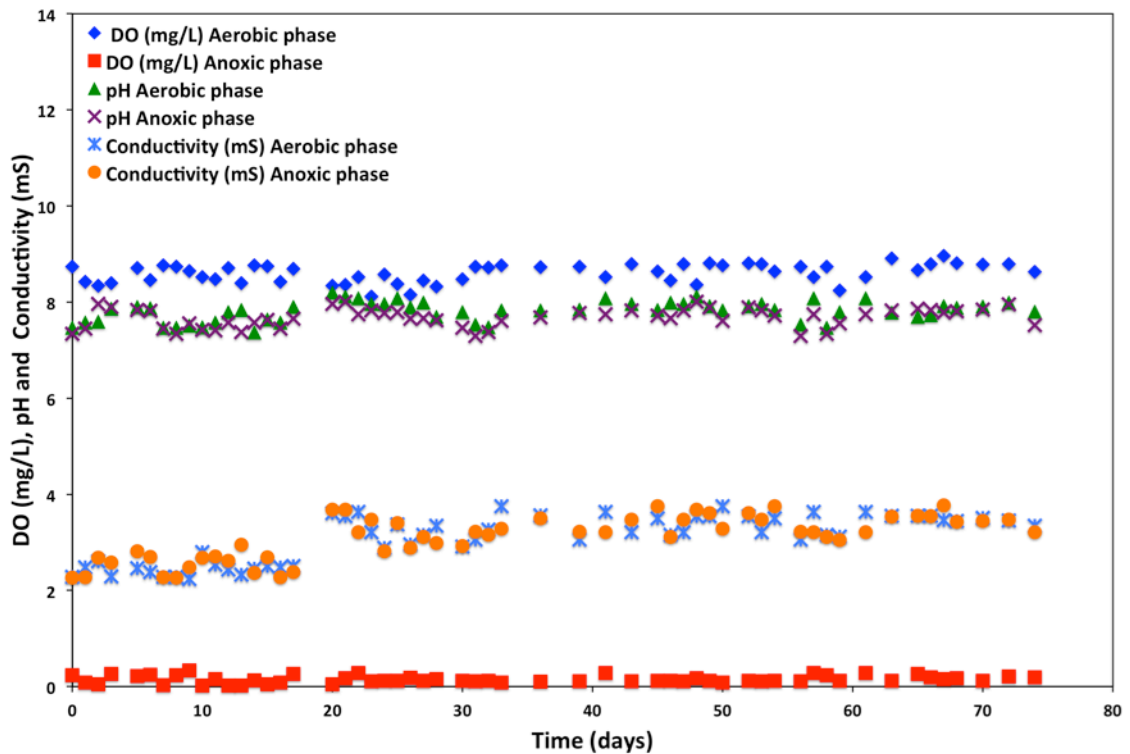


**Figure B.2.** Dissolved oxygen (mg/L), pH and conductivity (mS) measurements from the lab-scale MBR.

The reactor was fed with synthetic wastewater to simulate domestic wastewater with concentrations of  $404\pm 8.6$  mg/L COD and  $46\pm 1.5$  mg/L Ammonium, and the removal of COD and Ammonia were  $91.931\pm 2.8$  % and  $85.85\pm 6.2$  %, respectively

### Appendix C - Characterization of the hollow-fiber membranes.

The five clean hollow-fiber membranes were characterized by measuring FTIR (Figure C.1.), nominal pore size (Figure C.2.), zeta potential (Figure C.3.) and contact angle.

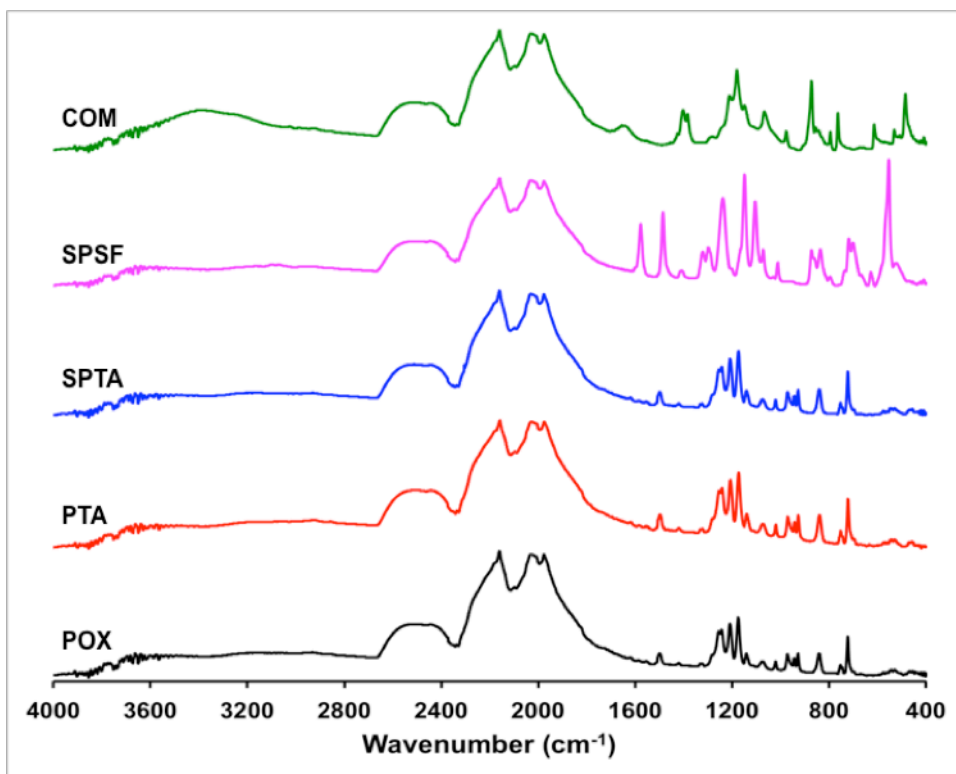


**Figure C.1.** Fourier transform infrared measurements of the five clean membranes.

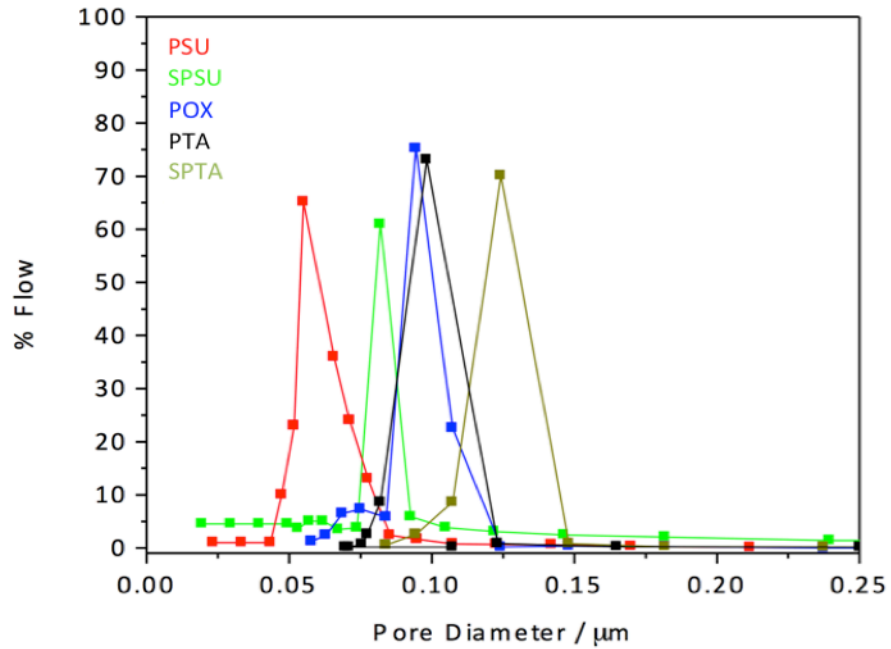


Figure C.2. Nominal pore size distribution for the four lab-made membranes.

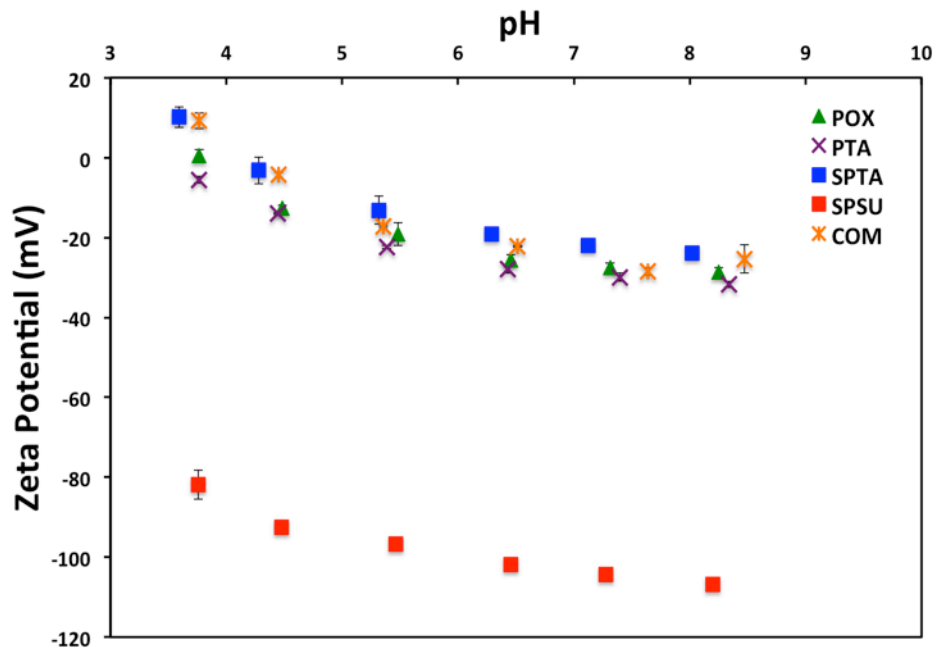
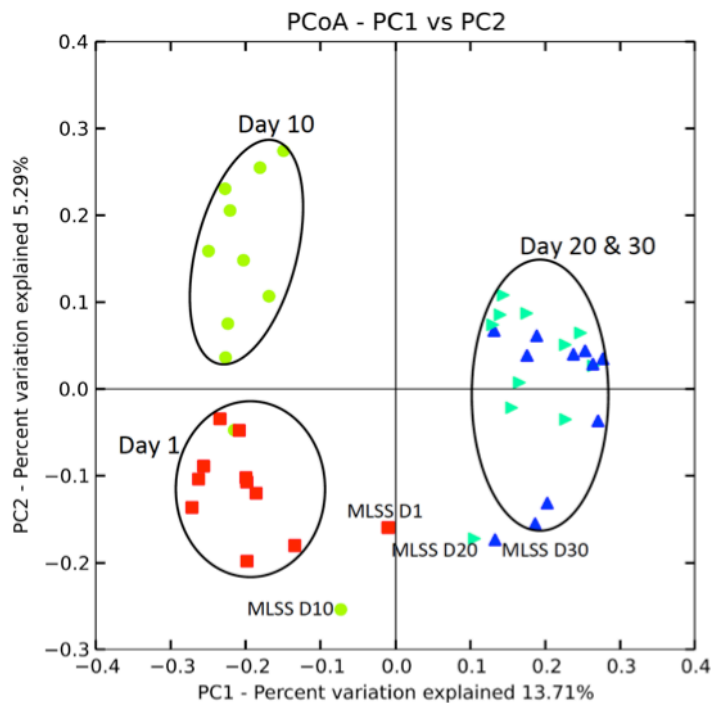


Figure C.3. Zeta potential measurements of the five clean membranes.

## Appendix D - Pyrosequencing results of RNA samples

Both DNA and RNA were extracted simultaneously from the membranes and mixed liquor samples using the MOBio PowerBiofilm RNA Isolation kit (MO BIO Laboratories, inc., Carlsbad, CA) with minor modifications. Consequently, the DNA was separated from the RNA using the ALLPrep DNA/RNA Mini Kit (Qiagen, Valencia, CA, USA). By targeting the RNA, it is possible to get insights on the active community and their function.



**Figure D.1.** Principal component analysis (PCoA) based on Unweighted Unifrac distance for the RNA samples extracted from the five different membranes operated with and without a permeate flux.

Preliminary sequencing results showed that the active microbial populations obtained through the analysis of RNA sequences demonstrated similar pattern to the DNA-derived populations. Figure D.1. shows the principal component analysis (PCoA) based on

unweighted unfrac distance of the RNA samples that clustered together according to the sampling day. RNA samples from days 1 and 10 clustered separately into two different groups while all samples from days 20 and 30 grouped together into one major cluster. In addition, the mixed liquor (MLSS) samples clustered separately from the membrane biofilm samples.

### **Appendix E - Optimization of different approaches for EPS extraction from hollow fiber membranes.**

Three different approaches to extract EPS from membrane surfaces were compared to optimize the best quantity and quality of EPS products. These approaches were adapted from Gonzalez-Gil et al., with minor modifications ([Gonzalez-Gil et al., 2015](#)). The membranes were immersed without filtration in an MBR tank for 24 h before starting the extraction protocols. The first three steps were identical and the major difference was at the 4<sup>th</sup> step. Briefly, 1) 10 cm of hollow-fiber membranes were cut into pieces and placed in 50 mL falcon tubes, 2) and 10 mL of 0.1 M NaCl were added to the membrane pieces. 3) Samples were subjected to vortexing for 45 min at full speed, to remove the EPS fractions within the biofilm from the membrane surface.

Figure E.1. shows the three different approaches and the corresponding EEM results of the EPS solutions. 5) A final extraction step consists of centrifugation the EPS solution at 12000g for 20 min at 4°C, to remove most of the remaining cells. According to the results presented above, approach C was adopted for the actual experiments.

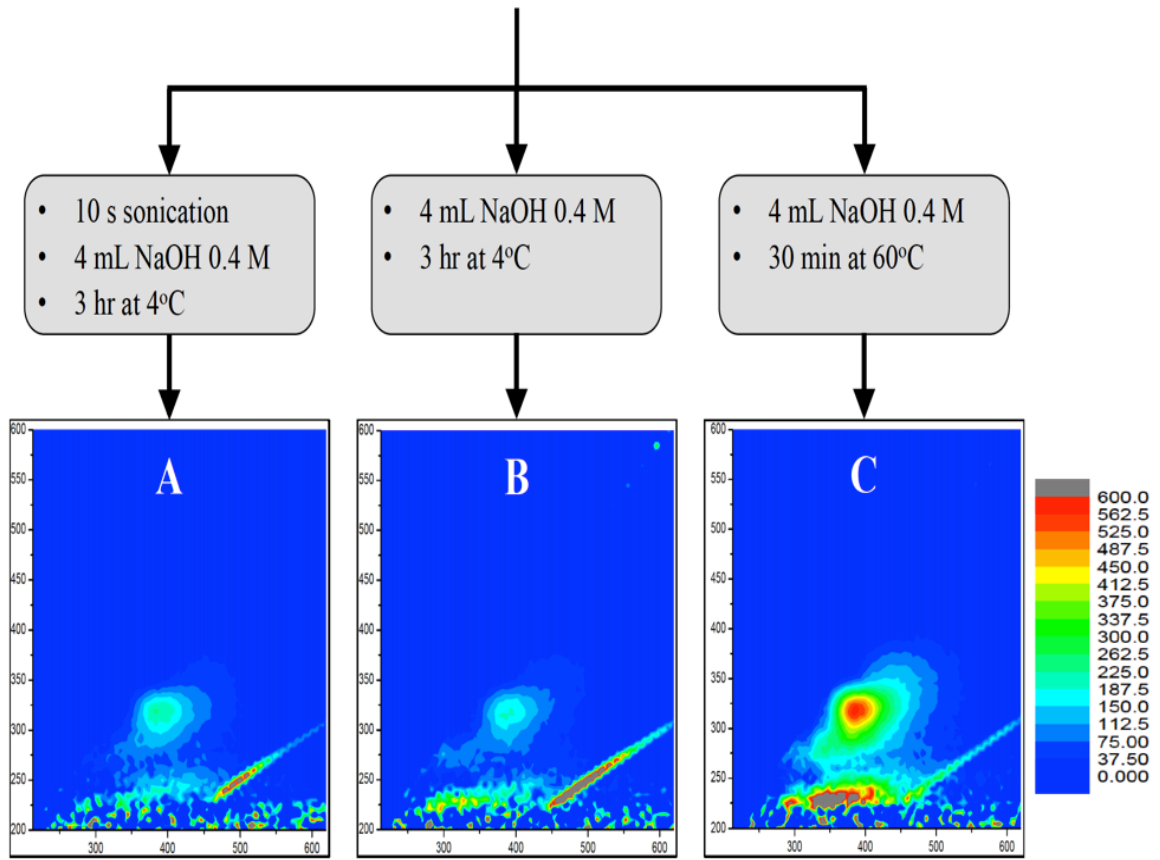
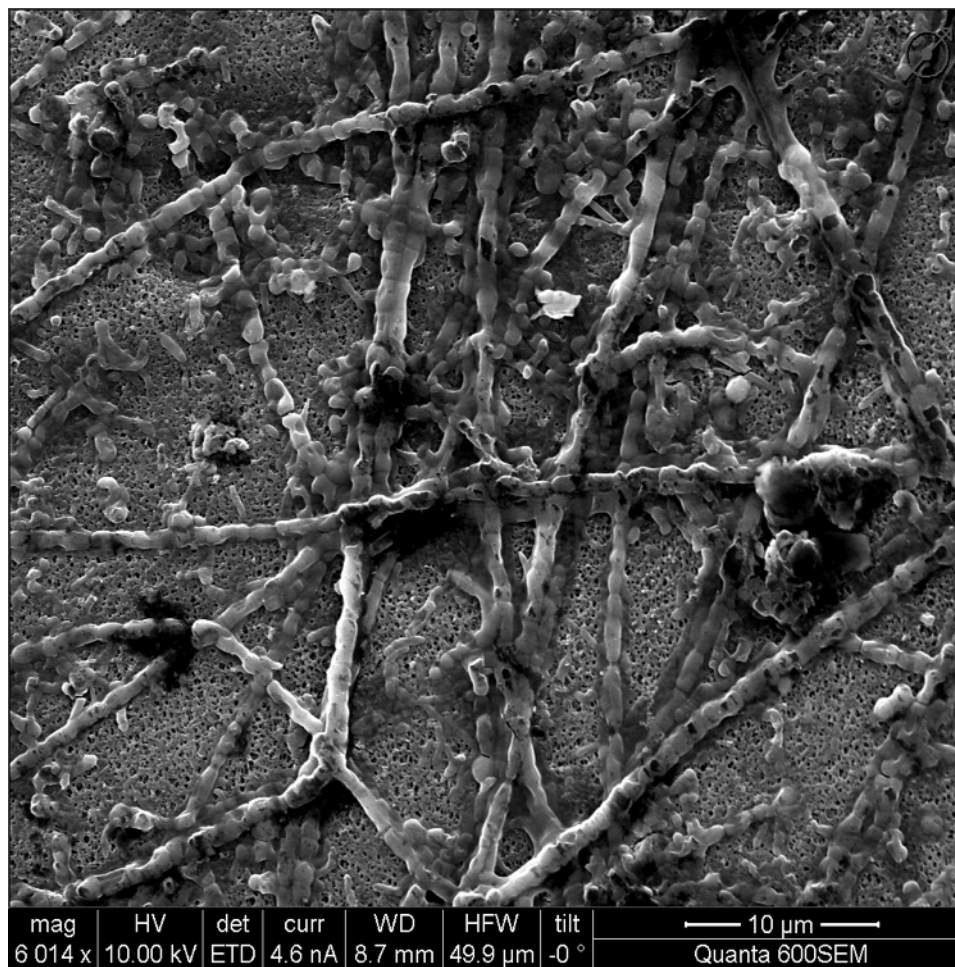


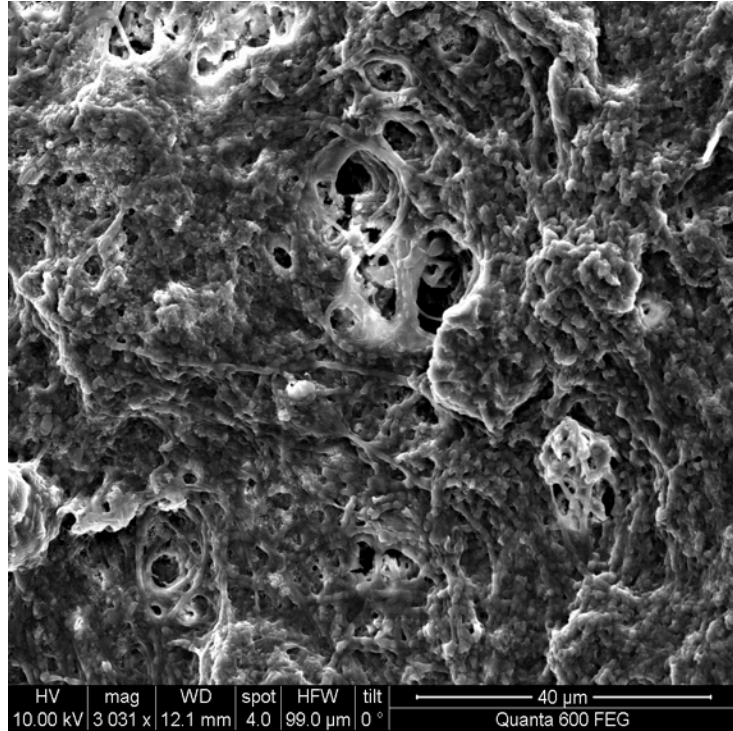
**Figure E.1.** Different approaches for EPS extraction and corresponding EEM results.

**Appendix F - Scanning electron micrographs and confocal laser scanning microscopy of biofilm samples on membrane surfaces.**

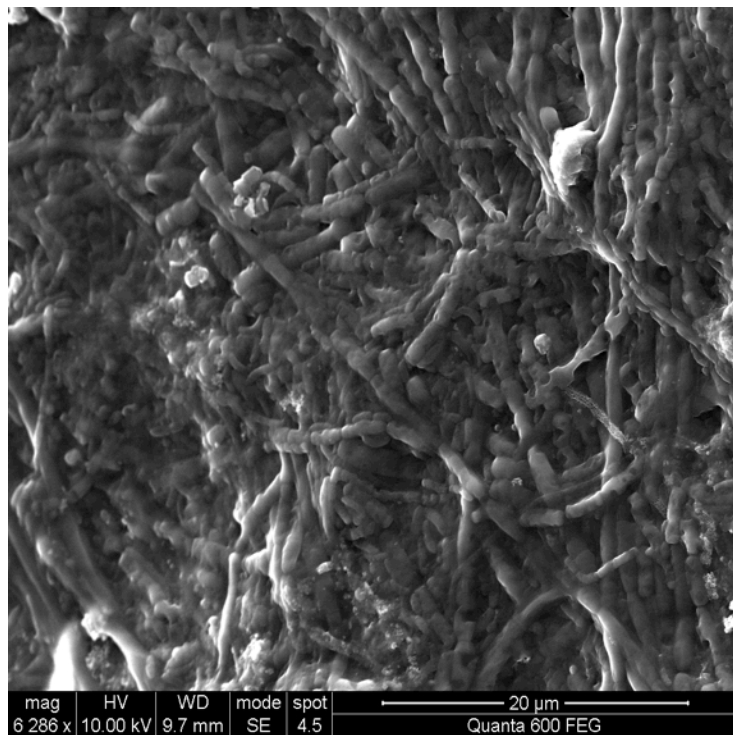
Membrane biofilm sections were fixed according to Katuri et al., (2012) and visualized using Quanta 600 scanning electron microscope (SEM). Random membrane samples from different sampling events are presented here.



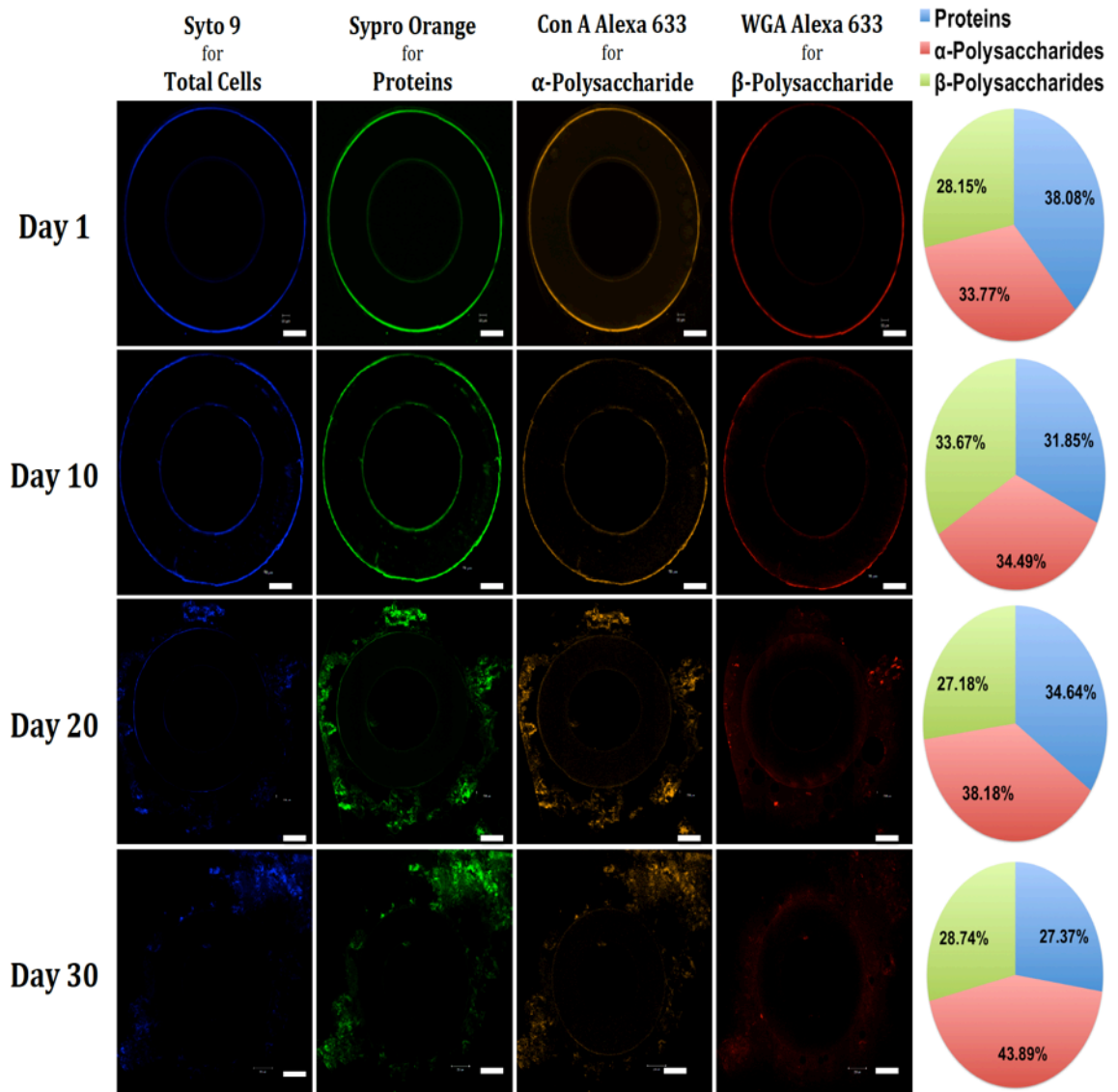
Attachment of early colonizers and their EPS products after 1 d filtration



Micro-channels formation within the biofilm on membrane surfaces after 20 d filtration



Dense biofilm covering completely the membrane surfaces after 30 d of filtration



Confocal laser scanning microscope images of the cryosectioned fibers collected from the commercial membrane modules

**Appendix G - Different lab-scale reactors designs and construction.**

Two different lab-scale MBRs were designed and constructed in the Water Desalination and Reuse Center (WDRC) to complete our research objectives. The first reactor was characterized with the ability to run 12 hollow-fiber membrane modules simultaneously. This reactor was used to complete the optimization work discussed in Appendix A. Figure G.1. shows the upper, frontal and side faces of the reactor, which accumulated biomass in the bottom corners. Therefore, a modified design was proposed to solve this biomass settlement problem.

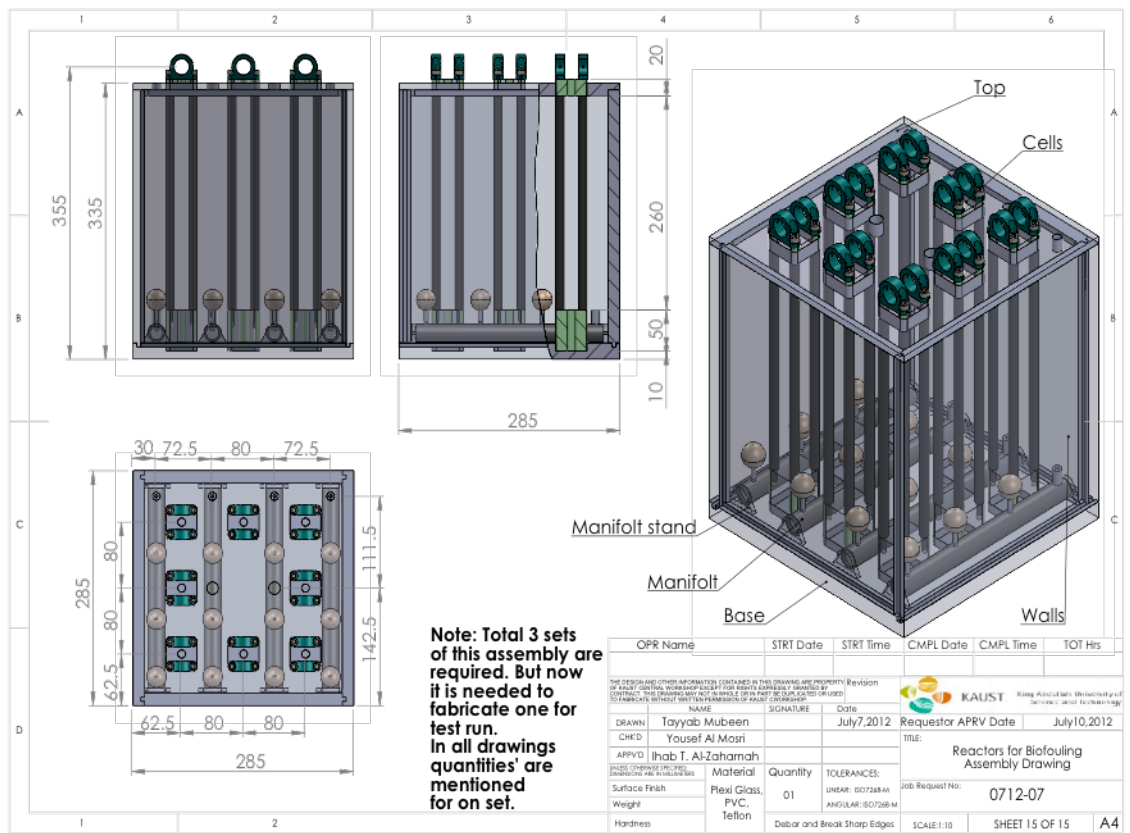


**Figure G.1.** Initial lab-scale MBR design.

The second lab-scale MBR presented in Figure G.2. solved the problem of biomass settlement, by adding slopes on both lateral sides. This reactor was used to complete all the lab-scale studies (chapters 3 and 4), and it can hold up to four membrane cassettes each of which can hold 6 different hollow-fiber membrane modules (total of 24 membrane modules).

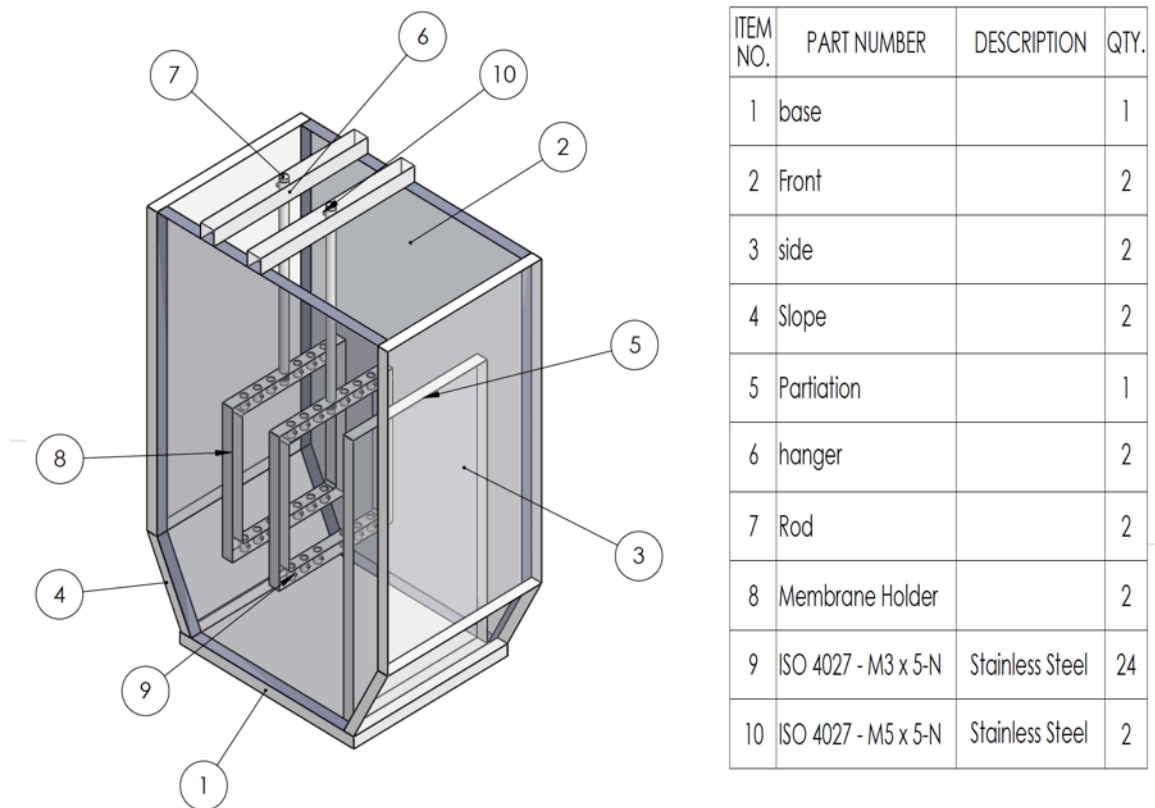


**Figure G.2.** Final design of the lab-scale MBR.

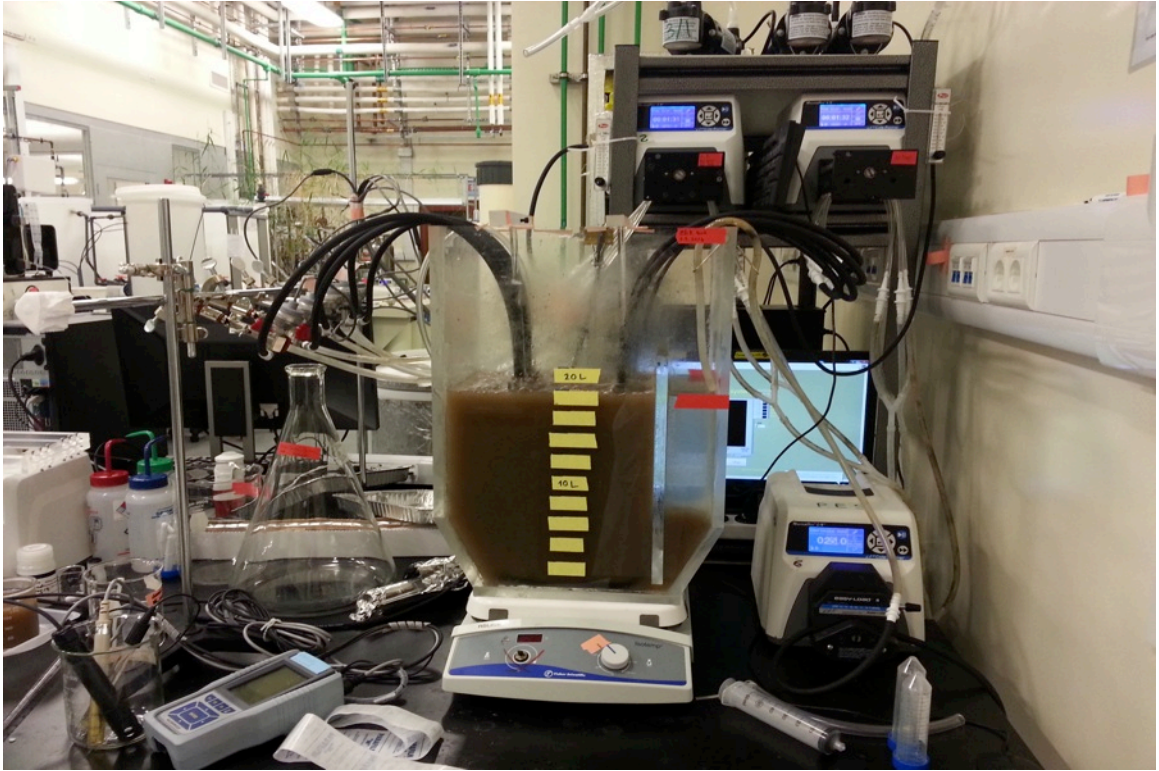


**Figure G.3.** Constructed lab-scale MBR in the Water Desalination and Reuse Center

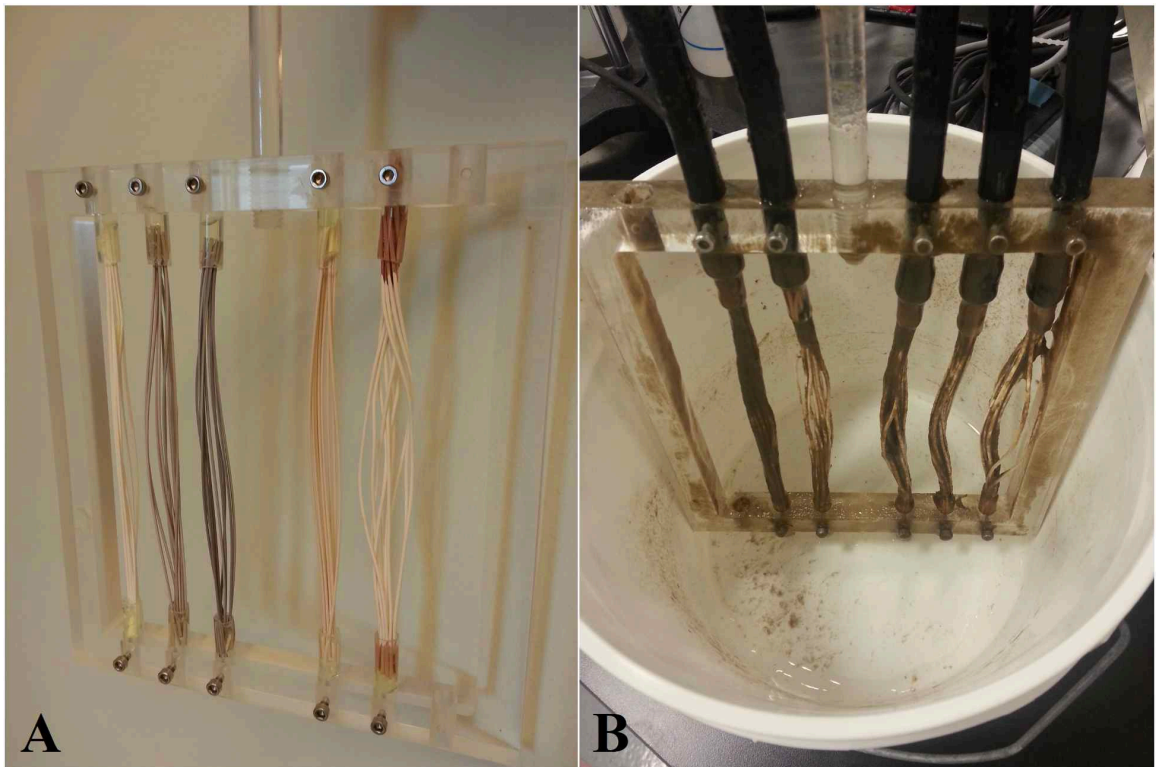


**Figure G.4.** Membrane cassette holding virgin (A) and biofouled membranes (B).